BIOINSPIRED SYNTHESIS AND REACTIVITY STUDIES OF NITRIC OXIDE IRON COMPLEXES

A Dissertation

by

JENNIFER LYNN HESS

Submitted to the Office of Graduate Studies of
Texas A&M University
in partial fulfillment of the requirements for the degree of

DOCTOR OF PHILOSOPHY

December 2011

Major Subject: Chemistry

BIOINSPIRED SYNTHESIS AND REACTIVITY STUDIES OF NITRIC OXIDE IRON COMPLEXES

A Dissertation

by

JENNIFER LYNN HESS

Submitted to the Office of Graduate Studies of
Texas A&M University
in partial fulfillment of the requirements for the degree of

DOCTOR OF PHILOSOPHY

Approved by:

Chair of Committee,	Marcetta Y. Darensbourg
Committee Members,	Janet Blümel
	Timothy R. Hughbanks
	Daniel F. Shantz
Head of Department,	David H. Russell

December 2011

Major Subject: Chemistry

ABSTRACT

Bioinspired Synthesis and Reactivity Studies of Nitric Oxide

Iron Complexes. (December 2011)

Jennifer Lynn Hess, B.S., Grove City College

Chair of Advisory Committee: Dr. Marcetta Y. Darensbourg

The significant role that nitric oxide (NO) plays in human physiology is linked to the ability of NO to bind to iron forming mono-nitrosyl iron complexes. Protein-bound and low-molecular-weight dinitrosyl iron complexes (DNICs) are known to form in excess NO. Studies of such biological DNICs have relied on their paramagnetism and characteristic EPR signal of g value of 2.03. It has been suggested that DNICs act *in vivo* as NO storage (when protein-bound) and transfer agents (when released by, for example, free cysteine). Biological DNICs, mainly resulting from iron-sulfur cluster degradation, are difficult to extract and isolate, thereby preventing their full characterization. Thus, development of synthetic DNICs is a promising approach to model and better understand the formation and function of biological DNICs, the scope of donor ligands that might coexist with $Fe(NO)_2$ units, the redox levels of bio-DNICs, and establish other spectroscopic techniques appropriate for characterization.

A series of N-heterocyclic carbene (NHC) and imidazole (Imid) complexes has been characterized as mimics of histidine-containing DNICs. The pseudo-tetrahedral $L_2Fe(NO)_2$ complexes have NO stretching frequencies and redox potentials that suggest

the NHCs are slightly better donors than Imids, however the two types of ligands have similar steric properties. Both the EPR-active, $\{Fe(NO)_2\}^9$ and the EPR-silent, $\{Fe(NO)_2\}^{10}$ states can be accessed and stabilized by the NHC. Nitric oxide transfer studies have shown that only the $\{Fe(NO)_2\}^9$ complexes are capable of transferring NO to a suitable NO trapping agent.

Deprotonation of the distal nitrogen functionality in the imidazolate ligands of $[(Imidazole)_2Fe(NO)_2]^-$ leads to aggregation forming molecular squares of $\{Fe(NO)_2\}^9$ units bridged by the imidazolates. These interesting tetrameric complexes are examined by X-ray diffraction, EPR, and Mössbauer studies. The paramagnetic tetrameric complexes have multiple redox events observed by cyclic voltammetry. Mössbauer spectral data of the tetrameric complexes are compared with Mössbauer data obtained for a series of NHC-containing DNICs.

Iron and cobalt-containing mononitrosyl N_2S_2 model complexes of the nitrile hydratase enzyme active site demonstrate sulfur-based reactivity resulting in the formation of polymetallic complexes. In all cases, shifts in the nitrosyl stretching frequencies demonstrate substantial transfer of electron density from the $(NO)M(N_2S_2)$ moiety to the metal-acceptor site.

DEDICATION

This dissertation is dedicated to my Lord and Savior, Jesus Christ. All I have and all I am are due to the blessing of God's grace in my life. My hope, strength, and comfort are found in Him and the greatest lesson I have learned over the past several years is that if I remain in Him, He will forever and faithfully remain in me (John 15:4). Thank you.

ACKNOWLEDGEMENTS

Graduate school has provided me with a wealth of opportunities—to learn, to meet new people from all over the world, to travel, and to grow as a scientist and an individual. At the forefront of these opportunities is my advisor, Marcetta Y. Darensbourg. Marcetta, your passion for great chemistry, your enthusiasm for teaching, and your dedication to your students is an inspiration. Thank you for never settling for mediocrity and for always pushing your students towards excellence. Thank you for instilling in me confidence, for teaching me how to write and present my work well, and for providing letters for all the various award and job applications, and for the opportunity and finances to travel to so many wonderful conferences and symposiums.

I would like to thank my committee members, Drs. Janet Blümel, Timothy R. Hughbanks, and Daniel F. Shantz, for their willingness to serve on my committee, for friendly advice, and for the helpful discussions involving my work. I would sincerely like to thank Dr. Joseph H. Reibenspies for all of his help with my many questions about x-ray crystallography. His patience, willingness to help, and speedy response whenever I had a problem with the instruments, are greatly appreciated. I would also like to thank Dr. Donald J. Darensbourg for all of his help and for the fun conversations in the lunch room. I would especially like to thank Dr. Elizabeth Binamira-Soriaga for a wonderful teaching assistant experience and for her help and patience in developing my teaching skills.

I must also thank all of the teachers in my life that have helped shape me and set the path for me to eventually attend graduate school. Specifically, I would like to acknowledge Mr. Griffiths, my high school Advanced Placement chemistry teacher. If it was not for you, I would have never developed a love for chemistry. To Mr. Doll, my high school band director, you always believed in me. Furthermore, I am grateful for the chemistry professors at Grove City College (GCC) (Drs. Joseph Augspurger, Harold Conder, Susan Cramer, Vincent DiStasi, Michael Falcetta, David Jones, and Charles Kriley). Your love for God, your students, and your unwavering willingness to help made my time at GCC so special and provided me with a model of the type of Christian educator I desire to be. Dr. Michael Falcetta, thank you for trying to calm me by giving me a 68% on all of my quizzes. You will be happy to know that I am much more relaxed these days, I think. Dr. Harold Conder, you have been my mentor and my friend, and I cannot express to you enough how grateful I am for that.

Thank you to all past and current Darensbourg group members (Elky Almaraz, Jeremy Andreatta, Shawn Fitch, William Foley, Eric Frantz, Kayla Green, Roxanne Jenkins, Osit Karroonnirun, Bin Li, Tianbiao Liu, Adriana Moncada, and Michael Singleton; Ryan Bethel, Scott Brothers, Danielle Crouthers, Jason Denny, Dr.Chung-Hung Hsieh, Tiffany Pinder, Ross Poland, Randara Pulukkody, Sheng-Hsuan Wei, and Stephanie Wilson). We are a family and I have enjoyed my interactions with each and every one of you. Kayla, your guidance, advice, and friendship over the years are second to none. Thank you for being such a great mentor, getting me going in my research and for being such a wonderful friend. Eric, I am so thankful that we have been

able to stay in touch. You are such a dear friend to me and I admire you greatly. Your ability to make me laugh, as well as have in-depth conversations, have been helpful on so many days. Jeremy (Jere-may!), what can I say other than that I will always be your Jen-nay. Jason, thanks for always being a friend and for helping me with so many different things, like moving my couch. Danielle, thanks for your laughter (you're the only one that ever laughs at my terrible jokes) and for always lending an ear to listen. Tiffany, thanks for your friendship, encouragement, and for allowing me to express my urban side. Mark, thank you for all your help and great insight on my project. Ross, thank you for providing me with Rock Band when I needed it, for so many laughs, and for being a very supportive friend. Hank (aka, Stephanie), I think our friendship is best described by that time we drove out to Snook at some ungodly hour. (Honk.) You are always there for me, always willing to help me out, and always willing to talk. Thank you so much for being such a cherished friend. Scott, my work husband, the glue that has held me together, thank you so much for your friendship and for always taking time to listen to me (over and over again).

Thank you to all of my friends from Grove City College. Our strong bond of friendship surpasses time and location, and I am so thankful for that. Jess, thank you for all the fun visits to New Orleans, for lending an ear when I have needed to vent, and for being a great, long-lasting roommate (I mean friend). Johannah, Natalie, Erin, Rebecca, Megan, Sarah, and Emily, I love you all dearly and I thank you for your friendship and support. Thank you also to my Solanco friends: Cody, Jess, Sherry, and Tasha. It is so

awesome and such a blessing that we have kept in touch. Your support and reminiscing whenever we can get together always keeps me going.

Most importantly, I would like to thank my mom and dad for their continuous love and support and for teaching me morals, values, and the importance of a good work ethic. Without you, I would not be here today and I would like to say thank you so much and I love you. To my brother Andy, my grandma and grandpa, my aunts and uncles, and all of my cousins, thank you for your love and support. You inspire me to be the best that I can be.

Emily Kleinhans, my best friend and my soul mate, I cannot adequately express to you how thankful I am that we are such great friends. You know me like no one else does. Thank you for all the support and encouraging words over the past couple of years. You are always the one I know I can go to to understand anything going on with me. I know for sure that we will always be there for each other. You are a model friend and I do not know what I would do without you.

And as tradition goes, the best is saved for last. Brian Young, you came into my life at just the right time and I am incredibly thankful to God for that every day. Your love, support, and patience know no bounds. You are an incredible person and make me a better person just by knowing you. I greatly look forward to seeing where life takes us. I love you.

Finally, thank you to all friends and colleagues that I unintentionally forgot to mention or just ran out of space to do so. I am grateful for your presence in my life and for all that you have done to help get me here.

TABLE OF CONTENTS

CHAPTER Page

Page

LIST OF FIGURES

FIGURE Page

FIGURE Page

FIGURE Page

FIGURE Page

FIGURE Page

LIST OF TABLES

CHAPTER I

INTRODUCTION

Biological Significance of Nitric Oxide

Though nitric oxide (NO) is known to be a toxic gas, over the past several decades this simple diatomic molecule has surprisingly emerged as a fundamental molecule in biological systems.[1] NO can exist in several redox states, as NO radical (NO•), oxidized nitrosonium cation (NO^+), or reduced nitroxyl anion (NO^-), resulting in its ability to be involved in a variety of different processes.[2] Interactions of NO with proteins and biomolecules are divided into three categories: protective, regulatory, and deleterious. Some of the main physiological activities in which NO plays a significant role include neurotransmission, blood pressure control, regulation of the immune system, and smooth muscle relaxation. On the other hand, interactions with NO can also result in negative responses such as inhibition of mitochondrial respiration, DNA damage, and septic shock.[2]

In biological systems, the synthesis of NO is exclusively regulated by the NO-synthase family of enzymes.[3] The NO-synthases (NOS) exist in three major isoforms: endothelial (eNOS), neuronal (nNOS), and inducible (iNOS). The eNOS are expressed in the cells lining the blood vessels. The nNOS are expressed in nerve cells mainly found in the brain and in skeletal muscle and heart muscle. The iNOS are expressed when their activity is triggered by a response to the immune system. The main role of

---

This dissertation follows the style of *Journal of the American Chemical Society*.

the eNOS and nNOS are in signaling activities, whereas, the iNOS is primarily a cytotoxic register.[4]

All of the NO-synthases catalyze the conversion of L-arginine to L-citrulline resulting in release of NO, Figure I-1.[5] The first step in the reaction requires delivery of two electrons from NADPH which aid in oxygen activation to form the intermediate N-ω-hydroxyl-L-arginine (NOHA). The second step requires only one electron to activate oxygen to form L-citrulline and NO. The NOS contain two functional domains to assist in this reaction sequence. The oxygenase domain is at the N-terminal end, which is the site of catalysis. This site consists of an Fe-heme that is ligated to the protein through a cysteine thiolate. The reductase domain is at the C-terminal end. Its main function is to receive electrons from NADPH and shuttle them through a series of flavins to the oxygenase domain. The oxygenase domain also contains a pterin cofactor (BH_4) that is hypothesized to function as an electron donor-acceptor in the final step of the catalytic reaction.[5] Interestingly, an extensive hydrogen-bonding network is found to associate all the components of these enzymes and guide the position of the reactive N of L-arginine to less than 5 Å from the heme iron.[4] While the complete mechanism of these enzymes is not fully understood, it is evident that this chemical reaction is unique to biological systems and serves as the source of NO *in vivo*.[4,5]

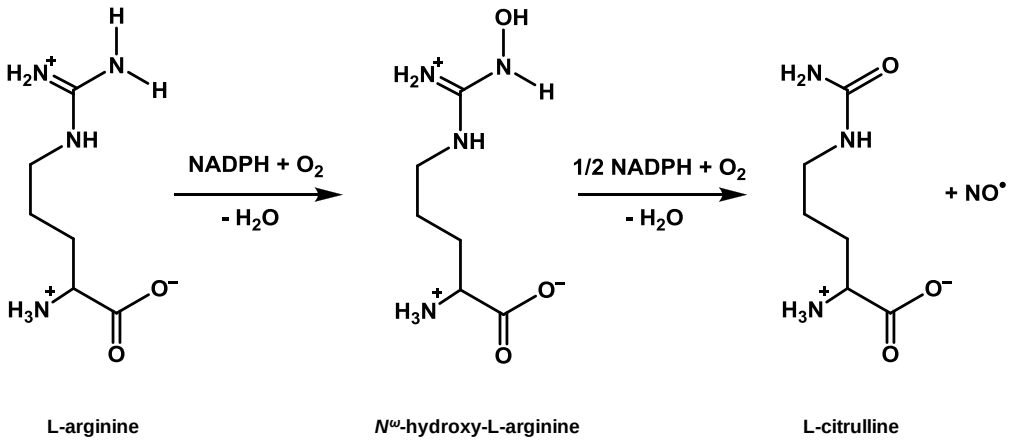

Figure I-1. Conversion of L-arginine to L-citrulline catalalyzed by NO synthase resulting in release of nitric oxide.[5]

Uncomplexed NO has a short lifespan; its half-life in the cellular milieu is on the order of 2 ms to 2 s.[6] Thus, the properties and cellular targets of NO are dependent on the concentration of NO. The protective effects of NO typically occur at low concentrations, i.e., when the amount of NO is in the picomolar to nanomolar range. When NO concentrations increase, cytotoxic effects or regulatory effects become more relevant.[7] It has been discovered that the stabilization, movement, and perhaps the function of NO *in vivo* is linked to the presence of S-nitrosothiols.[8] Dinitrosyl iron complexes have also been proposed to function as storage and/or transport units for NO.[3,7,8]

Discovery and Relevance of Dinitrosyl Iron Complexes (DNICs)

In the 1960's, Woolum and Commoner monitored purified liver tissue from carcinogen-fed rats via EPR spectroscopy. An unusual signal appeared at g = 2.035.[9] Previously, Vanin, Nalbandyan, and Shifman had reported that yeast cells grown in Reader's medium in the presence of nitrate (NO_3^-) also exhibit a g = 2.035 signal.[10,11,12] In order to elucidate the origin of this signal, Woolum and Commoner incubated a series of rat tissues with nitrite (NO_2^-) since nitrate is readily reduced to nitrite by animal tissues. Similar EPR signals were obtained from the nitrite incubated rat liver, skin, and brain tissues, Figure I-2.[9] These findings were compared to another study at the time in which McDonald, *et al*. had observed a similar signal, g = 2.033, upon mixing Fe^{2+} and NO with cysteine[13] suggesting that the nitrite was being reduced to NO in the rat tissues. These studies were corroborated by the EPR signal obtained upon nitrite incubation of aldolase, a protein containing thiol groups, resulting in a thiol-containing Fe^{2+}-NO complex.[9] With these studies, the first biologically relevant paramagnetic Fe-NO complexes with thiol-containing proteins were discovered, opening the door for an expansive field of investigation.

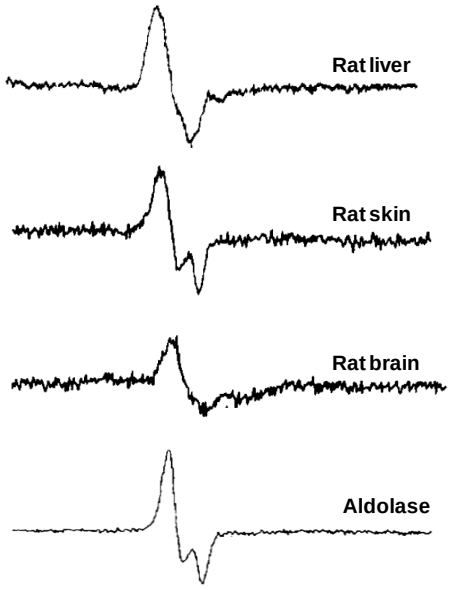

Figure I-2. EPR signals with g ~ 2.03 following incubation of rat liver, skin, and brain tissues with NO_2^-. These signals were compared with the signal from aldolase protein that forms a thiol containing Fe^{2+}-NO complex under similar incubation conditions.[9]

Since the 1960's, much research has been devoted to determining the structure, mechanism, and relation to biological activity of these thiol-containing nitrosyl iron complexes. It has been determined that these complexes are composed of a single tetrahedral iron coordinated by two nitrosyl ligands and, typically, two thiol/thiolate ligands resulting in the moniker: dinitrosyl iron complex (DNIC). These DNICs are EPR active and are characterized by their unique EPR signal with a g value at 2.03.[3,8] Following exposure to endogenous or exogenous NO, DNICs are generated in cells and tissues from a variety of sources. Nitric oxide binds to protein-based iron centers or iron-sulfur cluster-containing proteins to form protein-bound DNICs.[14-18] For example, interaction of NO with the 4Fe-4S cluster of FNR, an O_2-responsive regulator, results in

the formation of a DNIC as observed by EPR spectroscopy.[19] DNICs are also formed upon interaction of NO with thiol-rich proteins, as well as the cellular chelatable iron pool (CIP), a portion of cellular iron known as a dynamic iron reservoir capable of moving iron between metalloproteins.[20] Additionally, it has been suggested that free thiols, via thiolate exchange, can displace the ligated protein resulting in the formation of low molecular weight-DNICs (LMW-DNICs).[21]

A number of *in vivo* and *in vitro* studies have been performed to elucidate the direct physiological role of NO. For example, transfer of NO released from eNOS to the enzyme soluble guanylate cyclase in vascular smooth muscle cells stimulates the formation of cyclic guanosine-3′,5′-monophosphate, which induces vasodilation.[7] Under oxidative stress, high concentrations of NO rapidly react with superoxide to form peroxynitrite ($ONOO^-$), which is a known cytotoxin. This feature is utilized by inflammatory cells in response to invading pathogens in order to mediate apoptosis.[7] In these systems and others, it has been accepted that DNICs and S-nitrosothiols (formed in the presence of thiol and NO^+) may serve as NO storage agents with the ability to transport NO to its specific target when triggered by complex biological machinery.[3,6]

Additionally, NO is implicated in the degradation of several iron-sulfur cluster-containing proteins with concomitant formation of thiol-containing DNICs. This activity can have a positive effect in the example of SoxR (from the *E. coli soxRS* system), a redox-sensitive transcription activator. With NO exposure, the 2Fe-2S centers of this protein are cleaved to form protein-bound dithiol DNICs, resulting in activation of the transcriptional activity with an extended lifetime compared to the protein not exposed to

NO.[22] On the other hand, disassembly of Fe-S clusters can have a negative effect. For example, addition of NO to mammalian ferrochetolase results in degradation of its 2Fe-2S cluster and a decrease in enzyme activity.[14]

Only recently has a protein-bound DNIC been observed by x-ray crystallography; the $Fe(NO)_2$ unit, introduced exogenously to human glutathione transferase (GST P1-1) as bis-glutathionyl dinitrosyl iron, is found to bind within the active site of the enzyme through the phenolate oxygen of Tyr7 of the active site and the sulfur from glutathione that would normally be expected to reside in the active site.[23] Figure I-3 shows the reaction scheme and corresponding structure rendition as determined via X-ray crystallography.[23] While the presence of the DNIC guest, carried in with the glutathione, within this site correlates with diminished activity of GST, its identification encourages conjectures regarding protein chaperones or biomolecule transport agents.[23]

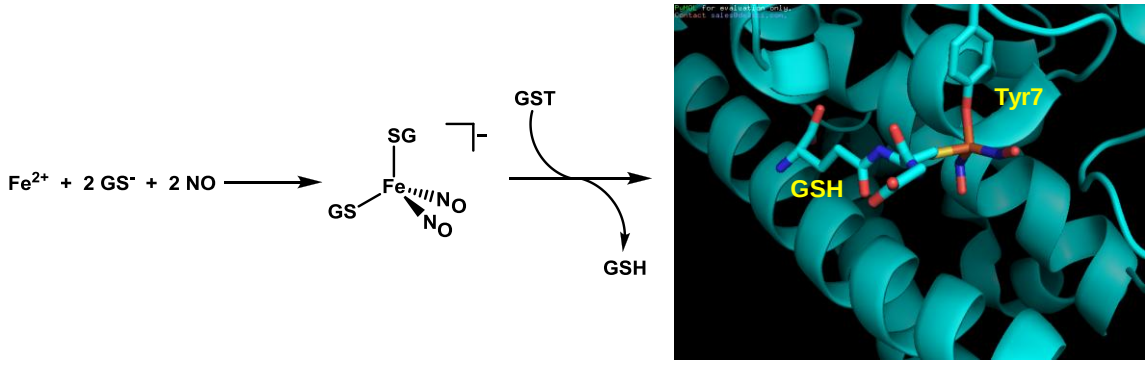

Figure I-3. Reaction scheme and X-ray crystallographic rendition of glutathione S-transferase (GST) protein-bound DNIC bound through glutathione (GSH) and tyrosine7 (Tyr7) following addition of bis-glutathionyl DNIC to the protein.[23]

Thus, while the mechanism of NO transport and the presence of DNICs in biological systems are not fully understood, it is evident that the interplay between the formation of DNICs and the bioactivity of NO could be of great significance.

Nitric Oxide Donor Drugs

Nitric oxide's vast array of functionality in the cardiovascular, nervous, and immune systems has generated a field of research devoted to developing NO donors as therapeutic agents.[7] Besides the processes mentioned above, NO has also been found to suppress aggregation of human platelets.[3] NO also induces fast healing of wounded skin tissue and prevents bacterial infection.[3] *In vivo* studies have suggested that NO plays an important part in inhibiting tumor cell adhesion and impedes further growth of tumor cells typically by inhibiting DNA synthesis of the tumor cells.[24-26] Additionally, endothelial dysfunction, which is a main culprit in cardiovascular diseases, leads to NO deficiency in human organisms. This NO deficiency derives from a deficit of NO synthesis, impaired availability of bioactive NO, or enhanced NO inactivation.[27] Thus, the need for strategic administration of exogenous NO for therapy or for the replacement of endogenous NO has provided a foundation for NO donors as pharmacological or therapeutic agents.

Currently, there are several agents available in clinical use. These can be divided into two categories: direct NO donors and drugs that modulate the bioactivity of endogenously produced NO.[28] Chart I-1 displays the chemical structures of several of these NO drugs.[7] Glyceryl trinitrite (GTN) mainly used for relief of pain associated with

angina, and sodium nitroprusside (SNP) typically used for cardiovascular emergencies and heart failure, are NO donor drugs that have been used for decades. In the case of GTN, one molar equivalent of NO is released upon bioactivation of this compound most likely by mitochondrial aldehyde dehydrogenase.[7] SNP generates NO through exposure to light when in solution or through a tissue-specific mode of release that has not fully been elucidated. This drug, however, is difficult to administer and can be quite potent making the dosage a difficult task to determine.[7] Other NO donors are NONOates (or diazeniumdiolates) and S-nitrosothiols.[7]

Two common examples of drugs that modulate the bioactivity of NO are Captopril and Sildenafil. Captopril is used to stimulate bradykinin-induced NO release, which inhibits the angiotensin-converting enzyme resulting in lowered blood pressure.[28] Sildenafil prolongs NO signaling by inhibiting cGMP-specific phosphodiesterase type 5 leading to increased vasodilation.[28] Adverse effects of these types of drugs could result in blood circulation problems and drug tolerance as well as detrimental effects related to the large amount of NO released upon administration of these drugs.[28]

Chart I-1. Examples of NO donor drugs.[7]

Direct NO Donors

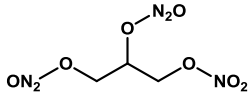

Glyceryl trinitrite (GTN)

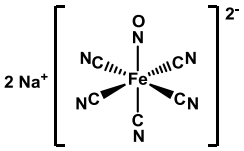

Sodium nitroprusside (SNP)

Diazeniumdiolates (NONOates)

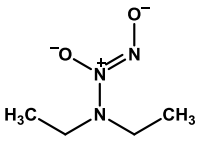

Diethylamine NONOate

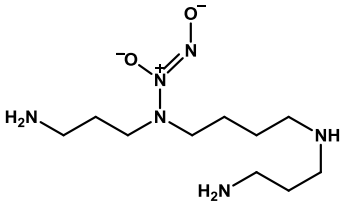

Spermine NONOate

S-Nitrosothiols

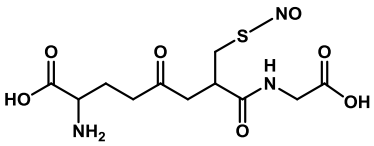

S-nitroso-glutathione (GSNO)

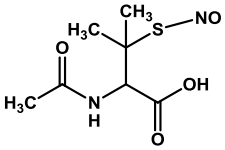

S-nitroso-N-acetylpenicillamine (SNAP)

Modulators of NO Bioactivity

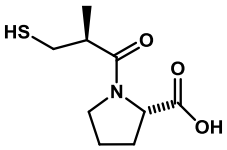

Captopril

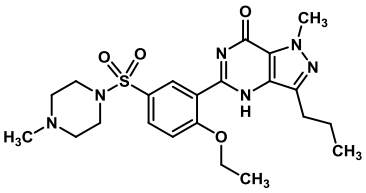

Sildenafil

Though these two classes of drugs are capable of delivering or modulating NO, efforts exist to develop other pharmaceuticals that are better at releasing NO slowly over long periods of time. The chemical properties of DNICs are favorable for their

development as NO transfer agents *in vivo*, so it is possible that these types of complexes could provide a new class of therapeutic agents.

Dinitrosyl Iron Model Complexes

Synthesis of inorganic DNICs and study of their reactivity and NO transfer ability can improve understanding of the function and reactivity of NO in biological systems. To date, most models of biological DNICs have relied on thiolate ligands which give rise to monomeric $[(RS)_2Fe(NO)_2]^-$ as well as dimeric, Roussin's red-ester type complex forms, i.e., $(\mu\text{-}RS)_2[Fe(NO)_2]_2$.[29-33] In both, the $Fe(NO)_2$ is in its oxidized form of $\{Fe(NO)_2\}^9$ electron configuration according to the Enemark-Feltham notation.[34] Abiological phosphine DNICs are known (stabilizing the reduced $\{Fe(NO)_2\}^{10}$ redox level) as well as DNICS containing nitrogen-donors.[35-37] These inorganic DNICs can be classified into five types: EPR-active, anionic $\{Fe(NO)_2\}^9$, neutral $\{Fe(NO)_2\}^9$, and cationic $\{Fe(NO)_2\}^9$ and EPR-silent, neutral $\{Fe(NO)_2\}^{10}$ and anionic $\{Fe(NO)_2\}^{10}$.[31,38] Figure I-4 provides structures of complexes representing each type of DNIC.

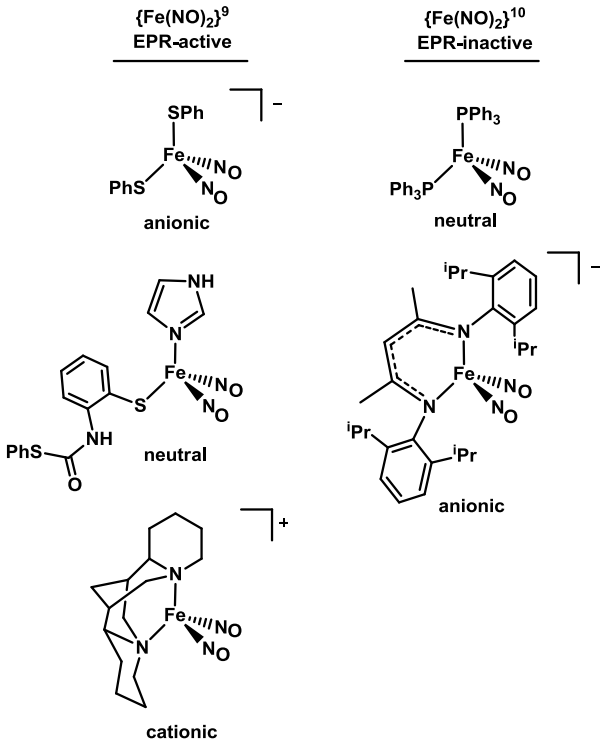

Figure I-4. Representative complexes of the types of inorganic DNICs: EPR-active, anionic $\{Fe(NO)_2\}^9$,[31] neutral $\{Fe(NO)_2\}^9$,[39] and cationic $\{Fe(NO)_2\}^9$ [31] and EPR-silent, neutral $\{Fe(NO)_2\}^{10}$ [40] and anionic $\{Fe(NO)_2\}^{10}$.[38]

Professor Wen-Feng Liaw and coworkers have provided myriad reports in the literature focused on the characterization of bis-thiolate DNICs and RRE-type complexes and the interconversion between these two forms. Liaw, *et al.* have demonstrated that the dimeric RREs can be cleaved by a variety of thiolates to form anionic bis-thiolate DNICs, eq I-1.[31,33,39] The stability of these complexes of the form $[(RS)_2Fe(NO)_2]^-$ are dependent on both the electronic and structural environment of the coordinated thiolate ligands; a stronger electron-donating thiolate can promote thiolate-ligand exchange, eq I-2.[30] For example, the thiolate ligands of [(2-*S*-

$C_7H_4NS)_2Fe(NO)_2]^-$ can be replaced by C_6H_4-*o*-NHC(O)-CH_3 to form $[(C_6H_4$-*o*-$NHC(O)$-$CH_3)_2Fe(NO)_2]^-$; the difference in electron-donating ability of the thiolates is demonstrated by the ν(NO) stretching frequencies according to typical π-backbonding arguments: 1716, 1766 cm^{-1} and 1705, 1752 cm^{-1}, respectively.[30] Furthermore, Liaw and coworkers proposed that the relative position of ν(NO) stretching frequencies and the difference between the two stretching frequencies may be a useful tool for determining the charge of the complex and the oxidation state of the $Fe(NO)_2$ unit.[31] For example, Liaw *et al.* reports that the $\Delta\nu_{(NO)}$ for a series of EPR-active, anionic $\{Fe(NO)_2\}^9$ is ~ 45 cm^{-1}, whereas for the EPR-active, cationic $\{Fe(NO)_2\}^9$ the Δν(NO) is ~ 65 cm^{-1} and for the EPR-silent, neutral $\{Fe(NO)_2\}^{10}$, the Δν(NO) is ~ 55 cm^{-1}.[31] They suggest that this $\Delta\nu_{(NO)}$ value may help establish the oxidation state of DNICs in biological systems.[39]

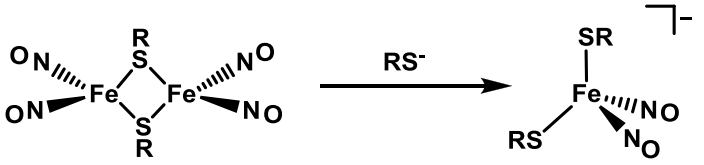

(eq I-1)

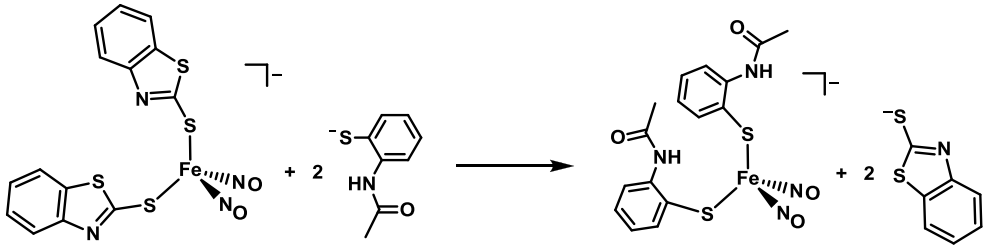

ν(NO) = 1716, 1766 cm^{-1}

ν(NO) = 1705, 1752 cm^{-1}

(eq I-2)

While the main components of biological DNICs are presumed to be thiolates, typically of cysteine or glutathione, DNICs containing other coordinated ligands (thiolate, amine and alkoxide) have been detected via EPR spectroscopic studies upon nitrosylation of several proteins.[14-19,41-44] Since the histidine amino acid residue is typically found as an adjunct to cysteine in metallobiomolecules, it is a reasonable assumption that the N-donors are from histidine amino acids. For example, nitrosylation of bovine serum albumin in which the cysteine groups were protected resulted in an EPR signal indicative of DNIC bound to the serum albumin protein via histidine.[42] Similarly, addition of NO to aconitase resulted in a transient iron-nitrosyl-histidyl-aconitase complex observed by EPR spectroscopy as well as formation of an iron-nitrosyl-thiol-aconitase complex.[15]

A more recent study by Tinberg and Lippard *et al.*, looked for evidence of both $(Cys\text{-}S)_2Fe(NO)_2^-$ and $(His\text{-}N)_2Fe(NO)_2$ that might be derived from a Rieske-type ferredoxin protein.[45] Excess NO (or an NO-donor molecule) was reacted with the toluene/*o*-xylene monooxygenase component C (ToMOC) from *Pseudomonas* sp. OX1), containing a [2Fe-2S] cluster with two histidines and two cysteine ligands as terminal ligands on individual irons. The observation of an EPR signal characteristic of an $\{Fe(NO)_2\}^9$ unit supported the expectation of bis-cysteine DNIC as seen with common 4Fe-4S clusters,[46] or of one of the possible forms of bis-histidine within an oxidized DNIC. As EPR spectroscopy is the major tool for detecting DNICs, the authors stated that the formation of histidine bound $\{Fe(NO)_2\}^{10}$ product was not verified but cannot be ruled out.[45]

In contrast to cysteine, histidine binding to metals offers additional complexities, including the basic nitrogen as a neutral donor and, on deprotonation of the weakly acidic N-H, a 1^- donor is obtained. Consequently, there are three possibilities for $(His)_2Fe(NO)_2$ complexes: a neutral EPR inactive $\{Fe(NO)_2\}^{10}$ complex; a neutral EPR active $\{Fe(NO)_2\}^9$ complex; or an anionic EPR active $\{Fe(NO)_2\}^9$ complex, Figure I-5. It is expected that the bioactivity of histidine-containing DNICs could critically depend on differences derived from these various redox/protonation levels.

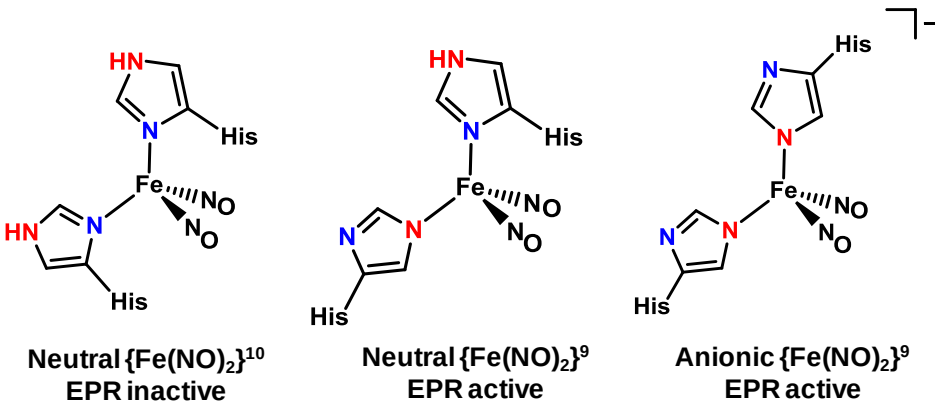

Figure I-5. Possible binding modes of biological histidine-containing DNICs.

Few studies have been reported that address synthetic analogues of histidine-containing DNICs. Li and coworkers have approached this difficult task and have ν(NO) infrared values for several neutral $(imidazole)_2Fe(NO)_2$ complexes mostly characterized *in situ*.[47] In one case, a neutral $(Imid\text{-}Me)_2Fe(NO)_2$ (Imid-Me = 1-

methylimidazole) complex of $\{Fe(NO)_2\}^{10}$ electron configuration was isolated and structurally characterized (Figure I-6a).[35] The extreme air sensitivity of this complex, and all other members of the series, led to detection of the oxidized $\{Fe(NO)_2\}^9$ species by EPR spectroscopy, presumably arising from adventitious O_2 as oxidant.[35,47] As in the $(RS)_2Fe(NO)_2^-$ complexes, the characteristic EPR signal is ~ 2.03.[29-33] Interestingly, Liaw *et al*. have synthesized, isolated, and structurally characterized the bis-imidazolate DNIC, an anionic $\{Fe(NO)_2\}^9$ complex, which is seemingly more stable than the neutral $\{Fe(NO)_2\}^{10}$ analogues, Figure I-6b.[36]

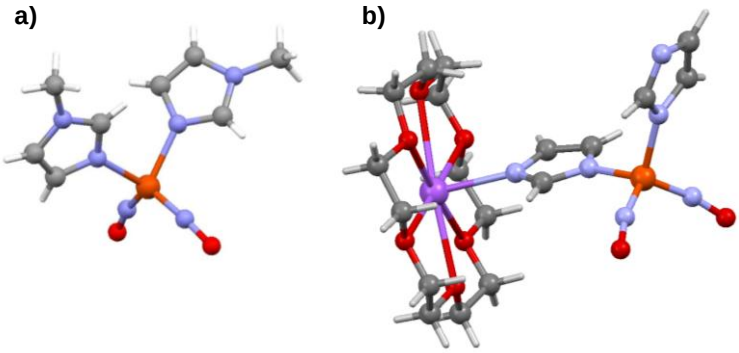

Figure I-6. Molecular structures of a) the neutral $\{Fe(NO)_2\}^{10}$ $(Imid\text{-}Me)_2Fe(NO)_2$ (Imid-Me = 1-methylimidazole) complex[35] and b) the anionic $\{Fe(NO)_2\}^9$ complex $(Imid^-)_2Fe(NO)_2$ ($Imid^-$ = imidazolate) as the sodium 18-crown-6-ether salt.[36]

NO Transfer Studies Involving Dinitrosyl Iron Model Complexes

In several cases, DNIC model complexes have demonstrated NO transfer ability to biologically relevant NO trapping agents. This type of NO transfer study may help to further elucidate *in vivo* NO transfer, as well as potentially discover a new class of

agents capable of stabilized, controlled release of NO. For example, Liaw and coworkers report that the water soluble RRE $[Fe(\mu\text{-}SC_2H_4COOH)(NO)_2]_2$ can be taken up by vascular endothelial cells.[48] An *in vitro* NO release assay demonstrated that the RRE was capable of stoichiometric NO release. This release was slower than that demonstrated by the common NO donor, *S*-nitroso-*N*-acetyl-penicillamine (SNAP). Additionally, EPR spectroscopic studies showed that this RRE could be transported into the cells and transformed into paramagnetic protein-bound DNIC in the presence of serum. Under serum-free conditions and in the presence of excess cysteine, the RRE was transformed into bis-cysteine DNIC. Both transformations occurred likely due to nitrosylation from NO release.[48]

Lippard and coworkers synthesized and characterized two DNICs containing a β-diketiminate ligand (Ar-nacnac) in both the $\{Fe(NO)_2\}^9$ and $\{Fe(NO)_2\}^{10}$ oxidation states[38] and studied their abilities to transfer NO to the well-known NO acceptor Fe^{III}(TPP)Cl (TPP = meso-tetraphenylporphine).[49] For the $\{Fe(NO)_2\}^9$ complex, NO transfer occurred immediately resulting in the formation of Fe(NO)Cl(Ar-nacnac) and Fe^{II}(NO)(TPP), Figure I-7.[49] However, for the $\{Fe(NO)_2\}^{10}$ complex, NO transfer only occurred upon reduction of Fe^{III}(TPP)Cl and consequent oxidation of the $\{Fe(NO)_2\}^{10}$ complex to the corresponding $\{Fe(NO)_2\}^9$ complex confirming a link between the iron redox state and NO transfer ability.[49]

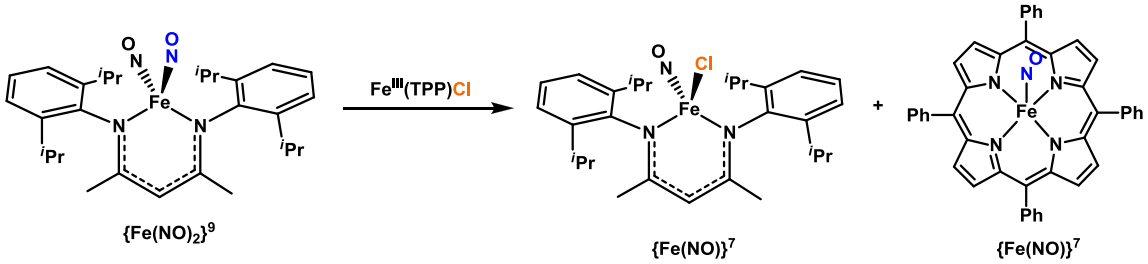

Figure I-7. NO transfer from $\{Fe(NO)_2\}^9$ diketiminate-bound DNIC to Fe porphyrin with simultaneous formation of $\{Fe(NO)\}^7$ diketiminate-bound mononitrosyl complex.[49]

Chiang and coworkers used the $(H^+bme\text{-}daco)Fe(NO)_2$ (bme-daco = *N,N'*-bis(2-mercaptoethyl)-1,4-diazacycloheptane) complex as an NO transfer agent to iron or cobalt porphyrins, Figure I-8.[50] Upon loss of a NO group from the bme-daco DNIC, the mononitrosylated Fe was captured in the N_2S_2 core of the bme-daco ligand. This led Chiang *et al*. to suggest the possible formation of mononitrosyl iron complexes (MNICs) in biological systems via capture by amide nitrogens from cysteines found in the protein backbone following the release of one NO ligand.[50]

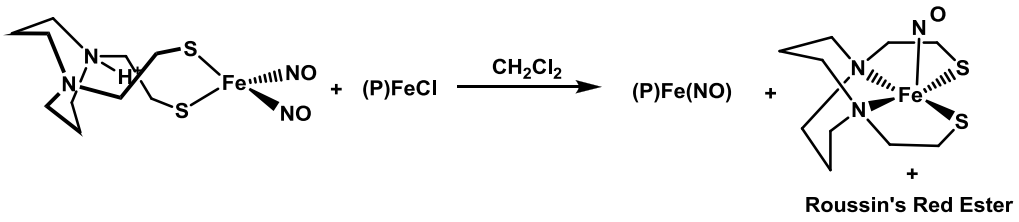

Scheme I-8. $(H^+bme\text{-}daco)Fe(NO)_2$ complex and corresponding NO transfer to an Fe porphyrin with concomitant formation of a mononitrosyl iron complex and Roussin's Red ester complex. (P)FeCl = α,β,γ,δ-Tetraphenylporphinato iron(III) chloride or 2,3,7,8,12,13,17,18-octaethyl-21H,23H-porphine iron(III) chloride.[50]

Such NO transfer studies and others demonstrate the potential for DNIC model complexes as viable NO transfer agents in a pharmaceutical context or for biomimetic studies. Such biomimetic studies may help to further understand the action of NO transfer from DNICs in biological systems, as well as the form of the DNIC, protein-bound or low-molecular-weight, from which NO transfer can occur. Additionally, determining the redox form of NO that is released in relation to the target molecule may help to provide information regarding the relationship between the NO redox state and the acceptor site (heme sites, oxidized heme sites, thiols, amines, or alcohols) in biological systems.

Nitrile Hydratase Enzyme Active Site

An additional example of the presence of NO in biological systems is found in a variety of bacteria and fungi within the nitrile hydratase (NHase) enzyme active site. This enzyme is responsible for the conversion of nitriles to their corresponding amides. In this active site, an iron or cobalt center is held in a square-planar contiguous N_2S_2 arrangement, in which the N_2S_2 binding motif originates from a cysteine-serine-cysteine tripeptide motif, Figure I-9.[51] The iron-containing NHase contains a NO ligand bound to the iron and activation of this "as-isolated" form occurs when the NO ligand is removed upon exposure to light.[51,52] While the source of the NO is still in question, crude extracts of *Rhodococcus* sp. R312 (a specific bacteria containing nitrile hydratase) contain a nitric oxide synthase, suggesting that NO release from the conversion of L-arginine to L-citrulline could be a possible source of the NO.[53] Studies of NO transfer from DNIC

moieties have been designed that would take advantage of the potential tetradentate ligating ability provided by the cysteinyl residues in the DNIC, resulting in mononitrosyl MNIC in an N_2S_2 donor set composed of carboxamido nitrogen/cysteine sulfur following an NO transfer reaction, Figure I-9.[50] Whether such MNICs are present and play a significant role in human and animal biological systems have yet to be discovered but biomimetic studies suggest that the notion is possible.

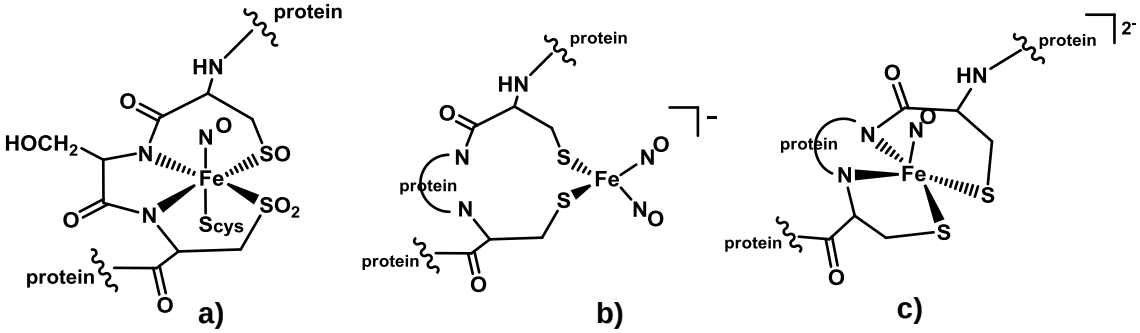

Figure I-9. a) NO inactivated iron nitrile hydratase enzyme active site,[51] an MNIC; b) proposed structure of protein-bound $(Cys)_2Fe(NO)_2$ DNIC; c) proposed structure of protein-bound $(Cys)_2Fe(NO)$ MNIC following loss of one NO from $(Cys)_2Fe(NO)_2$ and capture of the Fe(NO) unit within the tetradentate N_2S_2 binding motif.

Thus, this dissertation will focus on work inspired by the action of NO and the presence of dinitrosyl iron complexes in biological systems. To further model histidine-containing DNICs, we have utilized the N-heterocyclic carbene as a mimic of histidine/imidazole-type ligands. A series of DNICs and their corresponding reactivity are discussed in Chapter III. Additional investigation of imidazole-containing DNICs led to the formation of novel paramagnetic molecular squares containing four

$\{Fe(NO)_2\}^9$ units bridged by imidazolate ligands. Their unique, interesting structures, Mössbauer spectral data, and redox properties are presented in Chapter IV. The sulfur reactivity of several mononitrosyl NHase model complexes of the formula $(N_2S_2)M(NO)$ (M = Fe, Co) is explored in Chapter V. The first part describes the synthesis and properties of S-bound-$W(CO)_4$ heterobimetallics, while the second part describes the synthesis and properties of a Ag_2 paddlewheel complex ligated through the sulfurs of the $(N_2S_2)Fe(NO)$ paddles. The effect of the nitrosyl ligand on the donating ability of the metal-bound thiolate sulfurs is also discussed.

CHAPTER II

EXPERIMENTAL SECTION FOR CHAPTERS III-V

Abbreviations

DNIC = dinitrosyl iron complex

RRE = Roussin's red ester

NHC = N-heterocyclic carbene

NHC-iPr = 1,3-bis(isopropyl)imidazol-2-ylidene

NHC-Me = 1,3-bis(methyl)imidazol-2-ylidene

SPh = phenyl thiolate

Imid-iPr = 2-isopropylimidazole

Imid-H = imidazole

Imid-benz = benzimidazole

(bme-dach)Co(NO) = Co-1′(NO) = (*N*,*N*′-Bis(2-mercaptoethyl)-1,4-diazacycloheptane)-nitrosylcobalt

(bme-dach)Fe(NO) = Fe-1′(NO) = (*N*,*N*′-Bis(2-mercaptoethyl)-1,4-diazacycloheptane)-nitrosyliron

Co(TPP) = 5,10,15,20-tetraphenyl-21*H*,23*H*-porphine cobalt(II)

General Procedures and Physical Methods

All solvents were reagent grade and were purified and degassed by a Bruker solvent purification system and stored over molecular sieves. Standard Schlenk-line

techniques (N_2 atmosphere) and an Ar-filled glove box were used to maintain anaerobic conditions during preparation, isolation, and product storage.

Physical Measurements. Infrared spectra were recorded on a Bruker Tensor 27 FTIR spectrometer in CaF_2 solution cells of 0.1 mm pathlength. Solid state samples were run using the Pike MIRacleTM attachment from Pike Technologies for Attenuated Total Reflectance Infrared Spectra (ATR-FTIR). UV-Vis spectra were recorded on a Hewlett Packard HP8453 diode array spectrometer. NMR spectra were recorded using a Mercury 300 MHz NMR spectrometer. Mass spectrometry (ESI-MS) was performed by the Laboratory for Biological Mass Spectrometry at Texas A&M University. Nanoelectrospray ionization in positive mode was performed using an Applied Biosystems QSTAR Pulsar (Concord, ON, Canada) equipped with a nanoelectrospray ion source. Solution was flowed at 700 nL/min through a 50 μm ID fused-silica capillary that was tapered at the tip. Electrospray needle voltage was held at 1900 V. Elemental analyses of crystalline samples were determined by Atlantic Microlab, Inc., Norcross, GA.

EPR spectra were typically recorded in frozen THF or DMF at 10 K or in THF, DMF, or CH_2Cl_2 at 295 K, as indicated, using a Bruker ESP 300 equipped with an Oxford ER910 cryostat. The WinEPR Simfonia program was used to simulate spectral parameters.[54]

Mössbauer spectra were recorded with a MS4 WRC spectrometer (SEE Co., Edina, MN) with a 4.5 to 300 K closed-cycle refrigerated helium system. The spectra were collected at 5 K with a 700 G field applied parallel to the source of radiation. The

spectra were analyzed with the WMOSS software package (also SEE Co., Edina, MN). Chemical shifts were calibrated relative to Fe metal at 298 K.

Cyclic voltammograms were recorded on a BAS-100A electrochemical analyzer. All experiments were performed under an Ar blanket in the specified solution containing a 0.1 M [t-Bu_4N][BF_4] analyte at room temperature, a 3.0 mm glassy carbon working electrode, a $Ag/AgNO_3$ reference electrode, and a Pt coil counter electrode. All values have been internally referenced to Cp_2Fe/Cp_2Fe^+.

Magnetism measurements were obtained with the use of a Quantum Design SQUID magnetometer MPMS-XL equipped with a 7 T magnet. For paramagnetic substances' magnetic susceptibility measurements, the Evans' method was followed, using a Mercury 300 MHz NMR spectrometer and either d-DMSO/DMSO or CD_2Cl_2/CH_2Cl_2 solvent. Calculations were done on an Excel spreadsheet programmed with the Evans' method equation to determine χ.[55-57]

X-ray Crystallography. All samples were run at the X-ray Diffraction Laboratory in the Department of Chemistry at Texas A&M University. Crystal samples were coated in mineral oil, affixed to a Nylon loop, and placed under streaming N_2 (110 K) in a Bruker SMART 1000 CCD or single-crystal APEXii CCD diffractometer. X-ray diffraction data were collected by covering a hemisphere of space upon combination of three sets of exposures. The structures were solved by direct methods. H atoms were placed at idealized positions and refined with fixed isotropic displacement parameters and anisotropic displacement parameters were employed for all non-hydrogen atoms. The following programs were used: for data collection and cell refinement, SMART

WNT/2000, version 5.632[58] or APEX2[59]; data reductions, SAINTPLUS, version 6.63[60]; absorption correction, SADABS[61]; structure solutions, SHELXS-97[62]; structure refinement, SHELXL-97[63]. Structure plots were generated in either X-Seed 2.0,[64] Mercury, version 2.3,[65] or PyMol version 1.4.[66]

Experimental Details for Chapter III

Materials. Reagents, including nitrosonium tetrafluoroborate, 1,3-diisopropylimidazolium tetrafluoroborate, sodium *tert*-butoxide, ferrocenium tetrafluoroborate, sodium thiophenolate, 2-isopropylimidazole, and 5,10,15,20-tetraphenyl-21*H*,23*H*-porphine cobalt(II), Co(TPP), were purchased from Sigma-Aldrich Chemical Co. and were used as received. Standard Schlenk-line techniques (N_2 atmosphere) and an Ar-filled glove box were used to maintain anaerobic conditions during preparation, isolation, and product storage. $Fe(CO)_2(NO)_2$,[67] [Na-18-crown-6-ether][$Fe(CO)_3(NO)$],[68] and 1,3-dimethylimidazolium iodide[69] were prepared according to published procedures.

Preparation of Compounds

(NHC-iPr)(CO)Fe(NO)$_2$, Complex 1. In a 100 mL Schlenk flask, 1.00 g (2.20 mmol) [Na-18-crown-6-ether][$Fe(CO)_3(NO)$] and 0.26 g (2.23 mmol) $[NO]BF_4$ were dissolved in 15 mL THF and stirred for at least 10 min to produce $Fe(CO)_2(NO)_2$, which was vacuum transferred to a flask immersed in liquid N_2. A separate flask loaded with 0.52 g (2.18 mmol) of 1,3-diisopropylimidazolium tetrafluoroborate and 0.21 g (2.21 mmol) NaO^tBu was dissolved in 5 mL THF and stirred for at least 30 min. This pale

yellow solution was transferred via cannula to the flask of $Fe(CO)_2(NO)_2$ in THF and the mixture was stirred for at least an hour resulting in a brown opaque mixture. Solvent was removed in vacuo, a minimum amount of THF was added (~2 mL), followed by 30-40 mL hexanes. This mixture was filtered through Celite, the filtrate was dried in vacuo, and then dissolved in a minimum amount of pentane. The pentane solution was transferred via a "football" cannula (5.5 cm filter paper folded around and affixed to one end of the cannula with Teflon tape) to several stoppered and degassed test tubes, which were stored at 0 °C. Within several days, X-ray quality red-brown crystals were obtained. Isolation of the crystals afforded 0.24 g (37% yield) of product that is soluble in THF, CH_2Cl_2, hexane, pentane, and ether. $FeC_{10}H_{16}N_4O_3$ (MW = 296 g/mol) $^+$ESI-MS: *m/z* = 309 [M-CO+CH_3CN]; 268 [M-CO]; 238 [M-CO-NO]. IR (THF): ν(CO) 1986 (m), ν(NO) 1738 (m), 1696(s) cm^{-1}. Anal. Calcd. for $FeC_{10}H_{16}N_4O_3$ (found): C, 38.2 (38.7); H, 5.74 (6.31); N, 17.8 (15.1).

(NHC-Me)(CO)Fe(NO)$_2$, Complex 2. In a similar manner to that described above, $Fe(CO)_2(NO)_2$ was freshly prepared and added to a mixture of 0.49 g (2.19 mol) of 1,3-dimethylimidazolium iodide and 0.21 g (2.19 mmol) of NaO^tBu in 5 mL THF to ultimately produce 0.23 g (44.3%) of a red-brown crystalline solid. The product is soluble in THF, CH_2Cl_2, hexane, pentane, and ether. X-ray quality crystals were obtained by evaporation of pentane from the product mixture at 0 °C. $FeC_6H_8N_4O_3$ (MW = 240 g/mol) $^+$ESI-MS: m/z = 287 [M-CO+CH_3CN] IR (THF): ν(CO) 1988 (m), ν(NO) 1740 (m), 1697 (s) cm^{-1}. Anal. Calcd. for $FeC_6H_8N_4O_3$ (found): C, 30.0 (29.6); H, 3.34 (3.71); N, 23.4 (21.6).

(NHC-iPr)$_2$Fe(NO)$_2$, Complex 3. A pale yellow solution of NHC-iPr (prepared from 0.19 g (0.81 mmol) of 1,3-diisopropylimidazolium tetrafluoroborate and 0.078 g (0.81 mmol) in 5 mL THF) was transferred via cannula to a flask charged with 0.24 g (0.80 mmol) of complex **1** in 10 mL THF. The reaction mixture was stirred overnight and then dried in vacuo. Forty mL of hexanes were added, the mixture was stirred for 10 min, and the supernatant was separated from the precipitate via a "football" cannula. The precipitate was dissolved in THF and filtered through Celite. The solution was concentrated in vacuo, transferred to several degassed test tubes, and layered with hexanes to produce X-ray quality green-brown crystals at 0 °C. Isolation of the crystals afforded 0.13 g (38.0%) of analytically pure product that is soluble in THF and CH_2Cl_2. $FeC_{18}H_{32}N_6O_2$ (MW = 419 g/mol) $^+$ESI-MS: *m/z* = 420 $[M+H]^+$. IR (THF): ν(NO) 1664 (m), 1619 (s) cm^{-1}. Anal. Calcd. for $FeC_{18}H_{32}N_6O_2$ (found): C, 49.3 (49.3); H, 7.77 (7.62); N, 19.2 (18.5).

(NHC-Me)$_2$Fe(NO)$_2$, Complex 4. In a similar manner to that described above, a mixture of 0.14 g (0.60 mmol) of 1,3-dimethylimidazolium iodide and 0.058 g (0.60 mmol) of NaO^tBu dissolved in 5 mL THF was added to a flask charged with 0.14 g (0.60 mmol) of complex **2** in 10 mL THF ultimately producing 0.034 g (18.3%) of a brown crystalline solid. The product is soluble in THF and CH_2Cl_2. A THF solution of **4** was layered with hexanes at 0 °C to obtain X-ray quality crystals. $FeC_{10}H_{16}N_6O_2$ (FW = 307 g/mol) $^+$ESI-MS: *m/z* = 308 $[M+H]^+$; 278 [M-NO]. IR (THF): ν(NO) 1667 (m), 1624 (s) cm^{-1}. Anal. Calcd. for $FeC_{10}H_{16}N_6O_2$ (found): C, 39.0 (37.6); H, 5.20 (5.12); N, 27.3 (25.5).

[(NHC-iPr)Fe(NO)$_3$][BF$_4$], Complex 5$^+$. A 0.056 g (0.19 mmol) sample of complex **1** was dissolved in 10 mL THF and transferred via cannula to a Schlenk flask containing 0.024 g (0.21 mmol) [NO]BF$_4$. The mixture was stirred for 1 h resulting in a green precipitate, which was filtered anaerobically and washed with THF and ether to afford 0.026 g (35.7%) of a green powder. The product is soluble in CH_2Cl_2. X-ray quality crystals were obtained by layering a CH_2Cl_2 solution of the product with hexanes at 0 °C. IR (CH_2Cl_2): ν(NO) 1915 (m), 1826 (sh), 1810 (s) cm^{-1}. Anal. Calcd. for $FeC_9H_{16}N_5O_3BF_4$ (found): C, 28.1 (28.6); H, 4.16 (4.12); N, 18.2 (17.8).

[(NHC-Me)Fe(NO)$_3$][BF$_4$], Complex 6$^+$. In a similar manner to that described above, 0.097 g (0.34 mmol) of complex **2** was dissolved in 10 mL THF and transferred via cannula to a flask containing 0.037 g (0.32 mmol) [NO]BF$_4$. Isolation of the precipitate afforded 0.050 g (48.1%) of a green solid. IR (CH_2Cl_2): ν(NO) 1915 (m), 1826 (sh), 1814 (s) cm^{-1}. The green powder was not stable, even under an anaerobic environment, resulting in decomposition to an insoluble tan solid and loss of ν(NO) IR bands.

[(NHC-iPr)$_2$Fe(NO)$_2$][BF$_4$], Complex 3$^+$. Method A: A 0.024 g (0.10 mmol) sample of 1,3-diisopropylimidazolium tetrafluoroborate and 0.010 g (0.10 mmol) Na^{t}OBu were dissolved in 10 mL CH_2Cl_2 and stirred for at least 30 min prior to transfer to a Schlenk flask containing 0.044 g (0.11 mmol) of complex **5** in 5 mL CH_2Cl_2. The solution was stirred for 30 min and then solvent was reduced to ~ 2 mL in vacuo. To this, about 20-30 mL of hexanes were added to precipitate out a light brown powder (0.015 g, 29.6%), soluble in THF and CH_2Cl_2.

Method B: A sample of 0.025 g (0.060 mmol) of complex **3** and 0.020 g (0.073 mmol) ferrocenium tetrafluoroborate were dissolved in 10 mL CH_2Cl_2 and stirred for 1 h. Solvent was removed in vacuo and the resulting brown residue was washed with hexanes three times to remove ferrocene. The brown solid was dried in vacuo to afford 0.012 g (39.7 %) of a light brown powder. $FeC_{18}H_{32}N_6O_2(BF_4)$ (MW = 420 g/mol) $^+$ESI-MS: *m/z* = 420 $[M]^+$; 390 [M-NO]. IR (THF): ν(NO) 1789 (m), 1733 (s) cm^{-1}. The powder slowly degrades over the course of several days at 22°, even under an anaerobic environment, resulting in decomposition to an insoluble orange-brown solid and loss of ν(NO) IR bands. In solution under N_2, complex $\mathbf{3}^+$ as the BF_4^- (as well as the PF_6^-) salt is largely stable over the course of 8 h, however within 24 h there is major decomposition.

$[(NHC\text{-}Me)_2Fe(NO)_2][BF_4]$, Complex 4^+. In a manner similar to above, 0.014 g (0.063 mmol) of 1,3-dimethylimidazolium iodide and 0.006 g (0.062 mmol) of Na^tOBu were dissolved in 5 mL CH_2Cl_2 and the mixture was stirred for 30 min. This mixture was transferred to a Schlenk flask containing 0.020 g (0.061 mmol) of complex **6** in 5 mL CH_2Cl_2 to yield a yellow-brown solution. The unstable product was detected in solution by IR (THF): ν(NO) 1791 (m), 1723 (s) cm^{-1} and mass spectrometry: $FeC_{10}H_{16}N_6O_2(BF_4)$ (MW = 308 g/mol) $^+$ESI-MS: *m/z* = 308 $[M]^+$. Over the course of an hour, the color of solution bleached, ν(NO) IR bands disappearred, and an insoluble orange-brown precipitate formed.

$(NHC\text{-}iPr)(SPh)Fe(NO)_2$, Complex 7. Method A: A 0.027 g (0.13 mmol) sample of 1,3-diisopropylimidazolium tetrafluoroborate and 0.011 g (0.11 mmol) NaO^tBu were dissolved in 10 mL of THF and stirred for 30 min prior to transfer to a

Schlenk flask containing 0.025 g (0.056 mmol) of the Roussin's red ester (μ-$SPh)_2[Fe(NO)_2]_2$[70] in 5 mL of THF. The solution was stirred for 30 min and then the solvent was removed in vacuo. The resulting dark purple-red residue was dissolved in a minimum amount of pentane (~ 10 mL) and portioned out to 3 degassed and stoppered test tubes. This process was repeated several times until the entire product was dissolved in pentane and transferred to test tubes. The test tubes were put in the freezer at 0°C overnight to afford 0.030 g (71.4 %) of dark red crystalline material. X-ray quality crystals were obtained via slow evaporation from ether solution at 0 °C. $FeC_{15}H_{21}N_4O_2S$ (MW = 377 g/mol) $^+$ESI-MS: *m/z* = 378 $[M+H]^+$. IR (THF): ν(NO) 1757 (m), 1712 (s) cm^{-1}. Anal. Calcd. for $FeC_{15}H_{21}N_4O_2S$ (found): C, 47.8 (47.9); H, 5.57 (5.68); N, 14.9 (14.7).

Method B: A 0.036 g (0.094 mmol) sample of complex $\mathbf{5}^+$ was dissolved in 10 mL CH_2Cl_2, transferred to a Schlenk flask loaded with 0.022 g (0.17 mmol) of NaSPh. The mixture was stirred for 30 min resulting in a red solution. Solvent was removed in vacuo and the mixture was redissolved in 20 mL CH_2Cl_2, and filtered through Celite. Removal of solvent resulted in 0.021 g (74.7%) of a dark red solid. Product from this route and that of Method A above had identical properties. Method A is however preferred for simplicity.

(Imid-iPr)(CO)Fe(NO)$_2$, Complex 8. Fresh $Fe(CO)_2(NO)_2$ in 10 mL THF was prepared following the procedure above using 0.50 g (1.10 mmol) of [Na-18-crown-6-ether][$Fe(CO)_3(NO)$] and 0.13 g (1.11 mmol) of $[NO]BF_4$. A 0.12 g (1.1 mmol) sample of 2-isopropylimidazole (Imid-iPr) in 10 mL THF was added via cannula and stirred for

1 h. The IR spectrum taken on this solution indicated formation of product, but conversion to a tetramer (see below) occurred upon attempts to isolate product. IR (THF): ν(CO) 1992 (s), ν(NO) 1744 (m), 1698 (s) cm^{-1}.

[(Imid-iPr)Fe(NO)$_2$]$_4$, Complex 9. Attempts to form and isolate (Imid-iPr)$_2$Fe(NO)$_2$ with addition of one equivalent of Imid-iPr to complex **8** were unsuccessful and resulted in isolation of a tetramer. The optimized procedure for complex **9** follows: Fresh Fe(CO)$_2$(NO)$_2$ in CH_2Cl_2 was prepared following the procedure above using 0.75 g (1.64 mmol) of [Na-18-crown-6-ether][Fe(CO)$_3$(NO)] and 0.20 g (1.71 mmol) of [NO]BF_4. A 0.36 g (3.3 mmol) portion of Imid-iPr in 15 mL CH_2Cl_2 was added via cannula and the mixture was stirred overnight. [Note: Shorter reaction times could be achieved on deliberate addition of oxygen to the reaction vessel, however excess oxygen degrades product. Hence, best results were obtained as described with adventitious oxygen presumably serving as oxidant.] Solvent was removed in vacuo from the green-brown solution, 30-40 mL hexanes were added, and the solution was filtered through Celite. Solvent was removed in vacuo to afford 0.072 g (19.5%) of the red-brown solid product, soluble in THF, CH_2Cl_2 and partially soluble in hexanes and ether. X-ray quality crystals were grown via evaporation of solvent from an ether solution in septa-stoppered test tubes at 0 °C. IR (THF): ν(NO) 1794 (m), 1726 (s) cm^{-1}. Mass spectrometry (Nano-(+)-ESI MS): Low intensity parent ion ($Fe_4N_{16}O_8C_{24}H_{36}$) isotope bundle centered at m/z = 900; base (100%) peak centered at 538 ($Fe_3N_9O_5C_{12}H_{18}$, representing Fe$_3$(NO)$_5$(Imid-iPr)$_2$); other intense bundles centered at m/z 478.8 representing loss of 2 NO from the base peak, and at 647.9 representing

addition of one iPr-imidazole (+110 mass units) to the base peak. A portion of the yielded product (~ 20 mg) was redissolved in ~ 1 mL THF and ~ 5 mL of hexanes, filtered through Celite, and dried in vacuo. The resulting red-brown solid was washed with ether (not soluble in ether) and dried in vacuo. The polycrystalline solid was loaded into the glovebox, scraped into a vial, and sent for elemental analysis. The elemental analysis data resulted in C, H, and N percentages much higher than expected. The cause for this discrepancy is unclear but is discussed in Chapter IV.

Complex **9** reacted with [Na-18-crown-6-ether]$^{+}$ imidazolate-iPr^{-} (formed by deprotonation of Imid-iPr in THF solvent by Na^0 in the presence of 18-crown-6-ether) to yield a compound of IR and EPR parameters similar to that of [Na-18-crown-6-ether][$(Imid)_2Fe(NO)_2$].[36]

NO Trapping Experiments: Yellow-brown complex **3**$^{+}$ was formed in situ according to the procedure described above and transferred via cannula to a Schlenk flask containing Co(TPP) (0.013 g, 0.019 mmol in 10 mL THF, Co(TPP) = 5,10,15,20-Tetraphenyl-21*H*,23*H*-porphine cobalt(II)). Within minutes an absorption band at 1683 cm^{-1} assignable to (NO)CoTPP appeared and continued to grow in over the course of 6 h, along with a distinct color change of the solution from dark brown red to red. The reaction mixture was monitored by IR spectroscopy for 24 h. A decrease of complex **3**$^{+}$ IR bands at 1789 and 1733 cm^{-1} and an increase of the band at 1683 cm^{-1} was taken as indication of NO transfer.[50] The same procedure was performed for complex **3** (0.010 g, 0.024 mmol) with Co(TPP) (0.016 g 0.024 mmol); however, the IR bands associated

with complex **3** did not decrease and the band at 1683 cm^{-1} characteristic of (NO)Co(TPP) was not observed.

Experimental Details for Chapter IV

Materials. Reagents, including nitrosonium tetrafluoroborate and benzimidazole were purchased from Sigma-Aldrich Chemical Co. and were used as received. $Fe(CO)_2(NO)_2$[67] and [Na-18-crown-6-ether][$Fe(CO)_3(NO)$][68] were prepared according to published procedures. [(Imid)$Fe(NO)_2]_4$, complex **1**, was synthesized as reported by Li, *et al.*[71] [(Imid-iPr)$Fe(NO)_2]_4$, complex **2**, was synthesized as described in the experimental details for Chapter III.

[(Imid-benz)$Fe(NO)_2]_4$, Complex 3. Fresh $Fe(CO)_2(NO)_2$ in CH_2Cl_2 was prepared following the procedure described in the experimental details for Chapter III using 0.75 g (1.64 mmol) of [Na-18-crown-6-ether][$Fe(CO)_3(NO)$] and 0.20 g (1.71 mmol) of $[NO]BF_4$ in 15 mL CH_2Cl_2. To this was added a solution of 0.39 g (3.3 mmol) benzimidazole, Imid-benz, in 15 mL THF, via cannula. Following overnight stirring at 22°, solvent was removed in vacuo from the brown solution, and 30 mL of CH_2Cl_2 was added to dissolve the red-brown residue, leaving behind the excess benzimidazole. Following filtration of the extract through Celite, solvent was removed in vacuo to afford 0.235 g (68 %) of a red-brown solid, soluble in THF and CH_2Cl_2. X-ray quality crystals formed from slow diffusion of pentane into a CH_2Cl_2 solution of product at 0°C. ν(NO) IR (THF): 1801 (m), 1736 (s) cm^{-1}. Mass spectrometry: (Nano-(+)-ESI MS) : The parent ion ($Fe_4C_{28}H_{20}N_{16}O_8$, m/z = 931) isotope bundle was not observed in the

mass spectrum. Base (100%) peak was centered at m/z 538 ($Fe_3C_{14}H_{10}N_8O_5$, representing $Fe_3(NO)_4O(Imid\text{-}benz)_2$) with other intense bundles centered at m/z 478.9 representing loss of 2 NO from the base peak, and at m/z 655.9 representing addition of one benzimidazole (+118 mass units) to the base peak. A portion of the yielded product (~ 20 mg) was redissolved in ~ 5 mL of CH_2Cl_2 and filtered through Celite and dried in vacuo. The resulting red-brown solid was washed with ether (not soluble in ether) and dried in vacuo. The polycrystalline solid was loaded into the glovebox, scraped into a vial, and sent for elemental analysis. The elemental analysis data resulted in C, H, and N percentages much higher than expected. The cause for this discrepancy is unclear but is discussed in Chapter IV.

Experimental Details for Chapter V

Materials. The $(piperidine)_2W(CO)_4$ complex was prepared according to published procedures.[72]

Preparation of Compounds

(*N*,*N*′-Bis(2-mercaptoethyl)-1,4-diazacycloheptane)nitrosylcobalt, (bme-dach)Co(NO) or Co-1′(NO). In a 100 mL Schlenk flask, 0.352 g (0.634 mmol) of $[Co(bme\text{-}dach)]_2$ (synthesized according to published procedures[73,74]) was dissolved in 75 mL of methanol. The solution was heated to 60 °C, at which time the N_2 atmosphere was replaced with NO gas (1 atm) resulting in a color change of the solution from dark green to a dark purple-black. The solvent was removed in vacuo. The resulting solid was dissolved in CH_2Cl_2 and filtered through Celite. Pentane was added to the filtrate,

1:1 by volume, and the mixture was stirred overnight. The mixture was anaerobically filtered to afford 0.224 g (57.5%) of a dark-purple solid, soluble in CH_2Cl_2 and DMF. X-ray quality crystals of (bme-dach)Co(NO) were obtained by slow diffusion of ether into a CH_2Cl_2 solution of the product at 10 °C. UV–vis spectrum in CH_2Cl_2 [λ_{max} (ε, M^{-1} cm^{-1})]: 268 (8460), 298 (5990), 364 (1740), 635 (341), 657 (250). IR (CH_2Cl_2): ν(NO) 1604 (m) cm^{-1}. Anal. Calcd for $CoC_9H_{18}N_3OS_2$ (found): C, 35.15 (35.17); H, 5.86 (5.39); N, 13.67 (13.49).

(*N*,*N*′-Bis(2-mercaptoethyl)-1,4-diazacycloheptane)nitrosyliron, (bme-dach)Fe(NO) or Fe-1′(NO). This was prepared as previously reported.[73] Additional characterization of this complex was by electronic absorption spectroscopy. UV–vis spectrum in CH_2Cl_2 [λ_{max} (ε, M^{-1} cm^{-1})]: 242 (13 830), 293 (4990), 333 (4530), 345 (4540), 632 (192), 646 (532). The ν(NO) IR (CH_2Cl_2) = 1649 cm^{-1}.

[(bme-dach)M(NO)]W(CO)$_4$ Complexes: [(*N*,*N*′-Bis(2-mercaptoethyl)-1,4-diazacycloheptane)nitrosylcobalt]tungsten Tetracarbonyl, [(bme-dach)Co(NO)]W(CO)$_4$, or [Co-1′(NO)]W(CO)$_4$. In a 100 mL Schlenk flask, 0.118 g (0.25 mmol) of $(pip)_2W(CO)_4$[72] and 0.0762 g (0.25 mmol) of (bme-dach)Co(NO) were dissolved in 40.0 mL of CH_2Cl_2. The mixture was stirred at 40 °C for 10–15 min. The flask was cooled to room temperature, and the addition of 60 mL of hexanes led to a precipitate that formed over the course of a few hours. The resulting mixture was anaerobically filtered, and the solid was dried in vacuo to produce 0.112 g (75%) of a brown solid, soluble in DMF and partially soluble in CH_2Cl_2. A CH_2Cl_2 solution of [Co-1′(NO)]W(CO)$_4$ was layered with ether to obtain X-ray-quality crystals. UV–vis

spectrum in DMF [λ_{max} (ε, M^{-1} cm^{-1})]: 295 (22 420), 346 (4780), 379 (4590), 600 (696), 629 (107), 636 (56), 655 (787). IR (CH_2Cl_2): ν(NO) 1638 (m) cm^{-1}. IR (DMF): ν(CO) 1997 (m), 1878 (s), 1851 (s), 1824 (s) cm^{-1}. Anal. Calcd for $CoC_{13}H_{18}N_3O_5S_2W$ (found): C, 24.4 (25.9); H, 3.04 (2.98); N, 6.83 (6.96).

[(*N*,*N*′-Bis(2-mercaptoethyl)-1,4-diazacycloheptane)nitrosyliron]tungsten Tetracarbonyl], [(bme-dach)Fe(NO)]W(CO)$_4$ or [Fe-1′(NO)]W(CO)$_4$. In a manner similar to that described above, 0.166 g (0.350 mmol) of $(pip)_2W(CO)_4$ was mixed with 0.104 g (0.342 mmol) of (bme-dach)Fe(NO), Fe-1′(NO), ultimately producing 0.165 g (80.5%) of a dark-green solid, soluble in DMF and partially soluble in CH_2Cl_2. A CH_2Cl_2 solution of [Fe-1′(NO)]W(CO)$_4$ was layered with ether to obtain X-ray-quality crystals. UV–vis spectrum in DMF [λ_{max} (ε, M^{-1} cm^{-1})]: 268 (14 510), 362 (2360), 376 (1830), 446 (1320), 486 (1185), 626 (704), 659 (557). IR (CH_2Cl_2): ν(NO) 1697 (m) cm^{-1}. IR (DMF): ν(CO) 1998 (m), 1880 (s), 1854 (s), 1827 (s) cm^{-1}. Anal. Calcd $FeC_{13}H_{18}N_3O_5S_2W$ (found): C, 25.8 (26.0); H, 2.86 (3.00); N, 6.49 (7.00).

Preparation of {[Fe-1'(NO)]$_3$Ag$_2$}[BF$_4$]$_2$. The complete synthetic and isolation procedures of the compound were performed under an N_2 atmosphere. A 30 mg (0.099 mmol) portion of **Fe-1'**(NO)[73] was dissolved in 20 mL of CH_2Cl_2. A suspension of $AgBF_4$ (13 mg, 0.069 mmol, in 15 mL of CH_2Cl_2) was heated to 45°C and the dark green **Fe-1'**(NO) solution was transferred via cannula to the $AgBF_4$ suspension. With continued heating at 45°C and stirring for 15-20 min, a lighter green precipitate formed. The mixture was removed from the heat and further stirred for 1-2 h, after which solvent was removed *in vacuo*. The residual green solid was dissolved in a minimal amount of

CH_3CN and 50-70 mL of diethylether was added to the solution. The mixture was stirred for 1-2 h, followed by anaerobic filtration and drying in vacuo to produce 0.040 g (93.5 %) of a green solid that was soluble in CH_3CN and DMF. X-ray quality crystals were grown by vapor diffusion of diethylether into an CH_3CN solution of the product. UV-vis spectrum in DMF [λ_{max}, (ε, M^{-1} cm^{-1})]: 267(30,010) 299(22,915) 348(8635), 486(1003), 626(807), 634(799). ν(NO) IR (CH_3CN): 1690 (m) cm^{-1}. $^{+}$ESI-MS (CH_3CN solution) *m/z* (% abundance): 564 (100 %) {[**Fe-1'**$(NO)]_3Ag_2\}^{2+}$, 549 (61 %) {[**Fe-1'**$(NO)]_2$[**Fe-1'**$]Ag_2\}^{2+}$, 534 (28 %) {[**Fe-1'**(NO)][**Fe-1'**$]_2Ag_2\}^{2+}$, 519 (21 %) {[**Fe-1'**$]_3Ag_2\}^{2+}$, 717 (2 %) {[**Fe-1'**$(NO)]_2Ag\}^{+}$. Anal. Calcd (found), ({[**Fe-1'**$(NO)]_3Ag_2\}[BF_4]_2\cdot CH_2Cl_2$): C, 24.3 (24.0); H, 4.07 (4.20); N, 9.09 (8.51).

CHAPTER III

N-HETEROCYCLIC CARBENE LIGANDS AS MIMICS OF IMIDAZOLES/HISTIDINE FOR THE STABILIZATION OF DI- AND TRI-NITROSYL IRON COMPLEXES[†]

Introduction

The N-heterocyclic carbene (NHC) ligands have gained widespread use in organometallic chemistry for their strong σ-donating characteristics and ability to bind to and stabilize a range of transition metal complexes.[75,76] An example appropriate to Fe-NO chemistry is the observation of a trinitrosyl iron complex (TNIC) ligated by 1,3-bis(2,4,6-trimethylphenyl)imidazol-2-ylidene (NHC-Mes) that can be readily isolated and manipulated in solution under ambient conditions; the analogous $(R_3P)Fe(NO)_3^+$ (R = *p*-tolyl) immediately decomposes in solution at room temperature (22 °C).[77]

The planar NHC ligands mimic ligands such as imidazoles and pyridine; steric and electronic properties of the NHCs are largely influenced by the substituents on the N-atoms of the NHC ring. A structural comparison of three imidazoles with the dimethyl NHC complexed to square planar $Ni(N_2S)$, Ni(mmp-dach) (mmp-dach = 1-(2-mercapto-2-methyl-propyl-1,4-diazacycloheptane), found in all cases the plane of the ligands to be perpendicular to the NiN_2S plane with no significant differences in the Ni-

[†]Reproduced in part with permission from Hess, J. L.; Hsieh, C.-H.; Reibenspies, J. H.; Darensbourg, M. Y. *Inorg. Chem.* **2011**, ASAP. Copyright **2011** American Chemical Society.

N_{Imid} and Ni-C_{NHC} distances (1.89 Å- 1.90 Å), as well as the Ni-N or Ni-S spectator ligand distances, Figure III-1.[78] The barrier to rotation about the Ni-N bond of the imidazoles was experimentally determined by VT ^{1}H NMR studies, finding that for non-sterically hindered methylimidazole $\Delta G^{\ddagger} = 8.97$ kcal/mol, a value that was corroborated by DFT calculations. In contrast, the NHC derivative was sterically prohibited from such intramolecular dynamics over the accessible temperature range.[78]

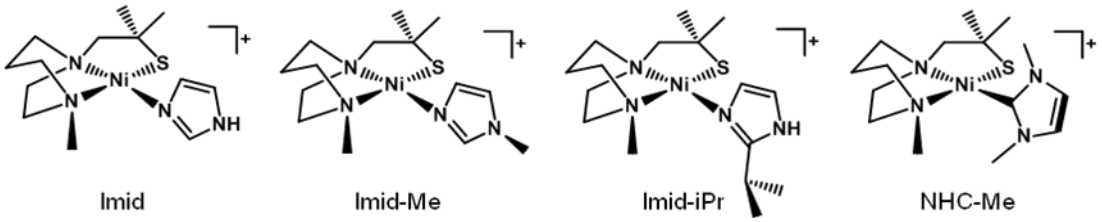

Figure III-1. Structures of $[LNi(N_2S)]^+$ complexes where plane of L is perpendicular to NiN_2S plane. L = Imid (imidazole), Imid-Me (1-methylimidazole), Imid-iPr (2-isopropylimidazole), and NHC-Me (dimethyl N-heterocyclic carbene).[78]

Crabtree and Eisenstein have described DFT computational results relating to the possibility of tautomerization from the N-bound to C-bound form of histidine in several metal derivatives of imidazoles, eq III-1. They concluded that N-binding is more favorable for first-row elements, while C-binding is preferred by second and third-row elements. Additionally, C- versus N-binding could be influenced by an imposed hydrogen bonding network around the histidine.[79] It should also be noted that the general preparation of NHCs involves the facile alkylation of imidazoles, eq III-2.[69] Relevant to this discussion, Erker, *et al.* reported the conversion of *L*-histidine in the

presence of excess *n*-propyl bromide or *iso*-propyl iodide to form the corresponding histidinium salt. Treatment of the histidinium salts with Ag^{I}, Pd^{II}, or Rh^{I} sources resulted in the formation of the respective transition metal NHC complex.[80] Such interconversions between imidazole and NHC are intriguing possibilities for biological systems, as yet undiscovered.

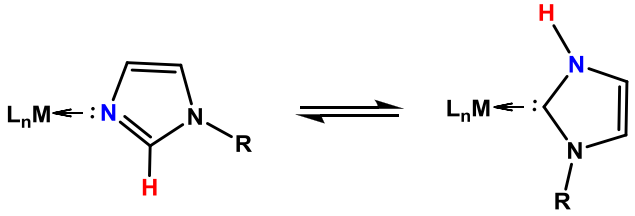

(eq III-1)

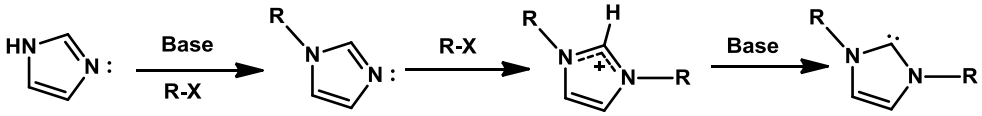

(eq III-2)

To further explore the analogy described above, as well as to develop the synthetic chemistry relating to $Fe(NO)_2$ as NO releasing agents, we present a series herein of DNICs containing NHCs and imidazoles in both the reduced $\{Fe(NO)_2\}^{10}$ and oxidized $\{Fe(NO)_2\}^{9}$ forms as mimics of histidine-containing DNICs.

Synthesis, Isolation, and Physical Properties

Synthetic access to reduced $\{Fe(NO)_2\}^{10}$ DNICs relies on the freshly prepared $Fe(CO)_2(NO)_2$ precursor, with CO/L exchange readily occurring for both L = N-heterocyclic carbenes (NHC) and imidazoles. As noted in **Scheme III-1**, on addition of

one equiv. of NHC, the mono-NHC complexes **1** and **2** were obtained, and with two equiv. of NHC, disubstituted complexes **3** and **4** were formed. Complex **8** was observed on reaction of the $Fe(CO)_2(NO)_2$ precursor with one equiv. of imidazole; however; excesses of imidazole led to the formation of a reddish brown tetrameric $\{Fe(NO)_2\}^9$ species, complex **9**. This product, presumed to require adventitious oxygen for oxidation, could be obtained in greater yield in the presence of excess imidazole. Its structure is further described in Chapter IV.

Scheme III-1. Reactions of NHC and imidazole with $\{Fe(NO)_2\}^{10}$ precursor

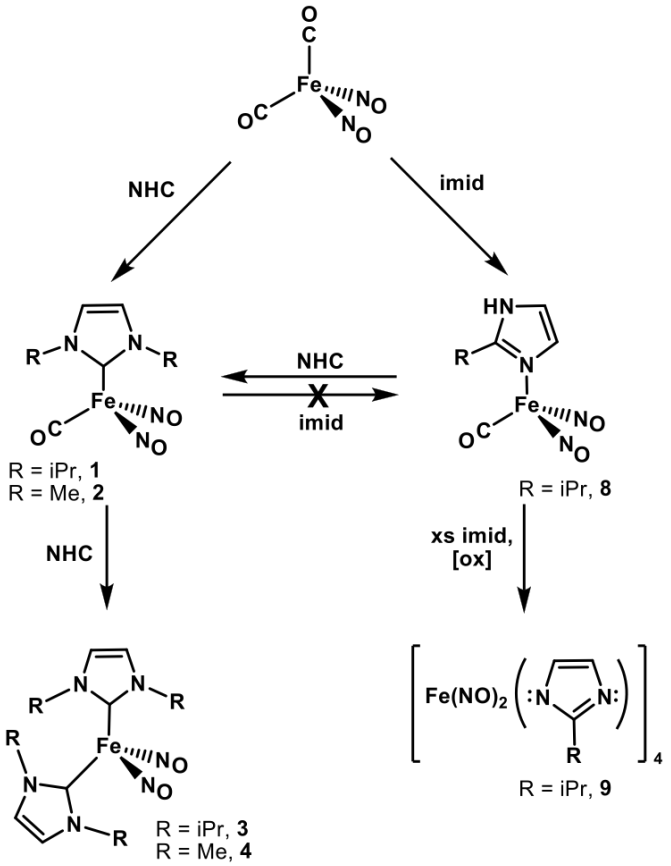

The NHC products **1-4** were isolated as air sensitive, but thermally stable, crystalline solids, and subjected to x-ray diffraction analysis, *vide infra*. Exposure of the $\{Fe(NO)_2\}^{10}$ NHC complexes **1-4** to air either as solids or in solution led to eventual degradation under ambient conditions. The air sensitivity in solution was found to be dependent on the NHC substituent, requiring ca. 24 h for degradation of the NHC-iPr DNICs **1** and **3**; within 1 h the NHC-Me complexes **2** and **4** are oxidized and degraded.

Nevertheless, intermediates in the oxidation process, especially of complexes **3** and **4**, can be observed. Reaction of complexes **3** and **4** with O_2 or NO^+ as oxidant leads to a color change from brown to yellow-brown, with ν(NO) band shifts to higher wavenumbers consistent with the formation of the $\mathbf{3}^+$ and $\mathbf{4}^+$ $\{Fe(NO)_2\}^9$ products, **Scheme III-2**. In contrast, addition of NO^+ to complexes **1** and **2** resulted in CO/NO^+ ligand exchange and formation of the green trinitrosyl complexes $\mathbf{5}^+$ and $\mathbf{6}^+$**,** respectively. Treatment of TNICs $\mathbf{5}^+$ and $\mathbf{6}^+$ with the appropriate NHC, proceeding with release of NO radicals (identified by capture of NO in a separate solution containing an NO trapping reagent, i.e., a double tube arrangement as described in ref. 77) resulted in the formation of complexes $\mathbf{3}^+$ and $\mathbf{4}^+$, respectively with the same color and ν(NO) bands as observed with direct oxidation of complexes **3** and **4**. This latter approach to $\mathbf{5}^+$ and $\mathbf{6}^+$ to the DNICs $\mathbf{3}^+$ and $\mathbf{4}^+$ appears to give cleaner compounds. Due to instability, as evidenced by bleaching of color and loss of ν(NO) IR bands, the cationic complexes $\mathbf{3}^+$ and $\mathbf{4}^+$ could not be isolated as pure and crystalline materials, however mass spectral results are consistent with the formulations given.

Scheme III-2. Synthetic routes to oxidized bis-NHC DNICs.

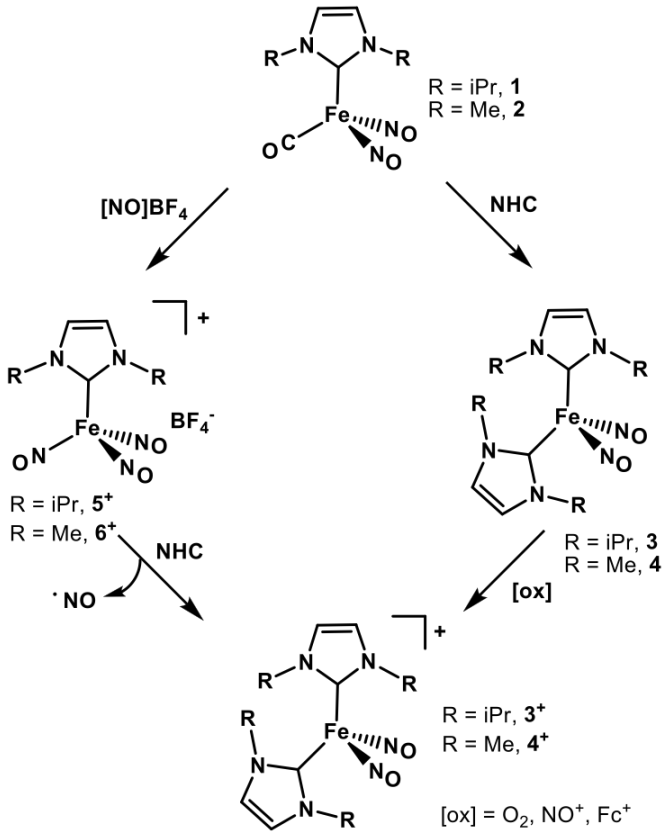

A common precursor to neutral $\{Fe(NO)_2\}^9$ DNICs is the Roussin's Red "ester", RRE $(\mu\text{-SPh})_2[Fe(NO)_2]_2$, **Scheme III-3**.[70] Cleavage of this dimeric complex by NHCs or imidazoles leads to analogous DNICs containing one NHC or imidazole and one SPh^- (complexes **7** and **10**). Complete conversion of the RRE dimer required excess (> 14 equiv.) imidazole, whereas only 2 equiv. of NHC were needed for complete conversion of the dimer to (NHC-iPr)(PhS)$Fe(NO)_2$ (**7),** which was isolated and structurally

characterized by X-ray diffraction. Complex **7** can also be formed by addition of NHC-iPr to complex $\mathbf{5}^{+}$ resulting in release of NO.[77] Subsequent reaction of complex **7**, with additional NHC-iPr resulted in bimolecular reductive elimination of PhSSPh, with formation of the reduced $\{Fe(NO)_2\}^{10}$ complex **3**. The imidazole complex **10** is unreactive with excess imidazole.

Scheme III-3. Comparison of NHC and imidazole reacting with $\{Fe(NO)_2\}^{9}$ precursor.

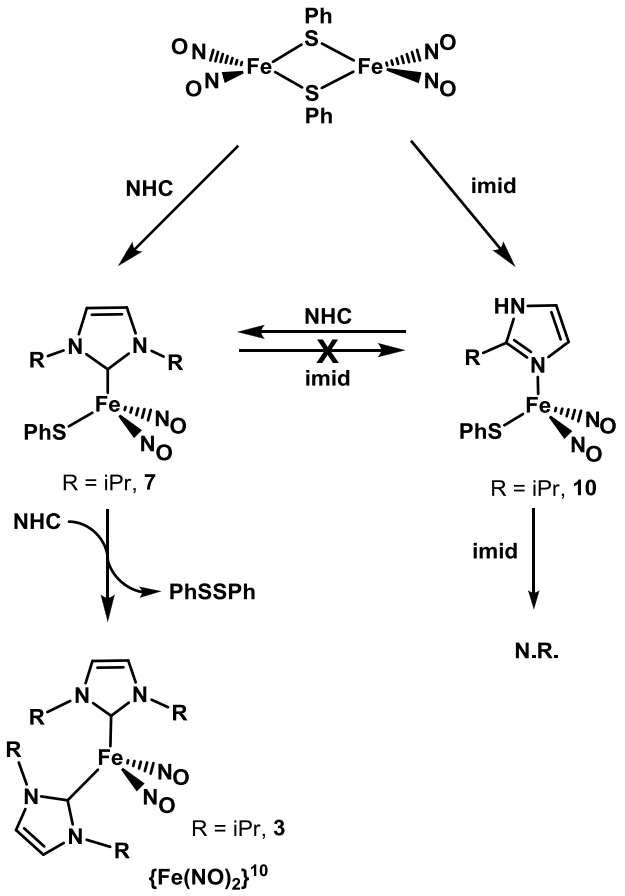

Molecular Structures

The molecular structures of complexes **1**, **2**, **3**, **4**, $\mathbf{5}^{+}$, and **7** were determined by X-ray diffraction analysis and are represented in ball and stick form in Figures III-2, III-3, and III-4. Selected metric data for these complexes are presented in Table III-1. The monomeric DNIC complexes are pseudo-tetrahedral, with average C_{NHC}-Fe-N_{NO} bond angles in the range of 107-109°. The N_{NO}-Fe-N_{NO} angles in complexes **3** and **4** are 119° and 122°, and the C_{NHC}-Fe-C_{NHC} bond angles of complexes **3** and **4** are 90° and 96°, respectively.

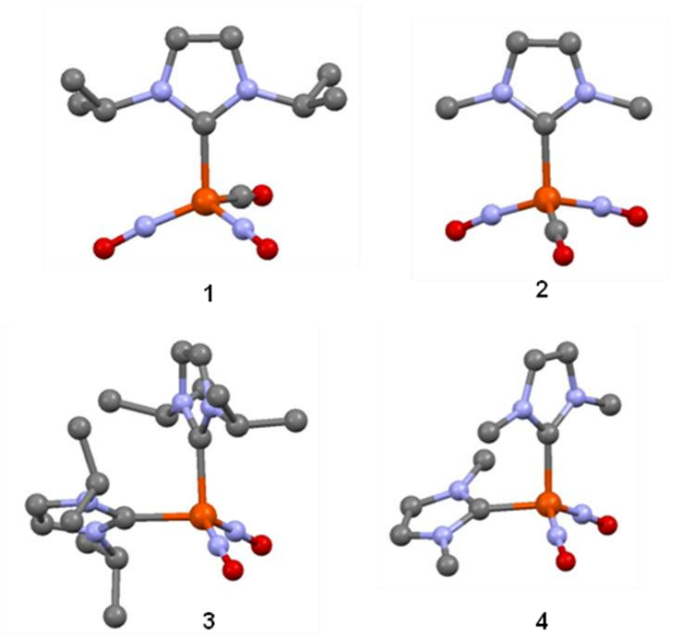

Figure III-2. As derived from X-ray diffraction analysis, ball and stick structures of the $\{Fe(NO)_2\}^{10}$ complexes: **1** = (NHC-iPr)(CO)Fe$(NO)_2$; **2** = (NHC-Me)(CO)Fe$(NO)_2$; **3** = (NHC-iPr)$_2$Fe$(NO)_2$; **4** = (NHC-Me)$_2$Fe$(NO)_2$. Hydrogen atoms have been removed for clarity. Selected metric data are in Table III-1.

This distortion from standard tetrahedral angles is similar to other neutral $L_2Fe(NO)_2$ complexes of $\{Fe(NO)_2\}^{10}$ composition including Wang, *et al.*'s $(Imid\text{-}Me)_2Fe(NO)_2$ complex, in which the $\angle N_{imid}\text{-}Fe\text{-}N_{imid}$ is 91.2°.[35] The Fe-N-O bond angles are substantially linear for the $\{Fe(NO)_2\}^{10}$ complexes with an average of 174°. The bis-imidazole complex $(Imid\text{-}Me)_2Fe(NO)_2$ has somewhat bent Fe-N-O angles of 168°. Likewise for complex **7**, Figure III-3, an $\{Fe(NO)_2\}^9$ complex, the ∠Fe-N-O averages to 167°, with the N-O ligands oriented inwards towards each other as was observed for the $\{Fe(NO)_2\}^9$ complex, $(NHC\text{-}Mes)(SPh)Fe(NO)_2$.[77] All in all, the $L_2Fe(NO)_2$ complex structures are similar to each other and to structures of $LXFe(NO)_2$ complexes, even when the spectator ligands are within bidentate frameworks.[46,47]

The $\{Fe(NO)_3\}^{10}$ complex $\mathbf{5}^+$ is an uncommon, trinitrosyliron complex, TNIC, stabilized by the NHC-iPr (Figure III-3a). The $(NHC\text{-}Mes)Fe(NO)_3^+$ complex is a precise analogue of $\mathbf{5}^+$.[77] An overlay of the molecular structures of TNIC $\mathbf{5}^+$ and $(NHC\text{-}Mes)Fe(NO)_3^+$ is given in Figure III-3b. The average $\angle N_{NO}\text{-}Fe\text{-}N_{NO}$ of 112.3° of the TNICs reflect a narrow range of angles; i.e., the bulk of the NHC does not influence one NO position over another. The steric bulk of the pendant N-substituents on the NHC rings undoubtedly contributes to the stability of these TNICs. In support of this conclusion, the $(NHC\text{-}Me)Fe(NO)_3^+$ cation, complex $\mathbf{6}^+$, did not lend itself to crystallization because of instability in solution. This is similar to other reported TNICs such as those derived from phosphines.[77,81]

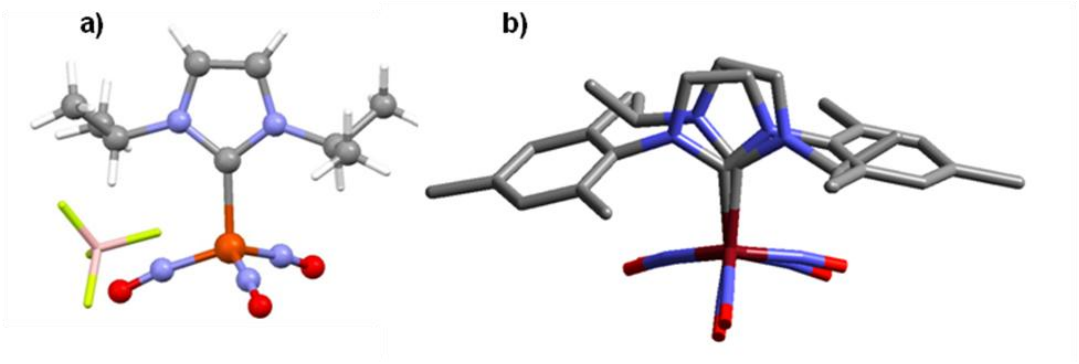

Figure III-3. a) Ball and stick structure of the trinitrosyl (NHC-iPr)$Fe(NO)_3^+$ BF_4^- salt, complex $\mathbf{5}^+$**.** b) Overlay of the (NHC-Mes)$Fe(NO)_3^+$ [77] with TNIC $\mathbf{5}^+$.

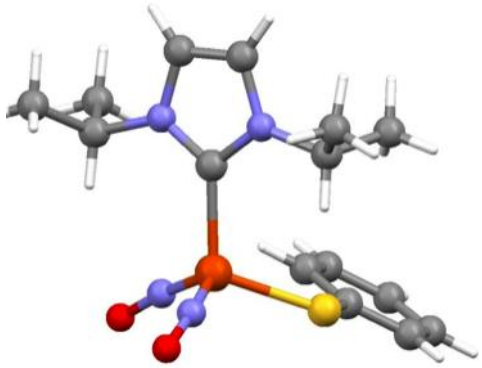

Figure III-4. The solid state molecular structure of (NHC-iPr)(PhS)$Fe(NO)_2$, complex **7** in ball and stick form.

Table III-1. Selected bond distances (Å) and angles (°) for molecular structures **1-5**$^{+}$, and **7**.

	1	**2**	**3**	**4**	**5**$^{+}$	**7**
Bond Distances (Å)						
Fe-C_{NHC}	2.005(2)	2.025(6)	2.015(3)	1.973(6)	2.004(5)	2.062(2)
Fe-NO avg	1.675(2)	1.727(6)	1.642(3)	1.659(6)	1.692(5)	1.668(3)
Fe-CO	1.784(2)	1.729(6)	--	--	--	--
Fe-S	--	--	--	--	--	2.256(11)
N-O avg	1.181(2)	1.176(7)	1.204(3)	1.202(6)	1.151(6)	1.172(3)
Bond Angles (°)						
N_{NO}-Fe-N_{NO}	119.07(10)	111.3(2)	119.48(19)	121.9(3)	112.3(3)[a]	113.80(13)
Fe-N-O avg	175.8(2)	173.3(5)	173.8(2)	174.0(5)	172.8(4)	166.8(3)
C_{NHC}-Fe-N_{NO} avg	107.9(8)	107.6(3)	109.39(11)	109.7(2)	106.5(2)	108.93(13)
C_{NHC}-Fe-C_{NHC}	--	--	89.72(17)	96.4(2)	--	--
C_{NHC}-Fe-S	--	--	--	--	--	110.79(9)
C_{NHC}-Fe- CO	99.04(9)	103.6(2)	--	--	--	--

[a]average of angles

The molecular structure of complex **9** was also determined by X-ray crystallographic analysis and is shown in Figure III-5. This tetrameric structure is similar to the unsubstituted imidazole-containing tetramer ($[(Im\text{-}H)Fe(NO)_2]_4$) reported by Wang and Li, *et al.*[71] The structures of complex 9, the $[(Im\text{-}H)Fe(NO)_2]_4$, and a benzimidazole tetramer will be examined in detail in Chapter IV.

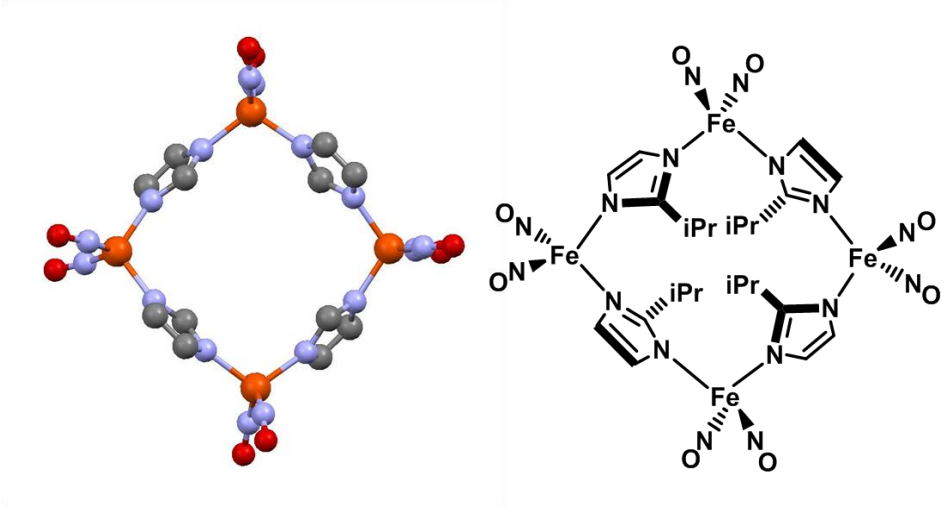

Figure III-5. *left*: From x-ray diffraction analysis, a ball and stick rendering of the molecular structure of complex **9** (isopropyl groups have been removed for clarity) and *right:* the analogous ChemDraw representations of **9**.

Infrared Spectral Data

Table III-2 lists the diatomic ligand stretching frequencies for the DNIC complexes of this study as well as other complexes selected for appropriate comparisons. Typically, DNICs of the $\{Fe(NO)_2\}^{10}$ configuration have ν(NO) stretching frequencies in the 1620-1740 cm^{-1} range, whereas those of the oxidized $\{Fe(NO)_2\}^9$ form are shifted positively into the 1700-1800 cm^{-1} regime. Cationic $\{Fe(NO)_2\}^9$ derivatives have higher ν(NO) than neutral analogues, demonstrated in this study by the differences in values for complex $\mathbf{3}^+$ and complex **7**. Notably, the difference between ν(NO) values of neutral complex **3**, of $\{Fe(NO)_2\}^{10}$ configuration, and cationic complex $\mathbf{3}^+$, is over 100 cm^{-1}, while the difference between the neutral $\{Fe(NO)_2\}^9$ complex, $(NHC\text{-}iPr)(PhS)Fe(NO)_2$, and the anionic $\{Fe(NO)_2\}^9$ complex, $(PhS)_2Fe(NO)_2^-$, is only 20 cm^{-1}.[31] This

phenomenon is consistent with the differences of ν(NO) stretching frequencies between (sparteine)$Fe(NO)_2^{0/+}$ and $(RS)_2Fe(NO)_2^-$ versus (Imid)(SR)$Fe(NO)_2$ (R = Ph-*o*-NH-CO-Ph).[31,39] As the structural differences in Fe-N-O distances and angles is minimal, the source of these major discrepancies awaits computational delineation.

Where comparisons of NHC and imidazole complexes are appropriate, both ν(NO) and ν(CO) values suggest the former is the (slightly) better donor. The better donating ability of NHC ligands as reported by ν(CO) values in NHC/CO transition metal complexes has been established. Thus in the case of the tetrahedral DNIC complexes, both steric properties and electron donor properties of the NHC ligands should make them suitable mimics of imidazole ligands.

Table III-3 lists ν(NO) infrared results for the cationic $\{Fe(NO)_3\}^{10}$ complexes with NHC and phosphine ligands. The higher stretching frequencies of these complexes speak to the replacement of CO by the isoelectronic NO^+ ligand in, for example, complexes **1** and **2** yielding a typical pattern of pseudo C_{3v} symmetry.

Table III-2. ν(NO) values for selected DNICs containing S, N, and C donors. THF solution measurements except where noted.

		LL'Fe(NO)$_2$		ν(CO) cm^{-1} (THF)	ν(NO) cm^{-1} (THF)	Ref.
	Complex	**L**	**L'**		Sym., Asym.	
Neutral {Fe(NO)$_2$}^{10}		CO	CO	2089(m), 2038(s)	1807(m), 1762(s)	67
	1	CO	NHC-iPr	1988(m)	1738(m), 1696(s)	a
	2	CO	NHC-Me	1986(m)	1740(m), 1697(s)	a
	8	CO	Imid-iPr	1992(m)	1744(m), 1698(s)	a
	3	NHC-iPr	NHC-iPr		1664(m), 1619(s)	a
	4	NHC-Me	NHC-Me		1667(m), 1624(s)	a
		Imid-Me	Imid-Me		1673(m), 1616(s)	35
		Sparteine[b]			1679(m), 1622(s)	31
Anionic {Fe(NO)$_2$}^{10}		Ar-nacnac[c]			1627(m), 1567(s)*	38
Cationic {Fe(NO)$_2$}^{9}	**3**$^+$	NHC-iPr	NHC-iPr		1791(m), 1723(s)	a
	4$^+$	NHC-Me	NHC-Me		1789(m), 1733(s)	a
		Sparteine			1808(m), 1739(s)	31
Neutral {Fe(NO)$_2$}^{9}	**7**	NHC-iPr	SPh		1757(m), 1712(s)	a
		NHC-Mes	SPh		1763(m), 1715(s)	77
	10	Imid-iPr	SPh		1767(m), 1715(s)	a
	9	Imid-iPr$^-$	Imid-iPr		1794(m), 1726(s)	a
		Ar-nacnac			1761(m), 1709(s)*	38
Anionic {Fe(NO)$_2$}^{9}		Imid-iPr$^-$	Imid-iPr$^-$		1765(m), 1699(s)	a
		Imid$^-$	Imid$^-$		1774(m), 1712(s)	36
		SPh	SPh		1737(m), 1693(s)	31

[a]This work. [b]Sparteine = (6*R*,8*S*,10*R*,12*S*)-7,15-diazatetracyclo[7.7.1.0^{2,7}.0^{10,15}]heptadecane. [c]Ar-nacnac = [(2,6-diisopropylphenyl)NC(Me)]$_2$CH, *Benzene-d$_6$ solution measurements

Table III-3. ν(NO) values for TNICs containing P, N, and C donors. CH_2Cl_2 solution measurements.

		L	ν(NO) cm^{-1}	Ref.
Cationic $\{Fe(NO)_3\}^{10}$	**5^+**	NHC-iPr	1915(m), 1826(sh), 1810(s)	a
	6^+	NHC-Me	1915(m), 1825(sh), 1814(s)	a
		NHC-Mes	1932(s), 1831(s), 1804(vs)[b]	77
		P(*p*-Tolyl)$_3$	1917(s), 1838(vs), 1813(vs)[c]	77
		$P(CH_2OH)_3$	1927(w), 1833(vs)[d]	81
		EtCN	1939(w), 1836(s)	82

[a]This work. [b]In THF. [c]Solid, ATR-FTIR. [d]In nitromethane.

Electron Paramagnetic Resonance Spectral Data and Magnetic Susceptibility of Complex 9

The EPR spectra for the following paramagnetic $\{Fe(NO)_2\}^9$ complexes prepared in this study were recorded at 10 K and 295 K in THF solution: **3^+**, **4^+**, **7**, **9**, and $(Imid\text{-}iPr^-)_2Fe(NO)_2^-$ (*vide infra*). At room temperature, complexes **3^+**, **4^+**, and **7** show isotropic signals at g = 2.028, 2.057, and 2.026, respectively. These are listed and compared with analogous complexes in Table III-4. Example spectra are displayed in Figure III-6. The EPR spectra for anionic, bis-imidazolate DNIC complexes show rhombicity with g values, for example, of 2.038, 2.027, and 2.008 for the complex $(Imid\text{-}iPr^-)_2Fe(NO)_2^-$.[36]

According to the report of Wang and Li, *et al*., the EPR spectrum of a frozen THF solution of tetrameric $[(Im\text{-}H)Fe(NO)_2]_4$ (based on the unsubstituted imidazolate) shows a nine-line spectrum with N-14 hyperfine coupling superimposed on a rhombic signal.[71] Preliminary EPR spectral data taken on a solution of the analogous complex **9**

shows a broad rhombic signal with g values of 2.055, 2.029, 2.012 at 10 K, that appears to be an unresolved rhombic envelope of the 9-line spectrum reported by Wang and Li, *et al*.[71] Further resolution of the spectrum of **9** into hyperfine features has not been achieved. At 295 K the signal becomes isotropic with a g value of 2.033.

Table III-4. g values of selected DNIC in THF solution at low temperatures as indicated

	g value	Temp (K)	Ref.
3^{+}	2.028	10	a
4^{+}	2.057	10	a
(Imid-Me)$_2$Fe(NO)$_2^{+}$	2.015	240	35
7	2.026	10	a
(NHC-Mes)(SPh)Fe(NO)$_2$	2.049, 2.029, 2.013	77	77
(Ar-nacnac)Fe(NO)$_2$	2.09, 2.06, 2.05	77	49
(Imid-iPr^{-})$_2$Fe(NO)$_2^{-}$	2.038, 2.027, 2.008	10	a
(Imid^{-})$_2$Fe(NO)$_2^{-}$	2.040, 2.022, 2.013	77	36
9	2.055, 2.029, 2.012	10	a
[(Im-H)Fe(NO)$_2$]$_4$	2.031	170	71
(Imid)(SPh-*o*-NH-CO-Ph)Fe(NO)$_2$	2.031	298	39

[a]This work.

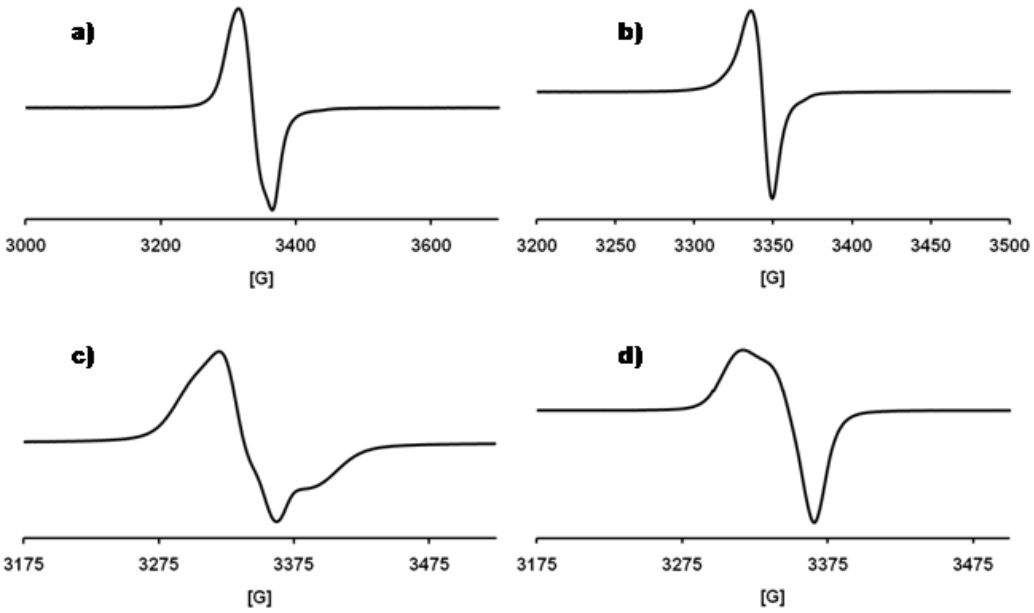

Figure III-6. X-band EPR spectra taken at 10 K in THF solution of a) complex $\mathbf{3}^{+}$ with a frequency at 9.468 GHz, b) complex **7** with a frequency at 9.482 GHz, c) complex **9** with a frequency at 9.468 GHz, and d) complex $(\text{Imid-iPr}^{-})_2\text{Fe(NO)}_2^{-}$ as Na-18-crown-6-ether salt with a frequency at 9.473 GHz.

It is well known that spin-spin coupling between $\{\text{Fe(NO)}_2\}^9$ units occurs in clusters such as Roussin's red ester (Fe···Fe separation = 2.5-2.6 Å) resulting in EPR silent complexes. In a dimer designed to have an Fe···Fe separation of ca. 4 Å, the EPR signal is observed.[41] Hence, as the separation between $\{\text{Fe(NO)}_2\}^9$ units in the imidazolate tetramers under discussion here is ca. 6 Å, spin-spin coupling is not expected. This is confirmed for complex **9** by the magnetic susceptibility measurement yielding an effective magnetic moment per Fe atom, μ_{eff}, of 1.75 BM (theoretical μ_{SO} value for one unpaired electron per Fe is 1.73 BM).

Rather than attribute the hyperfine observed in the EPR spectrum of [(Im-H)Fe(NO)$_2$]$_4$ to N-14 coupling within the intact tetramer, Wang and Li, *et al*., have suggested that the simpler complex dissociates in THF solvent, producing a monomeric DNIC [(Imid$^-$)(THF)Fe(NO)$_2$] with N-14 coupling from nitrogens of two nitrosyls and one imidazolate ligand accounting for the 9-line spectrum.[71] In support of this conclusion, Tsai and Liaw, *et al.*, report a monomeric {Fe(NO)$_2$}^{9} complex, (Imid)(SR)Fe(NO)$_2$ (R = Ph-*o*-NH-CO-Ph), with two nitrosyls and one imidazole, Figure III-7 which also exhibits a well-resolved 9-line EPR signal centered at g = 2.031 with hyperfine coupling constants 2.4 and 4.1 G at 298 K[39] these are amongst the few observations of such hyperfine coupling in paramagnetic DNICs. We note that the ν(NO) IR spectra of complex **9** in THF solution and in the solid state are identical. Hence at this stage of investigation there is no compelling evidence for breakup of the tetramer in solution, and the lack of resolvable features in the EPR spectrum of complex **9** will be further discussed in Chapter IV.

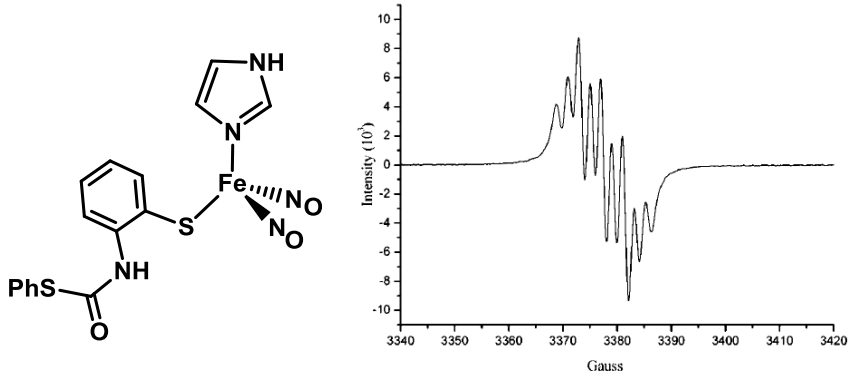

Figure III-7. A monomeric {Fe(NO)$_2$}^{9} complex, (Imid)(SR)Fe(NO)$_2$ (R = Ph-*o*-NH-CO-Ph), which exhibits a well-resolved 9-line EPR signal centered at g = 2.031 with hyperfine coupling constants 2.4 and 4.1 G at 298 K.[39]

Cyclic Voltammetry

Cyclic voltammograms of complexes **1**, **2**, **3**, **4**, and **7** were recorded in 2 mM THF solution and complex $\mathbf{5}^{+}$ was recorded in 2 mM CH_2Cl_2 solution with 100 mM [t-Bu_4N][BF_4] as the supporting electrolyte. All potentials were measured relative to a $Ag/AgNO_3$ electrode using a glassy carbon working electrode and are referenced to Cp_2Fe/Cp_2Fe^{+}. The redox potentials for each complex are given in Table III-5 and selected CVs are shown in Figure III-8. For complexes **1** and **2**, an irreversible oxidation event occurs at 0.14 and 0.12 V, respectively, whereas for complexes **3** and **4**, a reversible redox couple assigned to the $\{Fe(NO)_2\}^{9/10}$ couple is centered at -0.76 and -0.77 V, respectively, Figure III-8b. Compared to the previously reported neutral $\{Fe(NO)_2\}^{10}$, (bipy)$Fe(NO)_2$ (bipy = 2,2'-bipyridine), which has a reversible redox event at -0.48 V,[83] the neutral, bis-NHC-containing DNICs are oxidized at more negative values, ca. -0.76 V, which is consistent with the stronger electron donating characteristics of the NHC ligands. Despite the reversibility of the cationic complex $\mathbf{5}^{+}$ couple at 0.90 V (recorded in CH_2Cl_2 due to insolubility in THF), the TNIC rapidly decomposed with repeated scans. Note that the reversible reduction of the analogous NHC-Mes TNIC is more negative by a volt ($E_{1/2}$ = -0.29 V in THF and -0.39 in CH_2Cl_2) than that of $\mathbf{5}^{+}$.[77] This major discrepancy is not understood.

Table III-5. Electrochemical potentials of selected DNICs and TNICs.[a]

	E_{pc} (V)	$E_{1/2}$ (V)	Ref.
1	0.14	--	b
2	0.12	--	b
(CO)(NHC-Mes)Fe$(NO)_2$	-0.34	--	77
3	--	-0.76	b
4	--	-0.77	b
(bipy)Fe$(NO)_2$	--	-0.48	83
$\mathbf{5}^+$	--	0.90[c]	b
(NHC-Mes)Fe$(NO)_3^+$	--	-0.29	77
7	--	-1.33	b
(NHC-Mes)(SPh)Fe$(NO)_2$	--	-1.48	77
(Ar-nacnac)Fe$(NO)_2$	--	-1.34	38

[a]In THF solution (0.1 M $^tBu_4NBF_4$). All experiments were recorded using a glassy carbon working electrode and Pt counter electrode and referenced to Cp_2Fe/Cp_2Fe^+ at a scan rate of 100 mV/s. [b]This work. [c]In CH_2Cl_2 solution.

Complex **7** has a reversible redox event at -1.33 V (measured in THF) and, similarly to the previously reported (NHC-Mes)(PhS)Fe$(NO)_2$ complex, the reversible process is scan-rate dependent.[77] It is notable that the (Ar-nacnac)Fe$(NO)_2^{0/1-}$ complex couple is at -1.34 V in THF solution[38], closely matching the reversible $\{Fe(NO)_2\}^{9/10}$ couple of complexes **7** and (NHC-Mes)(PhS)Fe$(NO)_2$, but almost a volt more negative than the couple for (bipy)Fe$(NO)_2$.

Overall these data affirm the redox properties of the Fe$(NO)_2$ unit responds to ligand environment in a manner reflecting the typical donor/acceptor abilities of the spectator ligands.

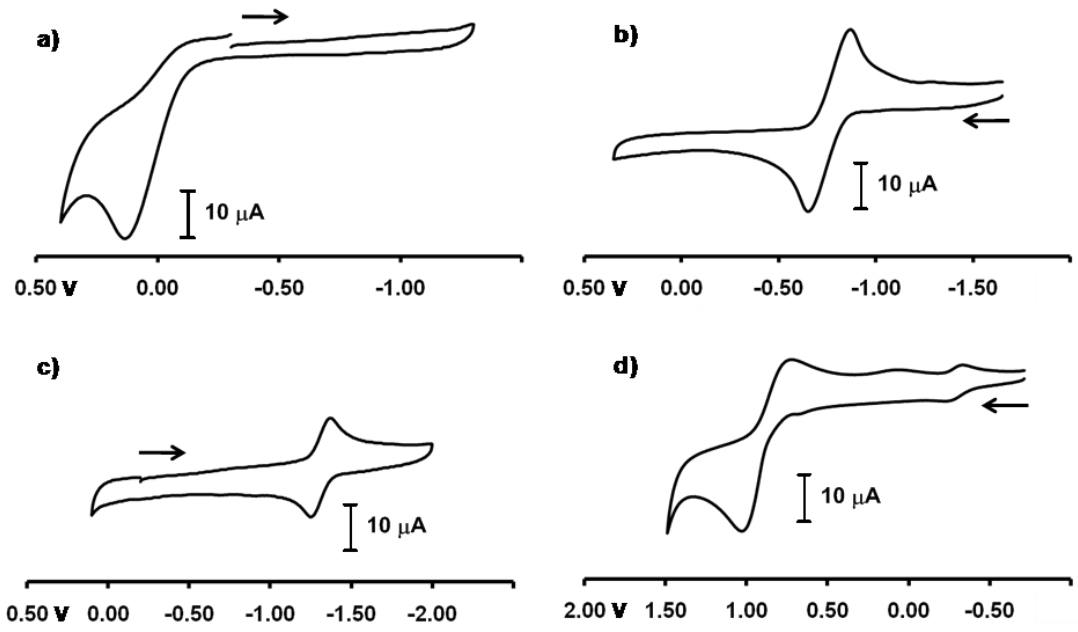

Figure III-8. Cyclic voltammograms of complexes a), **1**; b), **3**; c), **7** in 2 mM THF solution; and d), $\mathbf{5}^{+}$ in 2 mM CH_2Cl_2 solution. All are referenced to Cp_2Fe/Cp_2Fe^{+}.

Reactivity Studies

As noted above, imidazoles cleave the RRE $(\mu\text{-SPh})_2[Fe(NO)_2]_2$ to form the $(Imid\text{-}R)(SPh)Fe(NO)_2$ complex. The imidazole ligand can subsequently be displaced by addition of NHC-iPr to form complex **7**; addition of imidazole, even in large excesses, does not result in NHC displacement. Likewise, in the $\{Fe(NO)_2\}^{10}$ cases, addition of imidazole to $Fe(CO)_2(NO)_2$ results in the formation of $(Imid\text{-}R)(CO)Fe(NO)_2$. Again, the imidazole is readily (within minutes) displaced upon addition of NHC to form complexes **1** and **2**, in an irreversible reaction, **Scheme III-1**. Addition of excess NHC-iPr to complex **7** results in the formation of complex **3** with

bimolecular reductive elimination of diphenyl disulfide; however, addition of excess imidazole to (Imid)(SPh)Fe(NO)$_2$ had no effect as reported in **Scheme III-3**. No reaction occurred on addition of NaSPh to reduced complex **3**, however, one equivalent of NaSPh displaced NHC-iPr from oxidized complex **3**$^+$ within 5 minutes to form complex **7**, **Scheme III-4**. Further addition of an excess of NaSPh to **3** results in the formation of (SPh)$_2$Fe(NO)$_2^-$ within 5 minutes.

Scheme III-4. Reactivity of Complex **3**$^+$ with NaSPh in THF solvent.

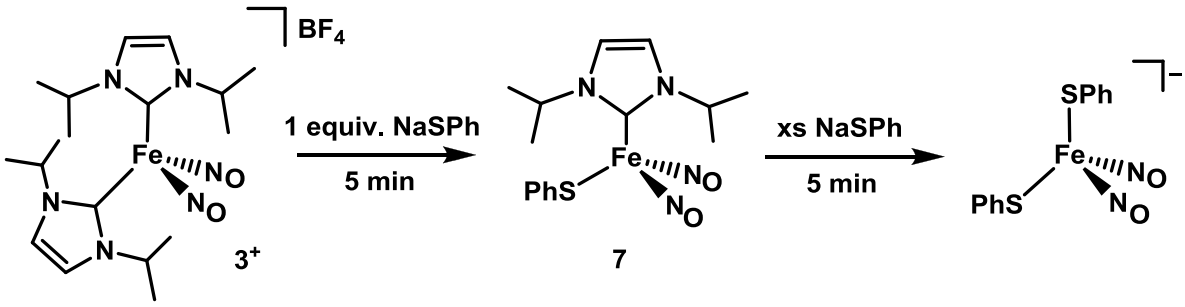

In the neutral {Fe(NO)$_2$}^{9} complexes, the replacement of imidazole by the stronger donating NHC likely results in a stabilized oxidized iron unit. Nevertheless, anionic thiolates are even better stabilizers of the oxidized {Fe(NO)$_2$}^{9} unit as exemplified by the instability of the cationic (NHC)$_2$Fe(NO)$_2^+$ complexes. The neutral, paramagnetic (NHC)(PhS)Fe(NO)$_2$ complexes are perhaps the most stable of the complexes explored in this study, while the neutral, diamagnetic (NHC)$_2$Fe(NO)$_2$ are the second most stable. Again the remarkable ability of the N-heterocyclic carbenes to

stabilize two redox levels is noted. Interestingly the PhS^- anions did not appear to extract NO, forming PhSNO, in a decomposition side reaction, in any of the reactions explored.

Imidazole-Containing Analogues

The tetrameric complex **9**, resulting from attempts to prepare monomeric complex **8**, **Scheme III-1**, can be cleaved with deprotonated Imid-iPr to form the anionic $(Imid\text{-}iPr^-)_2Fe(NO)_2^-$ complex, containing the oxidized $\{Fe(NO)_2\}^9$ unit as demonstrated via IR and EPR spectroscopies. Consistent with results of Chen, *et al*. working with the unsubstituted $[(Im\text{-}H)Fe(NO)_2]_4$ cluster, complex **9** can also be cleaved by deprotonated phenyl thiolate to form the mononuclear, $(Imid^-)(SPh)Fe(NO)_2^-$ DNIC.[37] Formation of clusters is highly relevant to thiolate-containing DNICs. Vanin, *et al*., have reported that this type of reactivity, under biological conditions using cysteine and glutathione, can be regulated by the pH where a decrease to pH = 5 results in formation of dinuclear $\{Fe(NO)_2\}^9$ DNICs and an increase to a pH of 9-10 results in the formation of mononuclear $\{Fe(NO)_2\}^9$ DNICs.[84] Additionally, it has been established that in biological systems in the absence of excess thiol, diamagnetic, spin-coupled dinuclear DNICs are formed rather than the paramagnetic mononuclear DNICs.[13] Thus, from our studies with imidazole-containing DNICs, it is reasonable that similar reactivity modulated by pH and the presence or absence of histidine/imidazole could control formation of polynuclear vs. mononuclear DNICs.

NO Transfer Studies

To probe the ability of the NHC-containing DNICs to release or transfer NO, the DNICs were combined with the NO-trapping reagent Co(TPP) in THF solution. Coupled with an almost immediate color change, an IR band that grew in at 1683 cm^{-1} concomitant with loss of bands from the DNIC, indicated (NO)Co(TPP) formation.[50] This reactivity of oxidized $\{Fe(NO)_2\}_9$ complexes $\mathbf{3}^+$ and $\mathbf{4}^+$ was in great contrast to the reduced $\{Fe(NO)_2\}^{10}$ complexes **3** and **4**, which showed no change upon mixing with THF solutions of Co(TPP). This preliminary study suggests that DNICs in the reduced $\{Fe(NO)_2\}^{10}$ oxidation level are inert to NO transfer, while DNICs in the oxidized $\{Fe(NO)_2\}^9$ oxidation state are capable of NO transfer in the presence of a suitable NO trapping agent. This conclusion is supported by work of Chiang, *et al*., and Tonzetich, *et al*.[50,49] Such assenting results encourage future studies to develop a biologically compatible DNIC that can be "turned on" by oxidation to deliver NO to a specific target. Nevertheless the mechanism of NO transfer is unknown; neither is the fate of the DNIC following loss of NO. From "double-tube" experiments we have shown that the cationic NHC-TNIC complex stabilized by the bulky NHC-Mes releases NO as free NO radical, which can diffuse into a solution containing a NO-trapping reagent.[77] Such a design to explore NO release from $\mathbf{3}^+$ or $\mathbf{4}^+$ was not successful.

CHAPTER IV

SELF ASSEMBLY OF DINITROSYL IRON UNITS INTO IMIDAZOLATE-EDGE-BRIDGED MOLECULAR SQUARES: CHARACTERIZATION INCLUDING MÖSSBAUER SPECTROSCOPY[†]

Introduction

Prominent ligand donor sites in metalloproteins result from thiolate sulfur and imidazole nitrogen as side chain amino acid residues from cysteine and histidine, respectively. In both cases deprotonated forms produce anionic ligands that may serve in bridging capacities, a feature of importance in the assembly of active sites as is found in the cysteinyl thiolate-bridged nickel-iron hydrogenase or in the bovine erythrocyte superoxide dismutase containing a histidine imidazolate-bridged Cu-Zn active site, Figure IV-1.[85,86] In the latter, copper may replace zinc resulting in a dicopper unit with noteworthy magnetic properties.[87,88] Approaches to small molecule models of these active sites have developed, in cases requiring heroic synthetic efforts to build in steric bulk within biomimetic ligands in order to prevent higher order aggregation and cluster formation.[87,89] In fact the clusters themselves may be of interest for molecular properties such as multiple redox events within a single molecule, or in the case of paramagnetic metal ion constituents, the possibility of temperature-dependent spin state switches.

[†]This chapter is to be submitted for review and publication with the following authorship list: Jennifer L. Hess, Chung-Hung Hsieh, Gregory P. Holmes-Hampton, Paul A. Lindahl, Scott M. Brothers, Michael B. Hall, and Marcetta Y. Darensbourg.

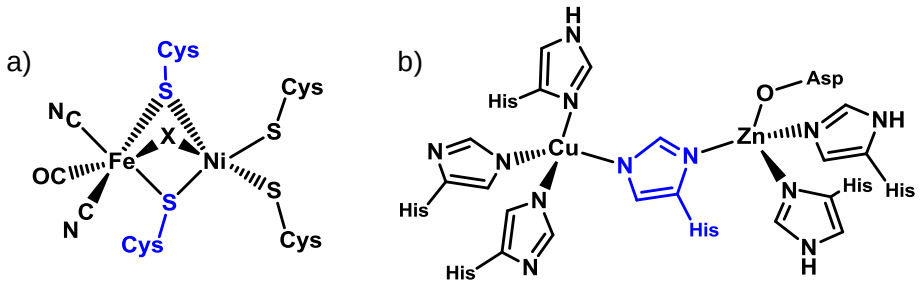

Figure IV-1. Structures of a) [NiFe]-hydrogenase and b) bovine erythrocyte superoxide dismutaste active sites demonstrating bridging cysteine or histidine (shown in blue) as found in metalloproteins.[85,86]

It was demonstrated in Chapter III that imidazoles, as neutral or anionic ligands can also support DNIC formation. When deprotonated, the distal nitrogen functionality in the imidazolate ligands of $[(Imid)_2Fe(NO)_2]^-$, can lead to aggregation through bridging, yielding interesting molecular squares comprised of $\{Fe(NO)_2\}^9$ units.[83,90] The self-assembly of cationic $\{Fe(NO)_2\}^9$ into clusters is also known for thiolates in the ubiquitous Roussin's red esters (RRE), $(\mu\text{-}SR)_2[Fe(NO)_2]_2$ for example.[70] Of note is that whereas the $\{Fe(NO)_2\}^9$ in the RRE complexes are spin coupled (the Fe···Fe distance is less than 3 Å), the imidazolate-bridged units in the tetramers described here are sufficiently spaced (~ 6 Å apart) to maintain paramagnetism at room temperature. Liaw, *et al.*, have a designed a variation on the RRE as shown in Figure IV-2 that spaces the $\{Fe(NO)_2\}^9$ units at 4 Å apart. This diiron complex was found to have two non-coupled S = ½ $\{Fe(NO)_2\}^9$ centers.[41]

Magnetic susceptibility data demonstrate that each Fe within the imidazolate tetramers reported by Li, *et al.*, $[(Imid)Fe(NO)_2]_4$ (complex **1**)[83] and by us, [(Imid-

iPr)Fe(NO)$_2$]$_4$ (complex **2**),[90] can also be considered as non-coupled, S = ½ units at room temperature. This chapter will further explore the effect of sterically encumbered imidazoles on the structure and aggregation of these interesting molecular squares.

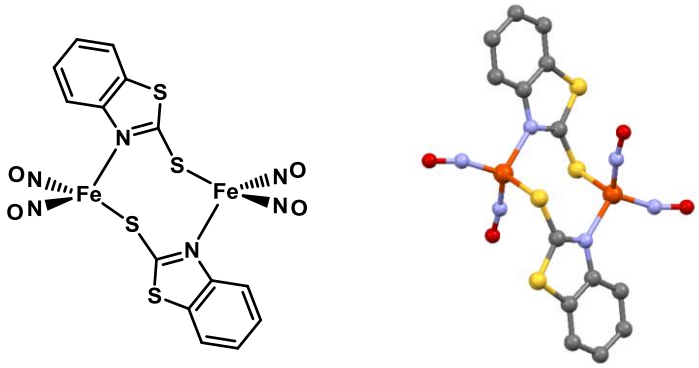

Figure IV-2. Structure and ball and stick rendition of a RRE in which the $\{Fe(NO)_2\}^9$ units are spaced 3.997 Å apart resulting in two non-coupled S = ½ $\{Fe(NO)_2\}^9$ centers.[41]

Synthesis and Composition

As was described for the preparation of the [(Imid-iPr)Fe(NO)$_2$]$_4$ complex **2** in Chapter III, addition of excess benzimidazole to freshly prepared Fe(CO)$_2$(NO)$_2$ in a mixture of THF/CH_2Cl_2 results in a color change from orange to red-brown and an infrared spectrum representative of an oxidized DNIC (ν(NO) in CH_2Cl_2 = 1805(m), 1739(s)) is observed.[90] Isolation and recrystallization from CH_2Cl_2/pentane yielded red-brown, x-ray quality crystals of complex **3**, [(Imid-benz)Fe(NO)$_2$]$_4$. An issue with all polymetallics is the possibility of dissociation in solution giving degraded species that might complicate analysis. Mass spectral data was obtained for complexes **2** and **3** using the nano-electron spray ionization technique in the positive mode. For complex **2**, a low

intensity parent ion ($Fe_4C_{24}H_{36}N_{16}O_8$) isotope bundle was observed centered at m/z = 900. The base (100%) peak was centered at m/z 538 ($Fe_3N_9O_5C_{12}H_{18}$, representing $Fe_3(NO)_5(Imid\text{-}iPr)_2$) with other intense bundles centered at m/z 478.8 representing loss of 2 NO from the base peak, and at m/z 647.9 representing addition of one iPr-imidazole (+110 mass units) to the base peak. For complex **3**, the parent ion ($Fe_4C_{28}H_{20}N_{16}O_8$, m/z = 931) isotope bundle was not observed in the mass spectrum. Similar to complex **2**, the base (100%) peak was centered at m/z 538 ($Fe_3C_{14}H_{10}N_8O_5$, representing $Fe_3(NO)_3(NO)_2(Imid\text{-}benz)_2$) with other intense bundles centered at m/z 478.9 representing loss of 2 NO from the base peak, and at m/z 655.9 representing addition of one benzimidazole (+118 mass units) to the base peak, forming an ion of composition $Fe_3(NO)_3(NO)_2(Imid\text{-}benz)_3$.

The elemental analyses of tetramers **2** and **3** were not readily interpreted. Elemental analysis was not reported for complex **1**. "Despite sending pure, crystalline samples" for analyses, the experimental C, H, and N percentages did not match the expected for $Fe_4(NO)_8(Imid\text{-}iPr)_4$ (complex **2**) and $Fe_4(NO)_8(Imid\text{-}benz)_4$ (complex **3**). For complexes **2** and **3**, samples from two different batches were sent for analysis and each reported a much higher carbon content than expected, Table IV-1. Interestingly, the results were reproducible, and the best match of formula to reported results is $FeC_{12}H_{18}N_6O_2$ for complex **2** possibly representing $Fe(NO)_2(Imid\text{-}iPr)_2$ and $FeC_{14}H_{10}N_5O$ for complex **3** possibly representing $Fe(NO)(Imid\text{-}benz)_2$. The high carbon content suggests that during combustion of the sample for analysis or introduction of the sample in to the combustion chamber, loss of iron is occurring. Such

a process may result in iron deposition in the combustion chamber and detection of fragments of the tetramer, which were also observed in the mass spectra. It should be noted that the crystals used in the X-ray diffraction study were obtained by a different procedure than those used for the elemental analyses (see experimental details in Chapter II).

Table IV-1. Elemental analysis results found compared to the theoretical values for elements C, H, and N for two separate preparation/isolations of complexes **2** and **3**.

	Complex **2**			Complex **3**		
		Batch			Batch	
		1	2		1	2
Element	Theory	Found		Theory	Found	
C	32.03	40.49	41.24	36.09	51.52	55.58
H	4.03	5.97	5.71	2.16	3.76	4.14
N	24.90	20.64	22.63	24.05	20.93	21.63

The X-ray diffraction analysis and the molecular structure of complex **3**, [(Imid-benz)$Fe(NO)_2]_4$ is first reported here and is compared to those previously reported of complexes **1**, [(Imid)$Fe(NO)_2]_4$, and **2**, [(Imid-iPr)$Fe(NO)_2]_4$.[83,90] Two views of the thermal ellipsoid plot of **3** is given in Figure IV-3. As was found for complexes **1** and **2**, Figure IV-4, the structure of **3** consists of an almost precise square plane of irons, with nitrosyl ligands capping the irons at the corners and imidazolates bridging the edges. The contrasting structural features of complexes **1** - **3** are revealed from side views of the Fe_4 plane, in Figures IV-4 and IV-5.

The shaded planes in Figure IV-4 display the canting of the imidazole planes with respect to the Fe_4 square plane. The angles of intersection of these planes and the orientation of the C_2 and C_1 units of the imidazole relative to the plane of the irons comprise the most significant differences in the three structures; the latter is more clearly seen in the abbreviated ball and stick displays of **1**-**3** in Figure IV-5. A fourth structure shown in Figure IV-5 is that of a copper analogue, described more fully below.[88] In complex **1**, the methylene units of the imidazole are all positioned to the same side and oriented in towards one another (angle of intersection of the Fe_4 plane and imidazole planes = 53°), closing off one side of the Fe_4 plane. On the opposite side the ethylene units, designated as the all "up" configuration in Figure IV-5, render a bowl-like open side that in the complete molecular structure includes an acetone solvent molecule of crystallization.[83]

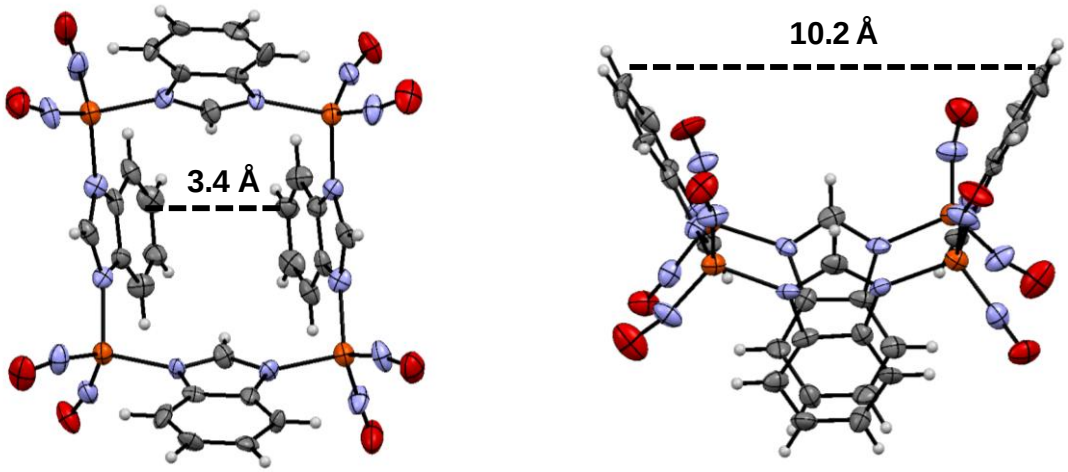

Figure IV-3. Two views of the thermal ellipsoid plot at 50% probability of [(Imid-benz)Fe$(NO)_2]_4$, complex **3**. The labels correspond to the distance between opposite aryl C-C bonds at the widest point (10.2 Å) and at the closest point (3.4 Å).

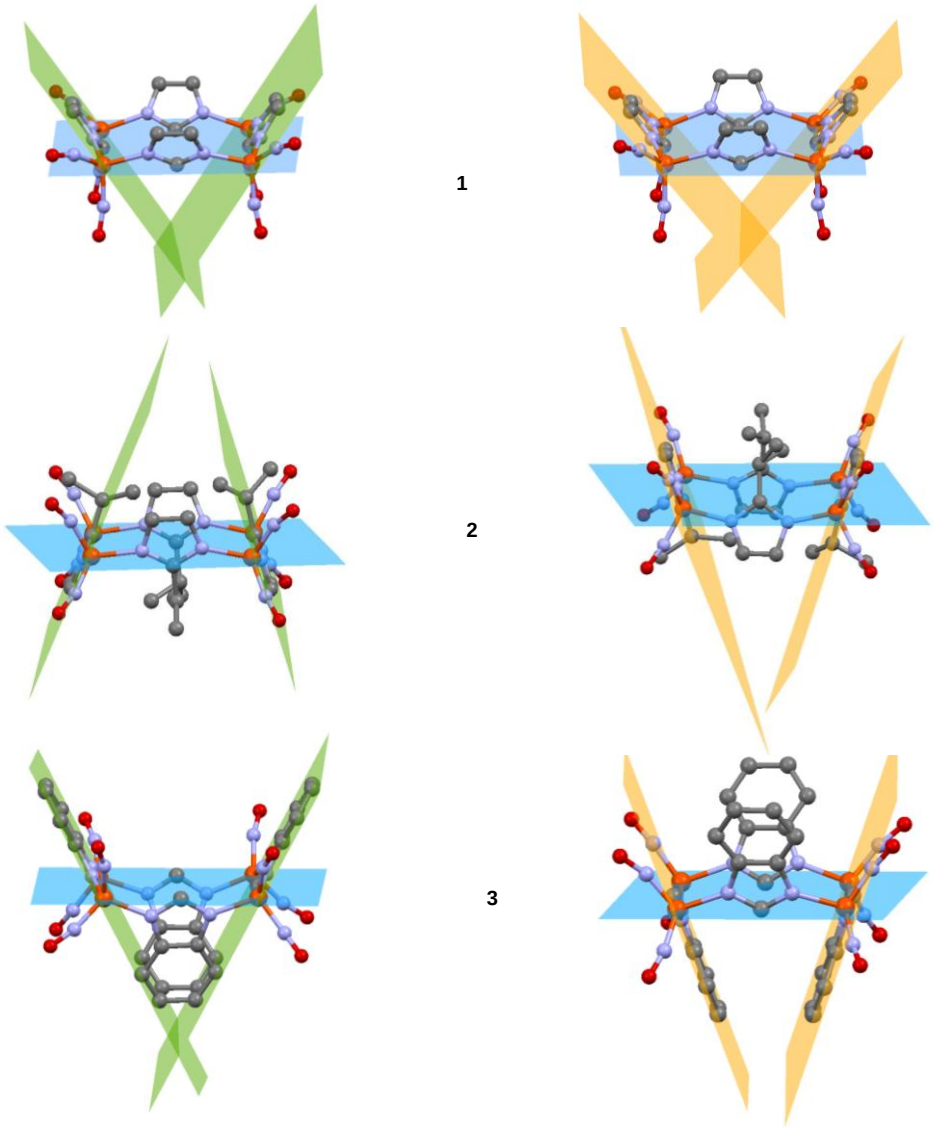

Figure IV-4. Ball and stick representations of the structures of complexes **1 - 3** as derived from X-ray diffraction analysis. In each case, the view on the right is from a rotation of 90° relative to the left.

In complex **2**, the C1 methylene carbons and the C2 ethylene units alternate up and down positions such that both sides of the Fe_4 square plane are blocked by the inwardly pointing isopropyl groups, Figure IV-4b; as in **1**, the ethylene units are

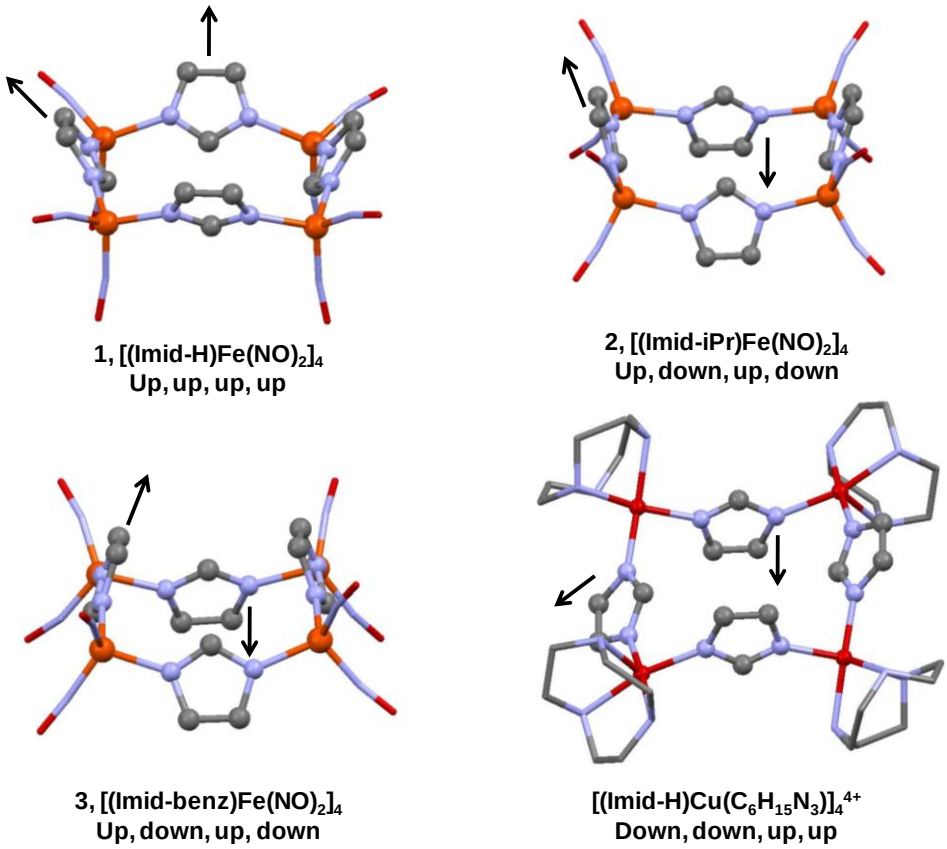

Figure IV-5. Up and/or down orientations of imidazolate ligands of complexes **1** – **3** and an analogous Cu-containing molecular square.[88] "Up" and "down" refers to the orientation of the ethenyl (HC=CH) group of the imidazolate with respect to the Fe_4 plane. Imidazole substituents (in the case of complex **2** and **3**) have been removed for clarity.

outwardly oriented. Complex **3**, Figures IV-4c and IV-5, shows another variation, in that the aryl groups attached to the ethylene unit are oriented outwardly and across from each other on one side of the Fe_4 square plane (10.2 Å across from aryl C-C bonds at widest point) and inwardly on the other two (3.4 Å apart at the closest point). This configuration has the effect of sterically blocking only one side of the Fe_4 plane and allows for highly efficient packing in the crystalline form as the closed side of one unit

can nest into the open side of another, see Figure IV-6. The nested benzimidazolates have the benzyl groups arranged edge to plane rather than π-stacked. While the closest intermolecular Fe···Fe distance is ~ 5.3 Å, the closest intermolecular C···C distance (from C10 of the nested benzimidazolate to C2 of the benzimidazolate of the open portion) is ~ 3.5 Å, Figure IV-6d. The separation of the nested benzyl groups measured by C11 to the methenyl carbon of the benzimidazolate of the open portion is ~ 3.6 Å.

A view down the center of the squares in the packing diagrams thus reveals a columnar cavity in complex **3**; the centers of complexes **1** and **2** are better blocked by the acetone molecule or isopropyl groups, respectively. Graphics displaying these views are given in Figure IV-7.

Metric parameters presented in Table IV-2 show similar $\angle N_{NO}$-Fe-N_{NO} in the range of 116.5 to 113.1° for **1** and **3**; the Imid-iPr analogue **2** average is 110.5°. The $\angle N_{Imid}$-Fe-N_{Imid} angles vary somewhat with complex **3** having the smallest, avg. = 105°. Complex **2** has a larger cavity as compared to **1** and **3**, as implied from Fe to Fe average edge distances of 6.24 Å, 0.2 Å larger than that of **1** and **3**; Fe to Fe cross distances are ca. 8.8 Å. The cavity is larger likely to accommodate the additional steric bulk of the isopropyl groups on position 2 of the imidazole ring. The iron atoms are positioned at ca. 120° relative to the carbons adjacent to the N-donors in the imidazolates, thus the vectors that connect the iron atoms do not include the imid-nitrogen donors.

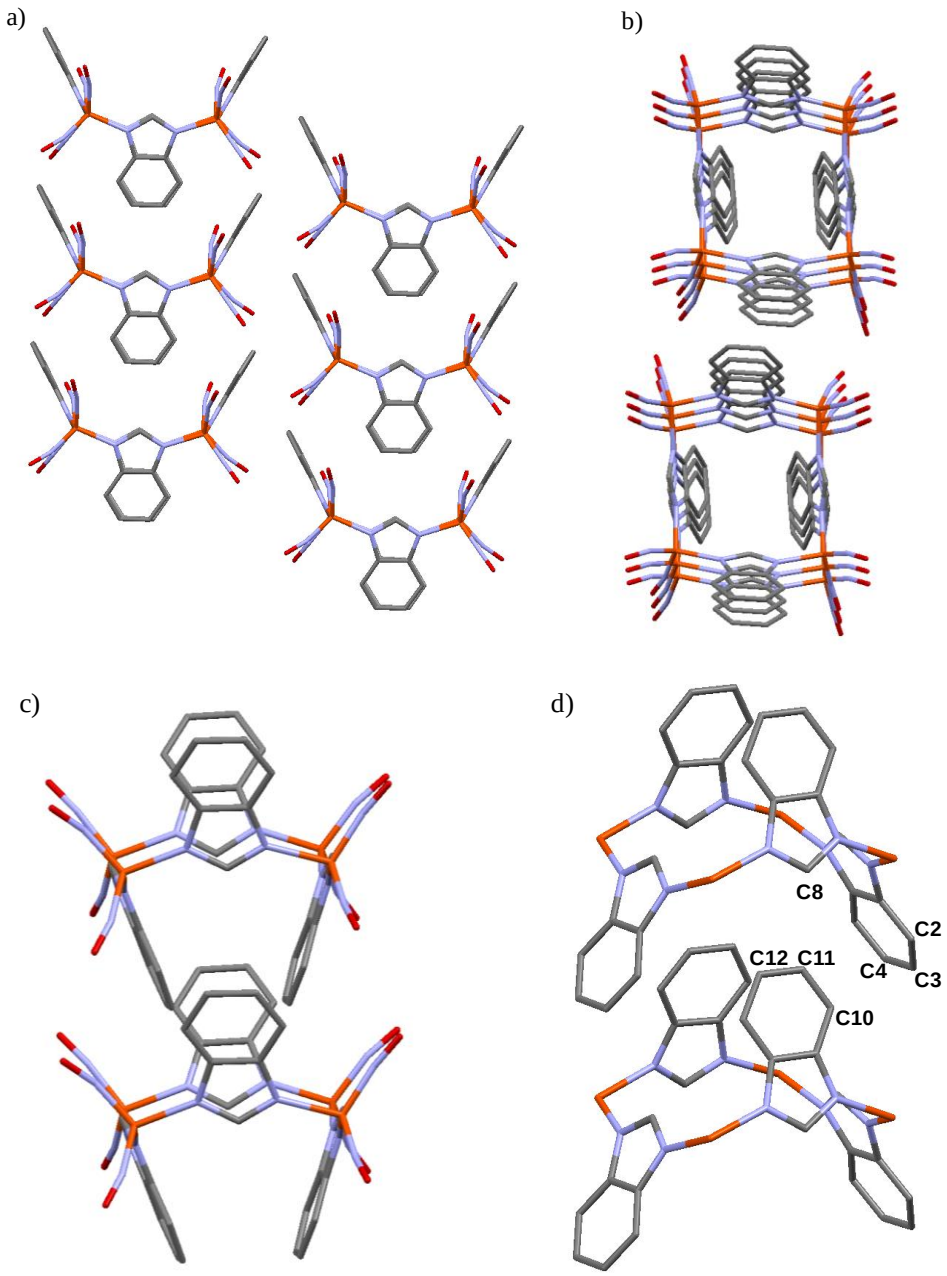

Figure IV-6. A portion of the extended packing diagram of complex **3** showing a) the nesting of the closed into the open portion of the clusters. b) This view is from a rotation of 90° relative to the view in a) looking down the cavities. c) Two molecules from the extended packing diagram rotated 180° from the view in a) to show the close contact of the benzyl groups of the closed portion to those of the open portion. d) Labeling scheme to demonstrate selected C-C distances between benzyl groups of the closed portion to the open portion. Nitrosyl groups have been removed for clarity. C-C distances, Å: C8-C12 3.610; C8-C11 3.587; C11-C4 4.926; C11-C3 4.497; C11-C2 3.837; C10-C2 3.506; C10-C3 3.940.

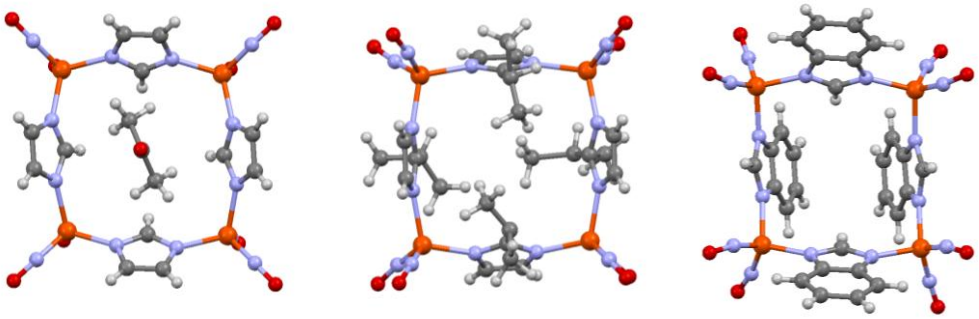

1 **2** **3**

Figure IV-7. A view down the center of the squares demonstrating blocked cavities for complexes **1** and **2** and an open cavity for complex **3**.

Table IV-2. Selected bond distances (Å) and angles (°) for complexes **1**, **2**, and **3**.

	1	**2**	**3**
Bond Distances (Å)			
Fe-$N_{Imid\ avg}$	2.005(5)	2.036(11)	1.982(7)
N-$O_{\ avg}$	1.166(6)	1.194(13)	1.161(10)
Fe-$N_{NO\ avg}$	1.694(5)	1.712(13)	1.683(10)
Fe---Fe (adj)	5.965	6.230	5.994
	5.977	6.253	5.961
Fe---Fe (cross)	8.697	8.755	8.693
	8.183	8.898	8.206
Bond Angles (°)			
N_{Imid}-Fe-$N_{Imid\ avg}$	109.24(17)	110.72(5)	105.2(3)
N_{NO}-Fe-$N_{NO\ avg}$	114.8(2)	110.39(5)	115.1(5)
Fe-N-$O_{\ avg}$	166.8(6)	164.02(11)	165.6(10)
Fe-N_{Imid}-$C_{Imid\ avg}$	128.9(3)	133.39(10)	127.4(7)
Deviation from Fe_4 Square Plane (Å)			
	0.0094	0.0145	0.0219
Angle of intersection of Fe_4 Square Plane With Imidazole Plane (°)			
	129.8	107.8	117.5
	55.7	68.5	70.3

These DNIC tetramer structures bear great similarity to imidazolate-bridged tetracopper squares.[87,88] The example shown in Figure IV-5, finds the Cu(II) corners capped by the 1,4,7-triazacyclononane or tacn ligand. The overall charge of the cluster is 4^+. Copper to copper distances along the edges are 5.89 and 5.99 Å, and the $\angle N_{Imid}$-Cu-N_{Imid} are in the range of 93°.[88] This tetramer and other copper-containing analogues were synthesized as mimics of histidine-containing metalloproteins and examined for the ability of the bridging imidazolate to mediate antiferromagnetic interactions. Variable temperature magnetic susceptibility studies found antiferromagnetic interactions between adjacent Cu(II) centers at low temperatures.[88] It is presumed that a σ-exchange pathway through the imidazolate bridge is responsible for this interaction.[87,88] To our knowledge, complexes **1** - **3** are the only known $Fe(NO)_2$-containing molecular squares.

Electron Paramagnetic Resonance Spectral Data

The EPR spectra for complexes **1** - **3** (Figure IV-8) originate from paramagnetic $\{Fe(NO)_2\}^9$ units. At 295 K, all display a broad isotropic signal at g = 2.03 in THF solution (~ 2 mM solutions for all three complexes), characteristic of DNIC complexes. At 10 K the tetrameric complex **2** in frozen THF shows a rhombic signal with g values of 2.055, 2.029, 2.012, whereas complex **3** in frozen THF (10 K) shows a broad isotropic

signal with a g value of 2.029 similar to the signal seen at room temperature. Complex **1** also shows a broad isotropic signal with a g value of 2.021 at 10 K in frozen THF. In contrast, Li and coworkers report a nine-line spectrum with N-14 hyperfine coupling centered around a g value of 2.031 at 170 K in THF solution.[83]

As discussed in Chapter III, Li and coworkers suggested, on the basis of its nine-line EPR spectrum, that complex **1** was dissociating in THF solvent to produce a THF-bound monomer DNIC.[83] In order to determine if there was any observable effect with a non-coordinating solvent on the signal shape or position of the g value, EPR spectra of complexes **1** – **3** were also obtained in CH_2Cl_2 solution at 298 K. In all three cases, a broad isotropic signal is observed with a g value closely matching the g value of the EPR spectra taken in THF solution. Even with lowering the concentration of the samples to ~0.5 mM and tweaking the spectral parameters (increasing scan time, increasing or decreasing the power, or lowering the modulation amplitude), no N-14 hyperfine was observed with either the THF or CH_2Cl_2 solutions. As the spectral line shapes and g values are similar in both THF and CH_2Cl_2, we assume that the tetramers remain intact in solution. The IR and cyclic voltammetry data support this assumption.

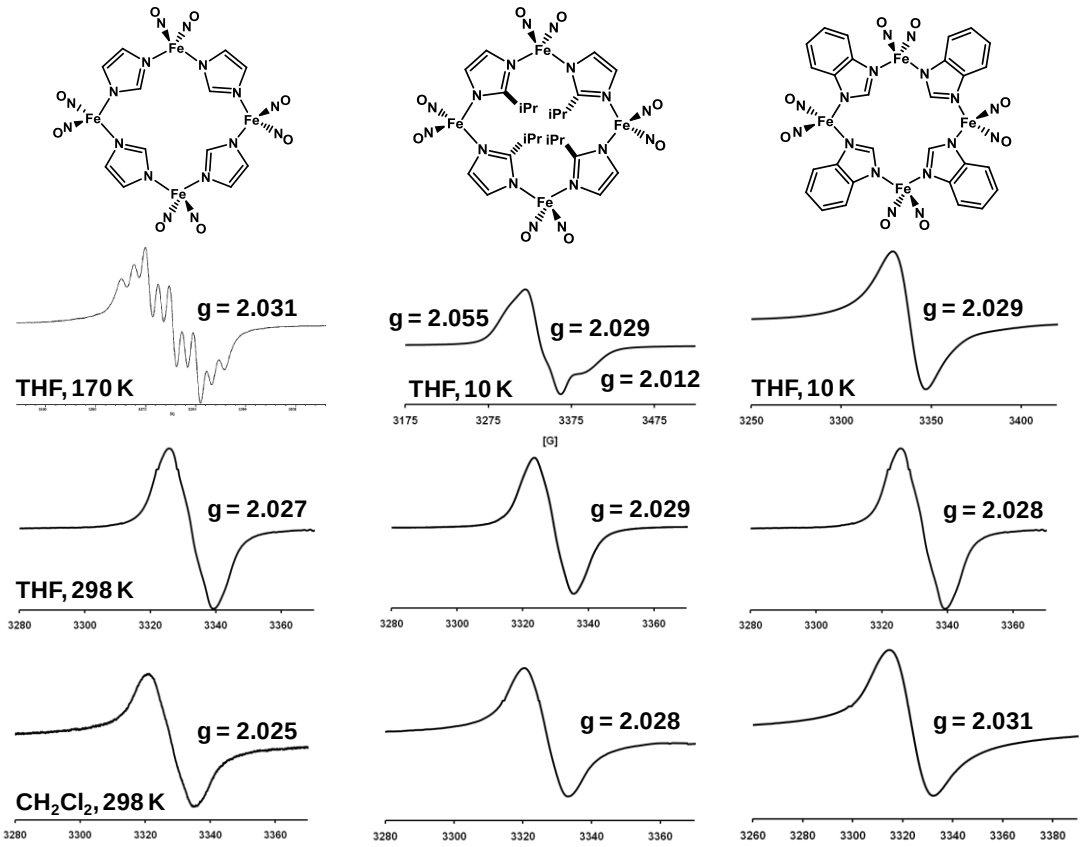

Figure IV-8. EPR spectra of complex **1** in THF at 170 K,[83] 298 K (frequency at 9.45 GHz), and in CH_2Cl_2 at 298 K (frequency at 9.45); complex **2** in THF at 10 K, 298 K (frequency at 9.45 GHz), and in CH_2Cl_2 at 298 K (frequency at 9.45); and complex **3** in THF at 10 K (frequency at 9.49 GHz), 298 K (frequency at 9.45 GHz), and in CH_2Cl_2 at 298 K (frequency at 9.44 GHz).

Cyclic Voltammetry

The cyclic voltammograms of complexes **1**, **2**, and **3** were recorded in 2 mM CH_2Cl_2 solution with 100 mM [t-Bu_4N][BF_4] as the supporting electrolyte. All potentials were measured relative to a $Ag/AgNO_3$ electrode using a glassy carbon working electrode and are referenced to Cp_2Fe/Cp_2Fe^+. As expected for polymetallics,[91,92] multiple and overlapping redox events are observed for each complex.

The cyclic voltammograms of complexes **1** – **3** in the cathodic region are given in Figure IV-9 with the corresponding square wave voltammograms as a means to amplify and validate the separate electrochemical events. Figure IV-10 shows the scan reversed at different potentials for each complex in attempts to isolate individual redox events. The redox potentials for each complex are given in Table IV-3.

Table IV-3. Reduction and oxidation values observed for complexes **1** – **3**.[a]

	E_{pc} (V)	E_{pa} (V)	$\Delta(E_{pa}-E_{pc})$ (V)	$\Delta(E_{pc2}-E_{pc1})$ (V)
1	-1.20	-1.03	0.17	0.19
	-1.39	-1.29	0.10	
2	-1.29	-1.09	0.20	0.38
	-1.67	-1.41	0.26	0.31[b]
	-1.98			
3	-1.12	-0.99	0.13	0.16
	-1.28	-1.21	0.07	

[a]In CH_2Cl_2 solution (0.1 M $^tBu_4NBF_4$). All experiments were recorded using a glassy carbon working electrode and Pt counter electrode and referenced to Cp_2Fe/Cp_2Fe^+ at a scan rate of 100 mV/s. [b]The potential difference refers to the difference between the second and third reductions.

For complexes **1** and **3**, two reductive events are observed at -1.20 and -1.39 V and -1.12 and -1.28 V, respectively. Isolation of the successive waves suggest that the oxidation events observed upon scan reversal are associated with the corresponding reduction, i.e. for complex **3**, the reductive event at -1.12 V is associated with the oxidative event at -0.99 V and the reductive event at -1.28 V is associated with the

oxidative event at -1.21 V. The square wave voltammograms display broad peaks, rather than well defined, separated peaks, suggesting that there are multiple overlapping events associated with the two observable events of the cyclic voltammograms. For complex **2**, three reduction events are observed at -1.29, -1.67, and -1.98 V. Again, isolation of the successive waves suggest that the oxidation events upon scan reversal at -1.09 and -1.41 V are associated with the events at -1.29 and -1.67 V, respectively. The square wave voltammogram is even broader, also suggesting the presence of several redox events in the -1.29 to -2.0 V region. The patterns of the cyclic voltammograms are consistent with previously observed polymetallics that have multiple redox events.[91,92]

Assuming that the tetramers remain intact in CH_2Cl_2 solution during the electrochemical experiment, we might expect to observe four individual, $\{Fe(NO)_2\}^{9/10}$ redox events. Broad and poorly defined events in both the cyclic voltammograms and square wave voltammograms suggest that these four reduction events may occur near similar voltage values, resulting in the apparent overlap of signal. Other neutral $\{Fe(NO)_2\}^9$ complexes, such as (NHC-iPr)(SPh)$Fe(NO)_2$[90] and (Ar-nacnac)$Fe(NO)_2$,[38] show reversible, well-defined redox couples in THF at $E_{1/2}$ = -1.33 and -1.34 V, respectively. For complexes **1**, **2**, and **3**, the first observable reduction events occur at -1.20, -1.29, and -1.12 V, respectively. As imidazole is a weaker donor compared to N-heterocyclic carbenes, and imidazolates are weaker donors than thiolates and diketiminates (discussed in Chapter III), we would expect reduction of **1**, **2**, and **3** to be slightly easier (more positive), on the basis of typical donor/acceptor ability arguments. This is observed for all three complexes.

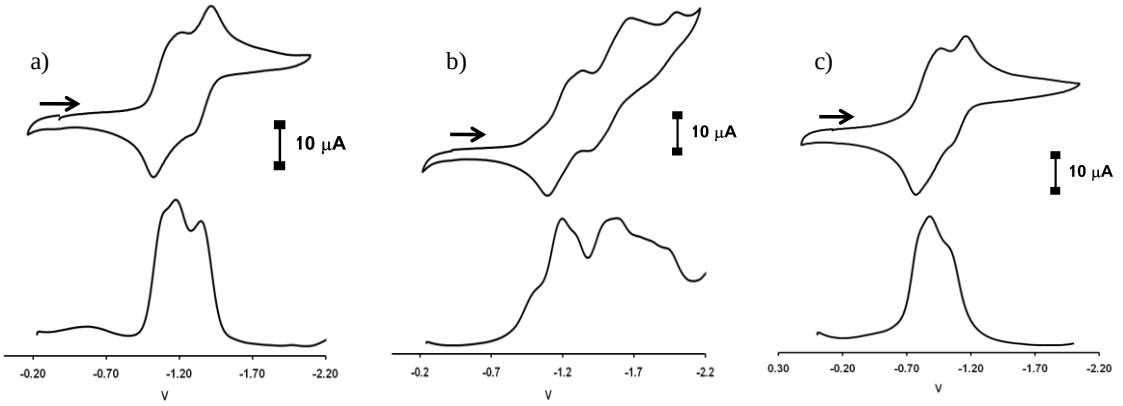

Figure IV-9. Cyclic and square wave voltammograms of complexes a), **1**; b), **2**; c), **3** in 2 mM CH_2Cl_2 solution. All are referenced to Cp_2Fe/Cp_2Fe^+.

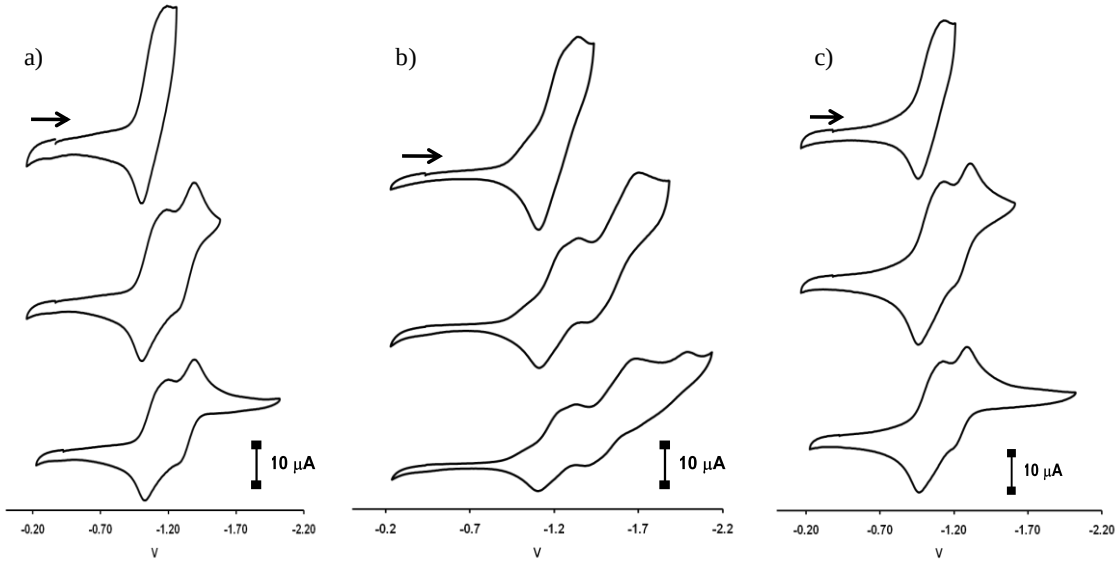

Figure IV-10. Scan reversals of the cyclic voltammograms to isolate successive waves of complexes a), **1**; b), **2**; c), **3** in 2 mM CH_2Cl_2 solution. All are referenced to Cp_2Fe/Cp_2Fe^+.

As previously reported, the difference between the first and second reduction potentials of polymetallic complexes provide a measure of the delocalization of the

mixed valence species and the stability of the species formed upon initial reduction.[92,93] In a nickel trimer, $[(Ni\text{-}1)_2Ni]^{2+}$ where "1" = 1,5-bis(mercaptoethyl)-1,5-diazacyclooctane, the ΔE of the reductions is 0.95 V, whereas the ΔE for a Ni-Zn paddlewheel complex, $(Ni\text{-}1)_3(ZnCl)_2^{2+}$, is 0.22 V (0.20 V for the difference between the second and third events).[92] As these two complexes are at the upper and lower ranges, respectively, for a series of Ni-containing polymetallics, it was determined that the larger value of ΔE for $[(Ni\text{-}1)_2Ni]^{2+}$ reflects delocalization between the three Ni^{II} and that the first reduction influences the subsequent reductions. However, for the Ni-Zn paddlewheel complex, the small ΔE suggests significant localization of the reduction events.[92] The ΔE values for complexes **1**, **2**, and **3** are listed in Table IV-3. The ΔE for complexes **1** and **3**, 0.19 and 0.16 V, respectively are small in magnitude compared with the Ni-containing polymetallic series[92] suggesting substantial localization of the reduction events. For complex **2**, the ΔE values (difference between the second and first reductions and the difference between the third and second reductions) are 0.38 and 0.31 V suggesting slightly greater delocalization of the reduction events; i.e., the first reduction seems to have a greater effect on the subsequent reductions.

Mössbauer Spectroscopic Studies

(Recorded by Gregory Holmes-Hampton of the P. A. Lindahl group.)

As solution samples at ~ 50 mM in THF solvent, complexes **1**, **2**, and **3** exhibit sharp quadrupole doublets at 5 K (Figure IV-11) with isomer shifts of 0.289, 0.276, and 0.270 mm/s, respectively, and quadrupole splitting parameters of 0.700, 0.717, and 0.768

mm/s, respectively. Mössbauer data were also obtained for a well-characterized set of test compounds, prepared as described in Chapter III, in order to provide a series of related compounds in which to compare with the Mössbauer spectral data of the tetramers. The Mössbauer data for the test compounds and corresponding structures are given in Figure IV-12.

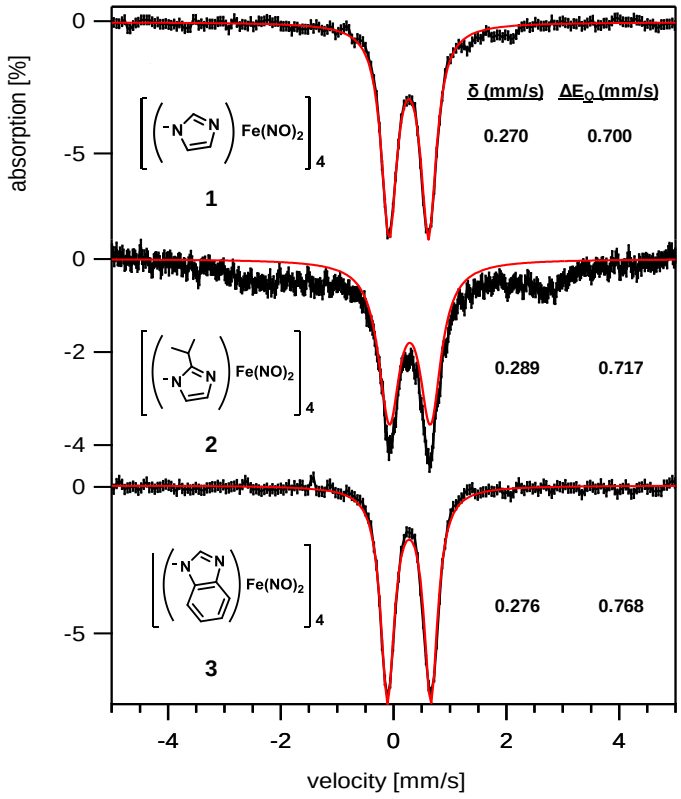

Figure IV-11. 5 K Mössbauer spectra for tetrameric complexes **1**, **2**, and **3** in frozen THF solution in an applied field of 700 G.

Typically, positive isomer shifts have been correlated with metal-based reductions in the presence of innocent donor ligands.[94] In these cases, reductions of the metal may result in longer M-L bonds. However, the presence and extent of π-backbonding onto the ligands results in a negative isomer shift.[94] Mössbauer data has been reported and interpreted for the reduced and oxidized $[(\text{Ar-nacnac})\text{Fe}(\text{NO})_2]^{-/0}$ complexes (Ar-nacnac = 2,6-diisopropylphenyl) prepared and characterized by the Lippard group.[38] The isomer shifts for the reduced and oxidized forms are extremely close, 0.22 and 0.19 mm/s, respectively.[95] As NO ligands are notoriously "non-innocent," and the Ar-nacnac ligand is also potentially redox-active, the question of ligand-based versus metal-based redox process in the Lippard system was approached by Ye and Neese in DFT studies.[95] The DFT calculations find that the 3d orbitals for iron in the reduced DNIC are energetically closer to the NO π* orbitals resulting in greater π-backbonding and thus a smaller isomer shift than what is expected for a metal-based reduction as compared to the oxidized analogue.[95] The role of the Ar-nacnac ligand as π-donor/ π-acceptor was not discussed.

The test compounds we have chosen as references for the tetramers contain spectator ligands with varying donor/acceptor properties, σ-donors (NHCs), π-acceptor (CO), and π-donor (SPh). Test compounds A and C are reduced $\{\text{Fe}(\text{NO})_2\}^{10}$ complexes. Complex A contains two strong σ-donating N-heterocyclic carbene ligands (NHC) bound to the $\text{Fe}(\text{NO})_2$ unit, whereas, for complex B one of the NHC ligands is replaced with CO, a weaker σ-donor, but a stronger π-backbonding ligand. Test

compounds B and D are oxidized $\{Fe(NO)_2\}^9$ complexes. Complex B is the cationic, oxidized analogue of complex A containing two strongly σ-donating NHCs. Complex

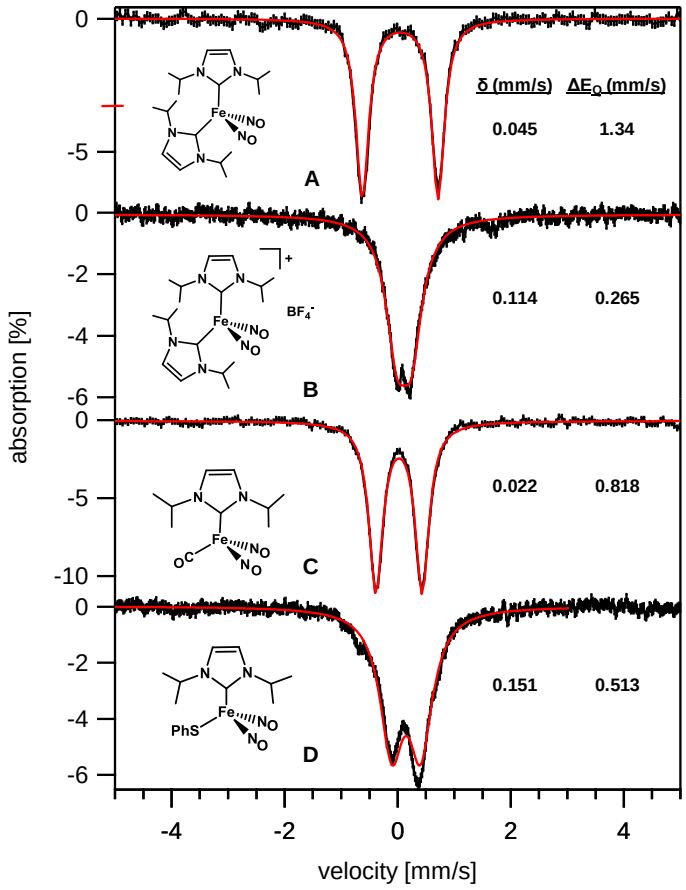

Figure IV-12. 5 K Mössbauer spectra of test complexes A-D in frozen THF solution in an applied field of 700 G.

D, on the other hand, is a neutral complex containing a strongly σ-donating NHC and a strong π-donor, phenyl thiolate (SPh). In the case of the test compounds where A and C are reduced $\{Fe(NO)_2\}^{10}$ complexes, the isomer shifts of 0.045 and 0.022 mm/s,

respectively are distinctly lower than for B and D, the oxidized $\{Fe(NO)_2\}^9$ complexes (0.114 and 0.151 mm/s, respectively). Even though A and C reflect Fe in a reduced state relative to B and D, the isomer shifts are shifted negatively as compared to those of B and D. Thus, the extent of π-backbonding is presumed to be greater in the reduced complexes accounting for the negative isomer shift. The π-backbonding of the NO ligands overwhelms the formal change in oxidation state. Additionally, the negative shift of A and C may also reflect the strong σ-donor character of the NHC ligands. Test complexes B and D also demonstrate this trend, where B contains two NHC ligands and has an isomer shift of 0.114 mm/s, while D only contains one NHC ligand, and a strong π-donor in the PhS^- ligand, and has a slightly larger isomer shift of 0.151 mm/s.

The isomer shifts of tetramers **1**, **2**, and **3** are significantly larger than those of the test complexes. Though the $Fe(NO)_2$ units are in the oxidized state, these larger shifts may be due to the fact that the σ-donating ability of the N-donors of the imidazole ligand, in a bridging mode, is less than that of the NHC.

As the extent of π-backbonding within compounds A and C is presumed to be greater than in test compounds B and D, our results are consistent with the Ye and Neese study that demonstrate that the extent of π-backbonding greatly affects the magnitude of the isomer shift.[95] Note that the similar isomer shifts of the Ar-nacnac DNIC redox pair and that of the tetrameric complexes **1** - **3** suggest a similar electronic environment induced by N-donors, one of which is anionic on the $\{Fe(NO)_2\}^9$ unit. Mössbauer spectral data of other N-containing DNICs, specifically of monomeric DNICs containing either imidazole or imidazolate donors for the purpose of comparing to the tetramer data

awaits future study. Additionally, DFT calculations of the electronic structures of the test complexes as well as the tetramers (underway by coworker Scott Brothers under the guidance of Prof. M. B. Hall) may provide a clear picture of the extent of orbital overlap and π-backbonding character as a means to support the claims made above.

Summary and Comments

Despite the presence of bridging imidazolates in biomolecules as well as a variety of inorganic complexes,[87,88,96,97] to our knowledge, only one DNIC containing bridging imidazolate ligands, complex **1**, was reported previous to this study.[83] Tetrameric complexes **1**, **2**, and **3** form as molecular squares; the orientation of the imidazolate ligand with respect to the Fe_4 plane in the crystal structures seem to be influenced by both steric interactions of the imidazolate substituents and crystal-packing forces. In solution, the orientation of the imidazolates may be flexible in that edges that are oriented outwardly may waggle to an inward position and vice versa.

EPR spectroscopic studies find g values of ~ 2.03 for all three tetrameric complexes, however, N-14 hyperfine coupling is not observed. There are only a few examples of DNICs that exhibit hyperfine coupling in the EPR spectra.[35-37,39,83] In fact, we do not see hyperfine features in an imidazole-containing DNIC, $(Imid)(PhS)Fe(NO)_2$ synthesized in the MYD laboratory. The correlation between DNIC structure and observation of hyperfine coupling to N-donor ligands or the NO ligands still remains unclear.

CHAPTER V

SYNTHETIC $(N_2S_2)M(NO)$ MODEL COMPLEXES (M = Fe, Co) AS METALLODITHIOLATE LIGANDS[†*]

A. Sulfur Reactivity and Electronic Effects of $(N_2S_2)M(NO)$ Complexes: Introduction

A series of $(N_2S_2)M(NO)$ (M = Fe, Co) model complexes bearing first coordination sphere compositional and structural similarity to the nitrile hydratase active site, where N_2S_2 = bme-daco (*N,N'*-bis(2-mercaptoethyl)-1,4-diazacycloheptane), designated as ligand **1**, and bme-dach (*N,N'*-bis(2-mercaptoethyl)-1,4-diazacyclooctane, **1′** was synthesized by earlier coworkers in the MYD laboratory.[73] These complexes are similar to a series of $Ni(N_2S_2)$ complexes reported by the MYD group and others, Figure V-1.[98,99] The $Ni(N_2S_2)$ complexes have demonstrated sulfur-based reactivity towards alkylating agents, such as 1,3-dibromopropane or methyliodide to form the corresponding thio-ether adducts[100,101] and towards oxygen, forming a variety of sulfinate (SO_2) or sulfenate (SO) complexes of the form $NiN_2S_{thiolate}S_{sulfinate}$, $NiN_2S_{sulfinate}S_{sulfinate}$, $NiN_2S_{thiolate}S_{sulfenate}$, and $NiN_2S_{sulfenate}S_{sulfenate}$.[102] This S-reactivity towards oxygen of the synthetic model complexes bears interesting similarities to the post-translationally modified cysteine sulfurs of the nitrile hydratase active site, in which

---

[†]Reproduced in part with permission from Hess, J. L.; Conder, H. L.; Green, K. N.; Darensbourg, M. Y. *Inorg. Chem.* **2008**, *47*, 2056-2063. Copyright **2008** American Chemical Society.

[*]Reproduced in part with permission from Hess, J. L.; Young, M. D.; Murillo, C. A.; Darensbourg, M. Y. *J. Mol. Struct.* **2008**, *890*, 70-74. Copyright **2008** Elsevier.

one sulfur is identified as a cysteine sulfinate (Cys-SO_2) and the other identified as a cysteine sulfenate (Cys-SO_2).[51]

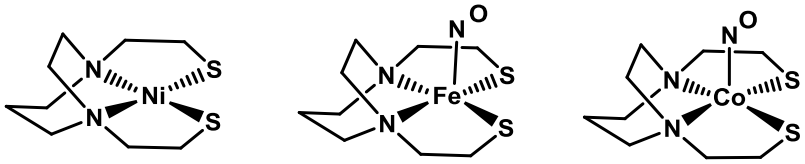

Figure V-1. Structures of (bme-dach)Ni,[98] (bme-dach)Fe(NO),[73] and (bme-dach)Co(NO),[73] where bme-dach = *N,N'*-bis(2-mercaptoethyl)-1,4-diazacyclooctane.

Further elucidation of the properties of these synthetic model complexes uncovered nearly identical one-electron reduction potentials for the (bme-dach)Co(NO) and (bme-dach)Fe(NO) complexes, despite their different Enemark-Feltham electron counts of $\{Co(NO)\}^8$ and $\{Fe(NO)\}^7$, respectively (Scheme V-1).[73] The former is isoelectronic with Ni^{II} (d^8) and the latter with Ni^{III} (d^7). This interesting concurrence of reduction potentials can possibly be explained by the structures of the nitrosyl complexes, which contain multiple points of electronic buffering, i.e., the M-N-O angle and the degree to which the M is displaced from the N_2S_2 plane, producing different levels of M-NR_3 and M-SR covalent interactions.[73]

Scheme V-1. Comparisons of the Reduction Potentials of (bme-dach)Ni^{II}, (bme-dach)Co(NO), and (bme-dach)Fe(NO)[103,73]

$$\text{(bme-dach)}Ni^{II}\ (d^8) \overset{e^-}{\rightleftharpoons} \text{(bme-dach)}Ni^{I}\ (d^9)$$

$$E_{1/2} = -2.1\ V$$

$$\text{(bme-dach)M(NO)} \overset{e^-}{\rightleftharpoons} [\text{(bme-dach)M(NO)}]^-$$

$$M(NO) = \{Co(NO)\}^8/\{Co(NO)\}^9;\quad E_{1/2} = -1.10\ V$$

$$= \{Fe(NO)\}^7/\{Fe(NO)\}^8;\quad E_{1/2} = -1.13\ V$$

In order to further probe the distinctive electronic properties in such $(N_2S_2)M(NO)$ complexes, we devised a study of such complexes as adducts of $W(CO)_4$, the formation of which ties up or neutralizes the sulfur electron density through thiolate bridging to the tungsten(0). Such $[(N_2S_2)M(NO)]W(CO)_4$ complexes would then have two spectroscopic reporters of electron distribution, the ν(NO) and ν(CO) vibrational probes. Furthermore, these heterobimetallics are of similar structure and geometry to $[(N_2S_2)Ni]W(CO)_4$ complexes, the ν(CO) values of which were used to rank the electron-donating ability of *cis*-dithiolate complexes as ligands with classic ligands such as phosphines and diimines.[103,104] The study described herein further explores the electronic character of the $(N_2S_2)M(NO)$ complexes and their capability to serve as metalloligands (see Figure V-2).

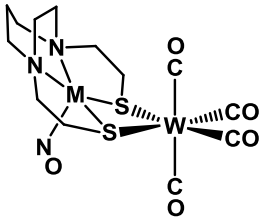

Figure V-2. Target compound (M = Co, Fe) displaying the $W(CO)_4$ adduct formed via the bridging dithiolate sulfurs of the (bme-dach)M(NO) metalloligands.

Physical Properties and Structures

The [Co-1′(NO)]$W(CO)_4$, and [Fe-1′(NO)]$W(CO)_4$ compounds were prepared on ligand displacement of piperidine in $(pip)_2W(CO)_4$ [72] by Co-1′(NO) or Fe-1′(NO), respectively at 40 °C over the course of 15 minutes. They were isolated as thermally stable (decomposition points at temperatures greater than 200 °C), intensely colored crystalline solids that are moderately air-stable. They degrade over the course of a few days in the absence of a strict anaerobic environment. The Co-1′(NO) and Fe-1′(NO) "free ligand" complexes are highly soluble in CH_2Cl_2 and DMF and moderately soluble in CH_3CN; the heterobimetallics [Co-1′(NO)]$W(CO)_4$ and [Fe-1′(NO)]$W(CO)_4$ are highly soluble in DMF, only moderately soluble in CH_2Cl_2, and sparingly soluble in CH_3CN. The cobalt derivatives are both diamagnetic, while Fe-1′(NO) and [Fe-1′(NO)]$W(CO)_4$ have μ_{obs} values (Evans method) of 1.6 ± 0.1 and 1.8 ± 0.1 μ_B, respectively, consistent with S = ½ in the $\{Fe(NO)\}^7$ electronic configuration and low-spin iron. The IR spectral properties and electrochemical data are presented below.

The paramagnetic Fe-1′(NO) and [Fe-1′(NO)]$W(CO)_4$ complexes both show a single isotropic signal in their EPR spectra with g values of 2.030 and 2.022, respectively. Experimental (frozen DMF solution) and simulated EPR spectra are given in Figure V-3. The isotropic signal and lack of hyperfine coupling suggest that the unpaired electron of the S = ½ systems is delocalized in the $\{Fe(NO)\}^7$ unit. The EPR spectrum of Fe-1′(NO) is similar to that previously reported, whose measurement was in CH_2Cl_2 at 298 K.[73] Interestingly, the isotropic signal in an analogous complex, (bme*-daco)Fe(NO), where bme*-daco = N,N-bis(2-methyl-2-mercaptoethyl)-1,5 diazacyclooctane, shows distinct hyperfine coupling to ^{14}N impinged on the isotropic signal, as has been seen in (tetraphenylporphyrin)Fe(NO).[105]

The molecular structures of Co-1′(NO), [Co-1′(NO)]$W(CO)_4$, and [Fe1′(NO)]$W(CO)_4$ were determined by X-ray diffraction analysis; thermal ellipsoid plots are shown in Figure V-4. Select metric data for Co-1′(NO), [Co-1′(NO)]$W(CO)_4$, Fe-1′(NO), and [Fe(bme-dach)NO]$W(CO)_4$ are presented in Table V-1, along with data for the analogous [Ni-1′]$W(CO)_4$ complex.[73,103]

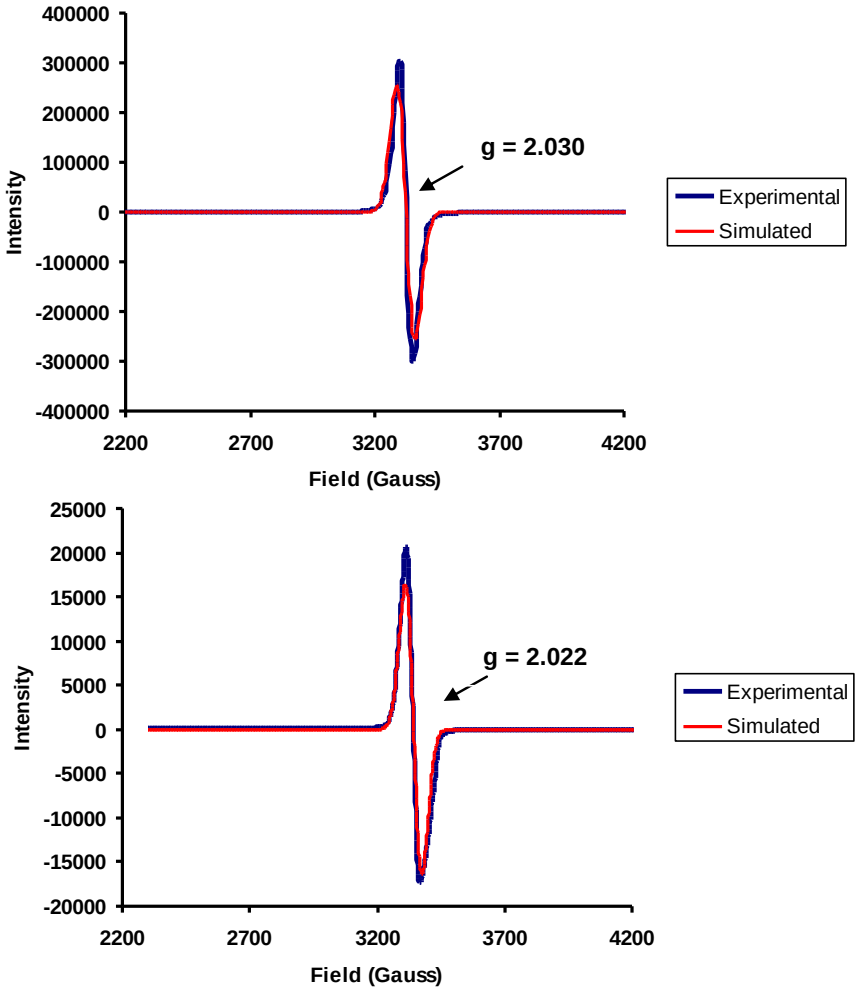

Figure V-3. Experimental and simulated EPR spectra of a) Fe-1'(NO) and b) [Fe-1'(NO)]$W(CO)_4$ at 9 K in DMF solution(glass).

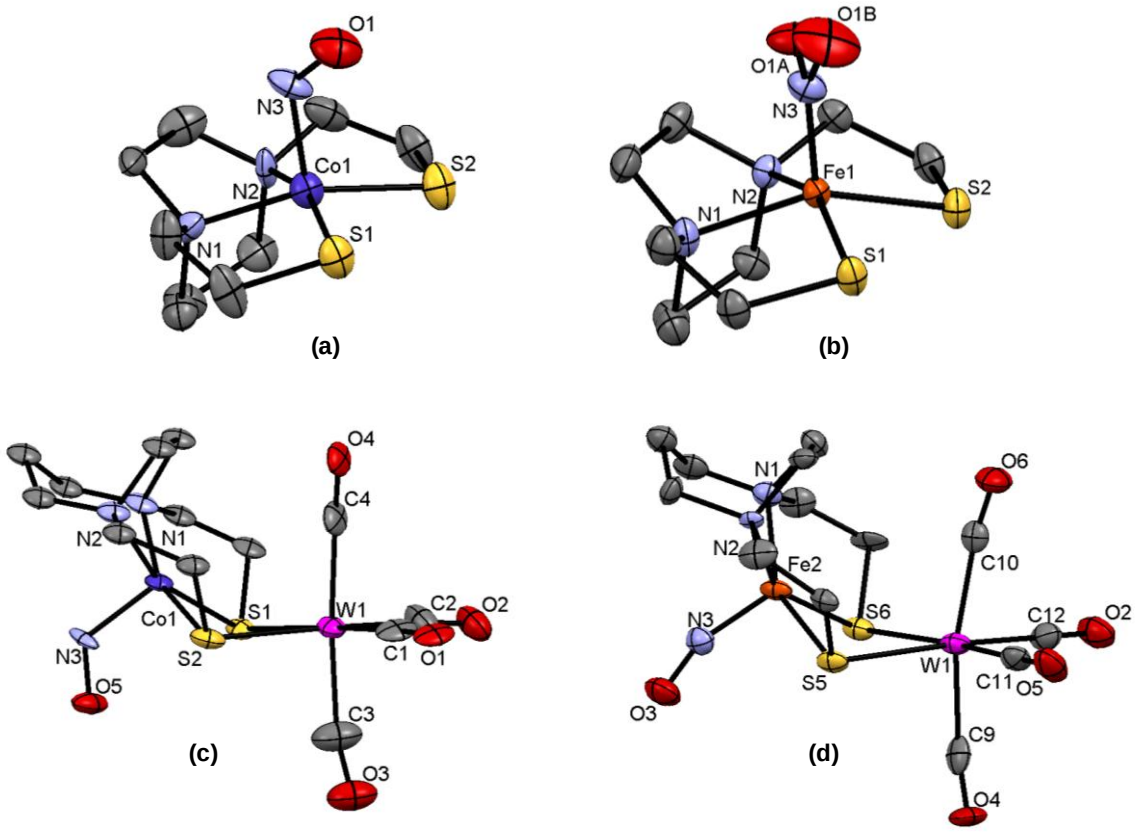

Figure V-4. Thermal ellipsoid plots of the molecular structures of a) (bme-dach)Co(NO) or Co-1'(NO); b) (bme-dach)Fe(NO) or Fe-1'(NO);[73] c) [(bme-dach)Co(NO)]$W(CO)_4$ or [Co-1'(NO)]$W(CO)_4$; and d) [(bme-dach)Fe(NO)]$W(CO)_4$ or [Fe-1'(NO)]$W(CO)_4$, with select atoms labeled and hydrogen atoms omitted.

The molecular structures of the [Co-1′(NO)]$W(CO)_4$, [Fe-1′(NO)]$W(CO)_4$, and [Ni-1′]$W(CO)_4$ complexes are similar in that the connection of the (N_2S_2)M unit to $W(CO)_4$ creates an octahedral geometry at tungsten with S-W-S bite angles of ca. 75° for all. The residual lone pair of each sulfur generates a hinge in the bridge between the two metals whose angle is calculated as the dihedral angle between the N_2S_2 and $S_2W(CO)_2$ best planes. This angle is 127.5° for the Co-1′(NO) and Ni-1′ adducts of $W(CO)_4$ and 121.2° for the Fe-1′(NO) analogue. Note that the M in the MNO units is displaced out of

the N_2S_2 planes and away from the $W(CO)_4$ unit, thus orienting the pendant N-O groups as distant as possible from the metal-carbonyl. This displacement is 0.076 Å greater in the Co-W adduct, while the same feature in the Fe(NO) analogue is unchanged.

As seen in Table V-1, the metric parameters of the metalloligands change little upon complexation to $W(CO)_4$. The most substantial difference occurs for the displacement of cobalt out of the N_2S_2 plane, which increases by ca. 0.08 Å from the Co-1′(NO) complex, 0.306 Å, to 0.382 Å for the [Co-1′(NO)]$W(CO)_4$ complex. In contrast, the same parameter for the Fe-1′(NO) analogue is constant. For both the cobalt and iron derivatives, the S-M-S angle is constricted by ca. 6° upon complexation to the $W(CO)_4$ unit.

While the M-N-O angle might be expected to respond to the electronic changes occurring at the cobalt or iron center with adduct formation, only minor changes are observed. The Co-N-O angle of 123.8° of Co-1′(NO) is largely the same as that in the $W(CO)_4$ derivative, 123.1°. For Fe-1′(NO), disorder in the NO group in the crystal structure results in two refined Fe-N-O angles of 152.4 and 144°, averaging to 148°.[73] There is a minor increase toward linearity in [Fe-1′(NO)]$W(CO)_4$: the Fe-N-O angle is 155.4°. The most impressive difference in the "free ligand", as contrasted to the $W(CO)_4$-bound form, is the position of the NO ligand with respect to the unsymmetric diazamesocycle. In the unbound Co-1′(NO) and Fe-1′(NO) units, the NO lies on the two-carbon side of the diazacycloheptane ring while, once bound, it is found on the three-carbon side, with metal displacement from the N_2S_2 planes toward the NO position

accordingly. The reason for this switch is as unclear as the mechanism whereby such isomerism might occur.

Table V-1. Selected bond distances and bond angles of Co-1'(NO), [Co-1'(NO)]$W(CO)_4$, Fe-1'(NO), [Fe-1'(NO)]$W(CO)_4$, and [Ni-1']$W(CO)_4$[73,103] . See Figure V-3 for atom labeling.

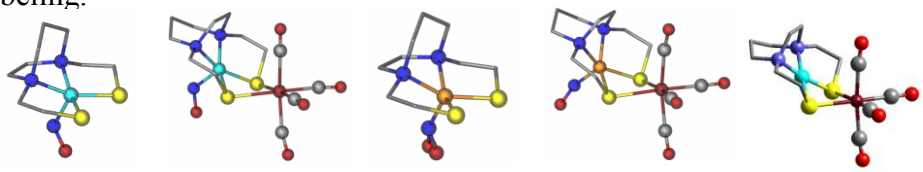

Complex	Co-1'(NO)	[Co-1'(NO)]-$W(CO)_4$	Fe-1'(NO) [73]	[Fe-1'(NO)]-$W(CO)_4$	[Ni-1']-$W(CO)_4$ [103]
M-W	--	3.386	--	3.432	3.249
M-C(4)	--	3.568	--	3.834	3.388
M-N (NO)	1.787(7)	1.80(2)	1.705(2)	1.697(8)	--
W-C(1)	--	2.00(2)	--	1.979(8)	2.03(4)
W-C(2)	--	2.01(2)	--	1.938(8)	2.03(8)
W-C(3)	--	2.05(2)	--	2.037(8)	1.96(15)
W-C(4)	--	2.05 (2)	--	2.052(8)	1.96(15)
W-S_{avg}	--	2.586(7)	--	2.574(2)	2.573(2)
M-S_{avg}	2.22 (2)	2.224(7)	2.2314(7)	2.26(2)	2.17(16)
M-N_{avg} (N_2S_2)	1.964(4)	2.00(2)	2.013(2)	2.033(1)	1.93(14)
M-N_2S_2 disp[a]	0.3063	0.3823	0.5525	0.5498	0.00
C(1)-W-C(2)	--	85.2(9)	--	91.0(3)	91(9)
C(3)-W-C(4)	--	175.5(9)	--	166.6(3)	172.6(10)
W-C(1)-O(1)	--	176.0(15)	--	179.9(9)	174.7(11)
W-C(2)-O(2)	--	174(2)	--	173.8(6)	174.9(10)
S(1)-W-S(2)	--	75.1(1)	--	75.64(5)	75(8)
S(1)-M-S(2)	96.4(1)	90.2(2)	94.91(3)	88.66(7)	92(9)
N(1)-M-N(2)	80.6(3)	82.2(5)	79.03(9)	79.9(2)	83(7)
M-N-O	123.8(7)	123.1(2)	148(2)	155.4(8)	--
Dihedral[b]	--	127.5	--	121.2	127.5

[a]Displacement of M from N_2S_2 best plane. [b]Angle between the N_2S_2 best plane and the $S_2W(CO)_2$ plane.

There is an apparent preference for the N-O bond vector to eclipse the M-S bond vector in the iron compounds,[73] whereas the N-O bond vectors of the cobalt compounds

bisect the two M-S bond vectors both in the tungsten adducts and in the free ligand. This observation is made clearer in the views of the structures shown in Figure V-5. Preliminary density functional theory (DFT) calculations by Jesse Tye and Roxanne Jenkins have suggested that the orientation of the NO bond vector of Co-1′(NO) does not greatly affect the stability of the complex because there is no more than a 2 kcal/mol difference between a variety of rotated NO bond vector positions.[ref] According to this result, crystal packing forces would be sufficient to control the position of the NO bond vector.[106]

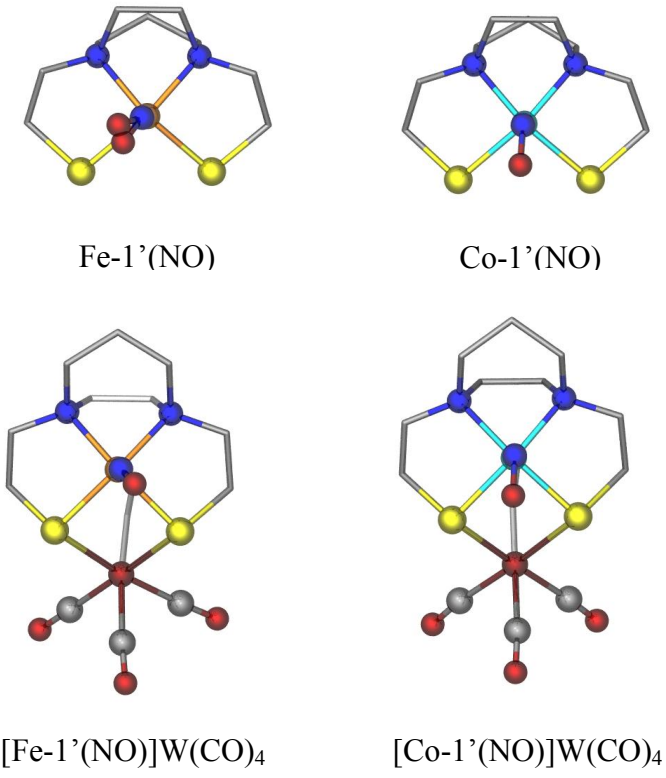

Figure V-5. A “bird’s eye” view of the M-1’(NO) units in the free metalloligand and in those complexed to $W(CO)_4$, focusing on the position of the NO bond vector (N of NO and the M are eclipsed).

Diatomic Ligand Vibrational Spectroscopy, ν(CO) and ν(NO)

The diatomic ligand IR spectra of [Co-1′(NO)]$W(CO)_4$ and [Fe-1′(NO)]$W(CO)_4$ were recorded in CH_2Cl_2 and DMF solvents. The latter gives a better resolution for the ν(CO) bands; however, the ν(NO) band is obscured by the strong absorbance of DMF in the same region. Hence, the ν(NO) absorbances are reported as measured in CH_2Cl_2. Four bands assignable to ν(CO) are observed in the 1800–2000 cm^{-1} range, with patterns similar to those reported for the [(N_2S_2)Ni]$W(CO)_4$ complexes.[103] The absorptions are listed in Table V-2 with assignments according to the pseudo-C_{2v} symmetry of the $W(CO)_4$ moiety. For comparison, the ν(CO) values of [Ni-1′]$W(CO)_4$, [(bme-daco)Ni]$W(CO)_4$, $\{[(ema)Ni]W(CO)_4\}^{2-}$, and $(pip)_2W(CO)_4$ are also given. Thus, assuming that the ν(CO) values are reporting electron density at the tungsten according to the typical σ-donor/π-back-bonding arguments,[107] the sulfur donors of the metallodithiolate ligands are seen to be better donors to $W(CO)_4$ than are piperidine ligands of $(pip)_2W(CO)_4$.[103] Furthermore, the electron donor abilities of [Co-1′(NO)] and [Fe-1′(NO)] toward $W(CO)_4$ are slightly poorer than those of the neutral NiN_2S_2 complexes, while, as expected, the dianionic $Ni(ema)^{2-}$ ligand appears to transfer most electron density to the $W(CO)_4$ acceptor.

The ν(NO) frequencies of the M-W bimetallic complexes compared to those of the free ligands, Co-1′(NO) and Fe-1′(NO), are also listed in Table V-2. The adduct formation with $W(CO)_4$ results in a positive shift in the ν(NO) values consistent with the withdrawal of electron density from the metallodithiolate ligand. The observation that the ν(NO) stretch of Fe-1′(NO) is affected more by $W(CO)_4$ adduct formation than is

that of Co-1′(NO), with positive shifts of 48 and 35 cm^{-1}, respectively, will be discussed below.

Table V-2. Diatomic ligand infrared data: ν(NO) and ν(CO) stretching frequencies (cm^{-1})[a,b, 103]

	ν(NO)	ν(CO)			
Compound		$\nu(A_1^1)$	$\nu(B_1)$	$\nu(A_1^2)$	$\nu(B_2)$
Co-1'(NO)	1603[b]				
[Co-1'(NO)]$W(CO)_4$	1638[b]	1997m	1878s	1851s	1824s
		(2002m)[b]	(1889s)	(1844s,br)	(1830s,br)
Fe-1'(NO)	1649[b]				
[Fe-1'(NO)]$W(CO)_4$	1697[b]	1998	1880	1854	1827
		(2004m)[b]	(1892s)	(1846s,br)	(1833s,br)
[Ni-1']$W(CO)_4$		1996	1873	1852	1817
[(bme-daco)Ni]$W(CO)_4$[c]		1995	1871	1853	1819
$[((ema)Ni)W(CO)_4]^{2-}(Et_4N)_2$[c]		1986	1853	1837	1791
$(pip)_2W(CO)_4$		2000	1863	1852	1809

[a]DMF solution spectra except where noted.
[b]Spectral measurements in CH_2Cl_2 solution.
[c](bme-daco = 1,5-Bis(2-mercaptoethyl)-1,5-diazacyclooctane)[103]; (ema = N,N'-ethylenebis(2-mercaptoacetamide))[103].

Electrochemical Studies

Cyclic voltammograms of Co-1′(NO), Fe-1′(NO), [Co-1′(NO)]$W(CO)_4$, and [Fe-1′(NO)]$W(CO)_4$ were recorded at room temperature in DMF solutions containing 0.1 M [*n*-Bu_4N][BF_4]. Selected scans are given in Figure V-6, and a summary of the electrochemical data is listed in Table V-3.

In general, the [Co-1′(NO)]$W(CO)_4$ and [Fe-1′(NO)]$W(CO)_4$ complexes undergo one reversible reduction and one irreversible oxidation, or quasi-reversible as is the case with [Fe-1′(NO)]$W(CO)_4$. The former occur at -0.59 and -0.47 V and are assigned to the $\{Co(NO)\}^{8/9}$ and $\{Fe(NO)\}^{7/8}$ redox couples, respectively. The greater ease of reduction in the $W(CO)_4$ adducts is indicated by the shift to more positive potentials by ca. 0.55 V as compared to the ca. -1.1 V redox events in the free Co-1′(NO) or Fe-1′(NO) ligands. This observation is compatible with the coordination of the $W(CO)_4$ moiety, which withdraws electron density from the metalloligand via the bridging thiolate sulfurs, resulting in a stabilization of the reduced M(NO) unit.

The oxidation events that occur at 0.60 and 0.46 V, respectively, are only slightly shifted (more positively) as compared to the free ligands. Furthermore, when the cyclic voltammogram of the [Co-1′(NO)]$W(CO)_4$ derivative is initiated at -1.5 V and recorded in the positive direction, two irreversible oxidation events appear at -0.12 and -0.23 V; a decomposition product likely from the 0.60 V event. Similarly, there are two additional oxidation events (+0.38 and -0.017 V) in the scan of [Fe-1′(NO)]$W(CO)_4$ that likely belong to a decomposition product from the 0.46 V event. Highly similar oxidative events with similarly small influences of the $W(CO)_4$ adduct are seen in the NiN_2S_2 or Ni-1' complex versus the [Ni-1′]$W(CO)_4$ adduct.[103] These were tentatively assigned to sulfur-based oxidations, and at this point we have no evidence that would confirm or refute this assignment and its validity here. It should be noted that oxidative events appropriate to the $W(CO)_4$ moiety are not accessible within the scan range.

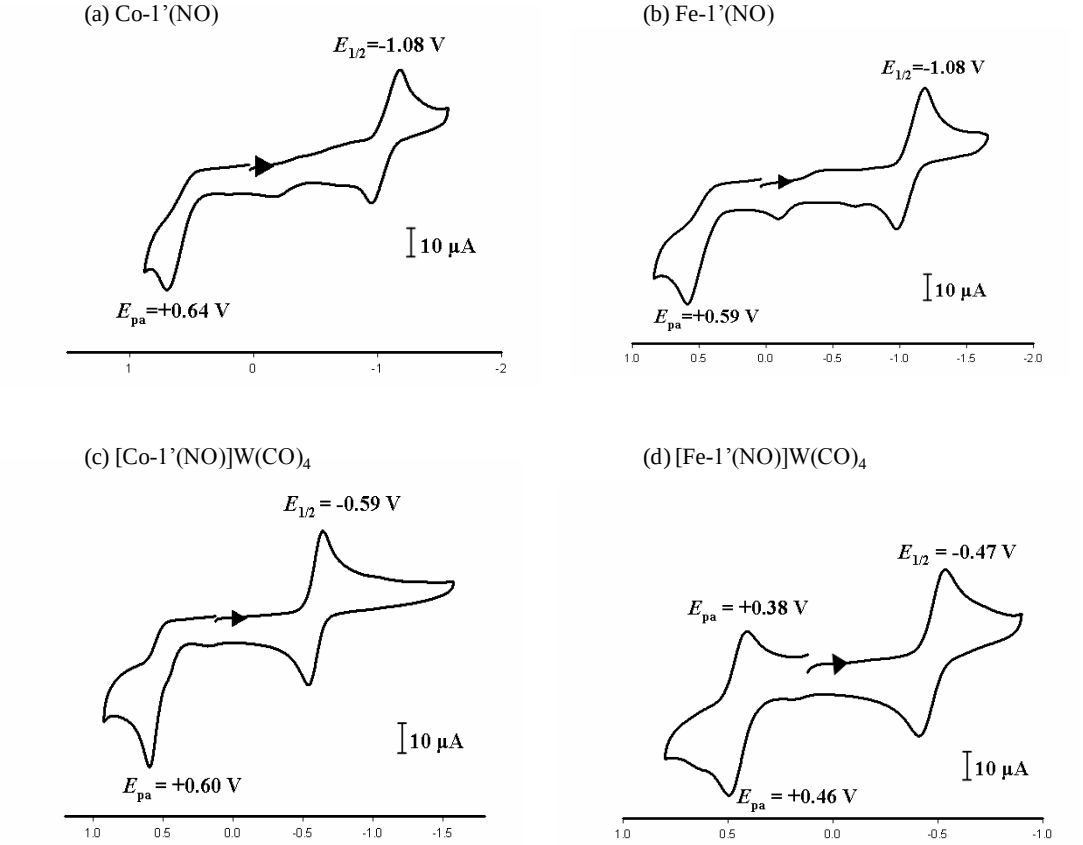

Figure V-6. Cyclic voltammograms of DMF solution of a) Co-1'(NO), b) Fe-1'(NO), c) [Co-1'(NO)]W(CO)$_4$, d) [Fe-1'(NO)]W(CO)$_4$ in 0.1 M n-Bu$_4$NBF$_4$ with a glassy carbon electrode at a scan rate of 200 mV/s.

Table V-3. Half-wave and anodic potentials for reductions and oxidations of Co-1'(NO), Fe-1'(NO), [Co-1'(NO)]W(CO)$_4$, and [Fe-1'(NO)]W(CO)$_4$ Complexes in DMF solvent.[a]

Compound	$E_{1/2}$(V) Rev. Reduction	E_{pa} Irr. Oxidation
Co-1'(NO)	-1.08	0.64
Fe-1'(NO)	-1.08	0.59
[Co-1'(NO)]W(CO)$_4$	-0.59	0.60
[Fe-1'(NO)]W(CO)$_4$	-0.47	0.46
Ni-1'	-2.03	0.21
[Ni-1']W(CO)$_4$	-1.51	0.30

[a]All potentials scaled to NHE as referenced to a Cp_2Fe/Cp_2Fe^+ standard ($E_{1/2}^{NHE}$ = 0.692 V; see Experimental Section). In DMF solutions, 0.1 M n-Bu$_4$NBF$_4$ electrolyte, glassy carbon working electrode, and Ag/AgCl reference electrode.

Comments and Comparisons

The overlay of [Co-1′(NO)]$W(CO)_4$, [Fe-1′(NO)]$W(CO)_4$, and [Ni-1′]$W(CO)_4$ structures (Figure V-7) displays similarities between the three structures that originate from the ability of all three metallodithiolates to serve as bidentate sulfur donor ligands to $W(CO)_4$ with bite angles of 75°. The graphic also impresses as to the inherent "hinge angle" that originates in the stereochemical effect of the residual lone pair on each sulfur atom donor.[108] A subtle but statistically significant difference in the Co-1′(NO) "free ligand" versus the [Co-1′(NO)]$W(CO)_4$ adduct is the displacement of cobalt out of the N_2S_2 best plane by 0.306 and 0.382, respectively. Such differences do not occur in the iron derivatives; however, a difference in the Fe-N-O angle is discernible. We conclude that the electronic effect of engaging the dithiolate as a ligand is experienced through the changes in metal displacement for the Co-1′(NO) complexes, whereas it is evidenced in a small measure through the changes in the M-N-O angles for the Fe-1′(NO) complexes. Such compensating steric features are expected to account for the concurrence of electrochemical or redox events as measured by cyclic voltammetry.

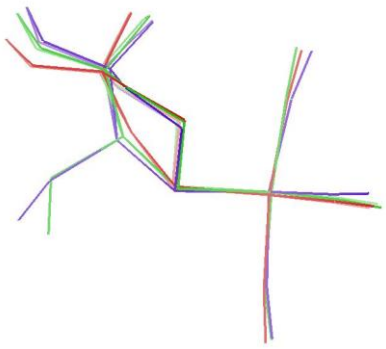

Figure V-7. Overlay of the [Co-1'(NO)]$W(CO)_4$, green, [Fe-1'(NO)]$W(CO)_4$, blue and [Ni-1']$W(CO)_4$,[103] red complexes.

It is instructive to contrast our square-pyramidal series of $(N_2S_2)M(NO)$ complexes with a set of $(N_4)M(NO)$ complexes (M = Fe, Co) derived from metalloporphyrins.[109] Within an $(N_4)[M(NO)]$ series, $\{M(NO)\}^6$, $\{M(NO)\}^7$, and $\{M(NO)\}^8$, there is reported "a systematic variation in the M-N-O angle, M-N(NO) bond length, and metal ion displacement (from the centroid of the N_4 porphyrin donor set)" according to the Enemark-Feltham electronic configuration of the $\{M(NO)\}^n$ unit, n = 6-8.[109] Greater M-N-O linearity correlates with higher oxidation levels of the Fe(NO) units; the linear $\{Fe(NO)\}^6$ unit (175°) has the greatest displacement (0.34 Å) from the N_4 plane, while in the $\{Fe(NO)\}^7$ complex (Fe-N-O is 145°), the deviation is less (0.28 Å). In contrast, $\{Co(NO)\}^8$ finds the cobalt almost coplanar (M_{disp} of 0.18 Å) and the Co-N-O angle is 122° (Chart V-1).[109]

In the case of the $(N_2S_2)M(NO)$ series (Chart V-1), iron displacement from the N_2S_2 plane (0.55 Å) is much more dramatic than it is in its $(N_4)\{Fe(NO)\}^7$ analogue, and neutralization of the thiolate sulfur charge by adduct formation with $W(CO)_4$ makes little difference. In contrast, the effect of diminishing the sulfur-donor ability to the $\{Co(NO)\}^8$ unit by $W(CO)_4$ adduct formation at thiolates, serves to increase the cobalt displacement out of the N_2S_2 plane. Because delocalization of electron density and the charge is less in the [Co(NO)] unit than in the [Fe(NO)] unit, there is expected to be a stronger electrostatic interaction between Co^{III} and the unfettered thiolate sulfur donors than to iron. Hence, the displacement of cobalt (reasonably assigned to Co^{III} in all cases here) out of the N_4, N_2S_2 and $N_2S'_2$ best planes correlates with the increasing soft character of the ligand donor set.

Chart V-1. Series of {Fe(NO)}^{7} and {Co(NO)}^{8} complexes focusing on the M-N-O angle and M ion displacement from the planar ligand donor set.[109] S' indicates modification by $W(CO)_4$ adduct formation. N_4 = porphyrin.[109]

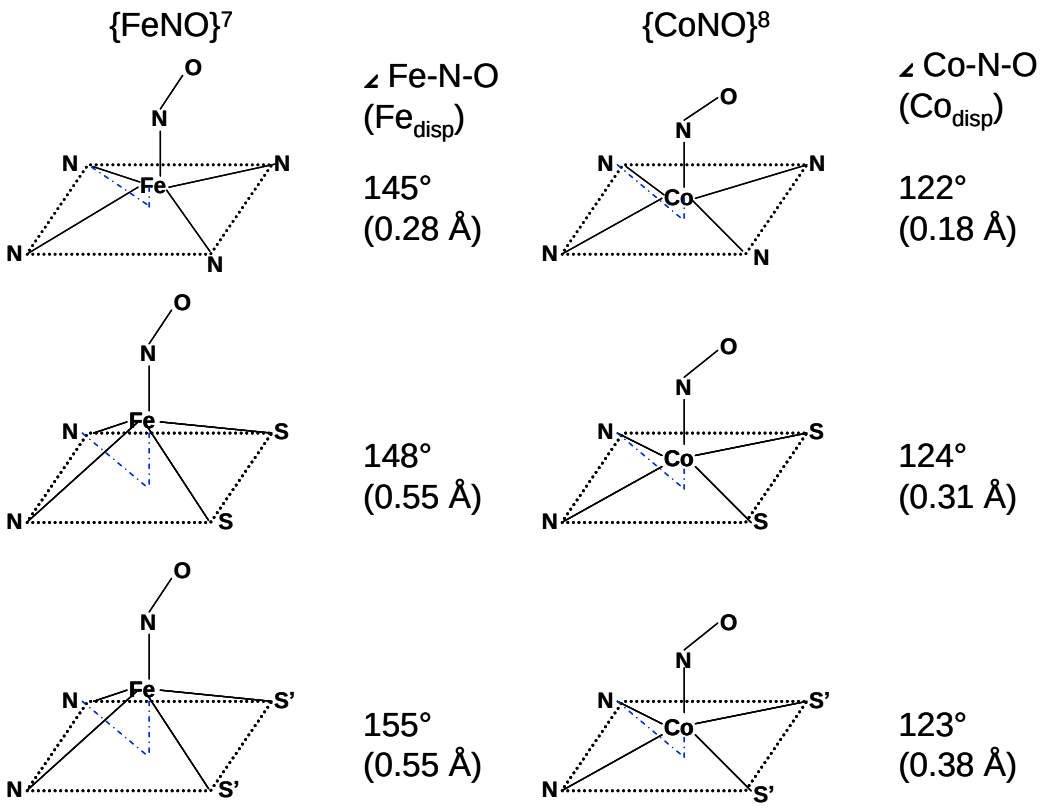

That the ligands transfer substantial electron density to tungsten is evidenced by shifts in the *v*(CO) and *v*(NO) stretching frequencies. The former reflects a donor ability of the Co-1′(NO) and Fe-1′(NO) ligands that is better than that of piperidine but poorer than the Ni-1′ dithiolate, while the *v*(NO) values suggest that the M(NO) unit experiences a less negative charge in the bimetallic, accountable to a shift in the thiolate electron density away from the M(NO) units as the $W(CO)_4$ adduct is formed.

Furthermore, electrochemical studies have shown that when bound to $W(CO)_4$, the [Co(NO)} and [Fe(NO)] moieties are more easily reduced by ca. 0.5 V, as compared to the Co-1′(NO) and Fe-1′(NO) free ligands. While the $Ni^{II/I}$ reduction is significantly more negative in both Ni-1′ and [Ni-1′]$W(CO)_4$, the differences between the reduction events of the free $Ni(N_2S_2)$ ligand and the $W(CO)_4$ adduct are very similar to those of the metal nitrosyl analogues.

B. $(N_2S_2)Fe(NO)$ as Ligand Paddles for the Construction of a Paramagnetic Trigonal Paddlewheel Complex: Introduction

As intimated above, the thiolate sulfurs of square planar $(N_2S_2)Ni$ complexes (N_2S_2 = bme-daco, N,N'-bis(2-mercapto-ethyl)-1,4-diazacycloheptane; bme-dach, N,N'-bis(2-mercapto-ethyl)-1,4-diazacycloheptane) have been well established as versatile metalloligands. The electron-donating ability of these dithiolates has been investigated through the formation of $[(N_2S_2)Ni]W(CO)_4$ adducts utilizing the CO ligand as a spectroscopic probe.[103] Through shifts in the ν(CO) stretching frequencies in a series of complexes, we have concluded that these $(N_2S_2)M$ metalloligands are comparable, if not better, donors than classic coordinating ligands, such as amines, diphosphines, and diimines,[103] and they form stable heterobimetallic complexes.

As a result, it is not a surprise that the $(N_2S_2)M$ dithiolate ligands serve as good donors to transition metals in various oxidation states. In addition to the W(0) complexes, they have been shown to form a variety of heterometallic cluster compounds, from octahedral Rh(III) complexed by three $(N_2S_2)Ni$ to square planar Ni(II) complexed

by two $(N_2S_2)Ni$.[110-112] As well, an assortment of C_4 and C_3 paddlewheel structures, $[(N_2S_2)Ni]_4M_2$ and $[(N_2S_2)Ni]_3M_2$, respectively, have been synthesized and characterized.[110-111,113,114] Our work has focused on the (bme-daco)Ni and (bme-dach)Ni complexes as paddles with dimetal axes (M = Mo, Rh, Pd, Cu, Ag, and Zn). Figure V-8 presents representative structures and the impressive range of metal-metal distances spanned by the nickeldithiolato ligands.[110-111,91,92,115-118]

Spanning five decades, similar types of paddlewheel structures using classical binucleating ligands were the focus of the late Professor F.A. Cotton's studies. These studies provided a template for exploration of metal-metal multiple bonds and laid the foundations for the fundamental understanding of metal-metal interactions in discrete transition metal complexes, their reactivity, response to electronic and steric effects introduced by coordinating ligands, and interplay of transition metal and ligand molecular orbitals.[119]

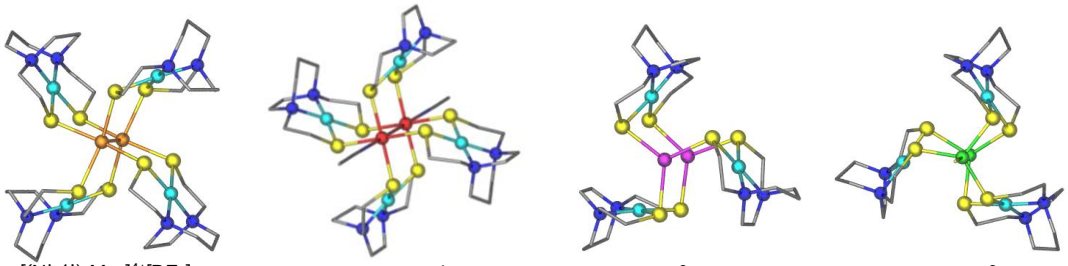

Figure V-8. Ball-and-stick representations of (bme-dach)Ni (or **Ni-1'**) paddlewheel structures where M_2 = Mo, Rh, Ag, and Zn.[117,110,92] Counter anions have been omitted for clarity.

In this work we explore the use of the paramagnetic metalloligand, (bme-dach)Fe(NO), or **Fe-1'**(NO)[73] to compare its properties to those of the diamagnetic (N_2S_2)Ni units. Following the Enemark-Feltham notation,[34] this compound is an S = ½, $\{Fe(NO)\}^7$ complex, which has an electronic count analogous to that of the Ni^{III} centers of sulfur-protected, oxidized (N_2S_2)Ni complexes.[101,120] Adduct formation with $W(CO)_4$ groups, similar to those with (N_2S_2)Ni, *vide supra*, have indicated that **Fe-1'**(NO) is also as good a donor as phosphines and diimines but not as good as the Ni^{II} analogues.[103] Thus, it became our objective to determine whether the **Fe-1'**(NO) ligand would binucleate metal ions into paddlewheel complexes and to further examine the magnetic properties of such species.

Hence, a synthesis targeting $\{[\textbf{Fe-1'}(NO)]_3Ag_2\}^{2+}$ as a paddlewheel complex was developed. In addition to single crystal x-ray diffraction analysis, characterization of this complex employed ν(NO) IR and EPR spectroscopies, variable temperature magnetism (SQUID) analysis, and cyclic voltammetry.

Synthesis and Properties

Addition of a dark green solution of **Fe-1'**(NO) in CH_2Cl_2 to a suspension of $AgBF_4$ in CH_2Cl_2 resulted in uptake of the poorly soluble Ag^+ salt and immediate formation of a light-green precipitate. In CH_3CN solution this compound shows a ν(NO) band that is 57 cm^{-1} higher than that of the free **Fe-1'**(NO) ligand. As isolated, the $\{[\textbf{Fe-1'}(NO)]_3Ag_2\}[BF_4]_2$ compound is a thermally stable (decomposition temperature of over 230°C) crystalline solid, which is moderately air stable in the solid state. The compound

decomposes if left in solution over the course of a few hours both in the absence and in the presence of air. The complex is highly soluble in CH_3CN and DMF, partially soluble in CH_3OH, and sparingly soluble in CH_2Cl_2. The parent ion is observed in the mass spectrum as a major signal with m/z daughter ions reflecting successive losses of NO ligands. Single crystals suitable for X-ray studies were obtained by vapor diffusion of ether into an acetonitrile solution of the product.

Molecular Structure of {[Fe-1'(NO)]$_3$Ag$_2$}[BF$_4$]$_2$

The molecular structure of the pentametallic paddlewheel complex, {[**Fe-1'**(NO)]$_3$Ag$_2$}[BF$_4$]$_2$, is shown in Figure V-9. The {[**Fe-1'**(NO)]$_3$Ag$_2$}[BF$_4$]$_2$ structure exists as two independent but chemically equivalent molecules in the asymmetric unit cell, each having unique geometric parameters with minor differences within each "paddle" of the paddlewheel complex.

The general structure consists of two silver(I) metal ions separated by 2.88 Å and 2.85 Å, respectively with three **Fe-1'**(NO) ligands attached to the silver ions through the thiolate sulfurs resulting in trigonal planar coordination of the Ag^+ ions by sulfurs from three different **Fe-1'** groups. The NO ligands coordinated to each Fe all point in the same direction, i.e., each is oriented towards the thiolate sulfurs with the NO bond vector displaced from the center of the S-Fe-S angle towards one Fe-S bond vector. The average dihedral angle, defined by the intersection of planes comprised of O-N-Fe and N-Fe-S in each **Fe-1'**(NO) paddle, is 33.8°. Each paddlewheel molecule possesses local C_3 symmetry with a three-fold rotation axis through the two silver centers. A pseudo

mirror plane, containing the three Fe atoms, bisects the Ag···Ag axis as well as the N-Fe-N and S-Fe-S angles. A tetrafluoroborate counter anion is in close proximity to a Ag^{+} of each molecule (Ag1A-Boron, 3.774 Å and Ag2B-Boron, 3.868 Å) with the second tetrafluoroborate counter anion for each molecule positioned more than 8 to 9 Å from the silver centers. As can be seen by the space filling diagrams in Figure V-10, each close BF_4 anion lines up with the corresponding Ag^{+} along the C_3 axis, whereas the distant BF_4 anions are nestled outside the Fe-1'(NO) paddles.

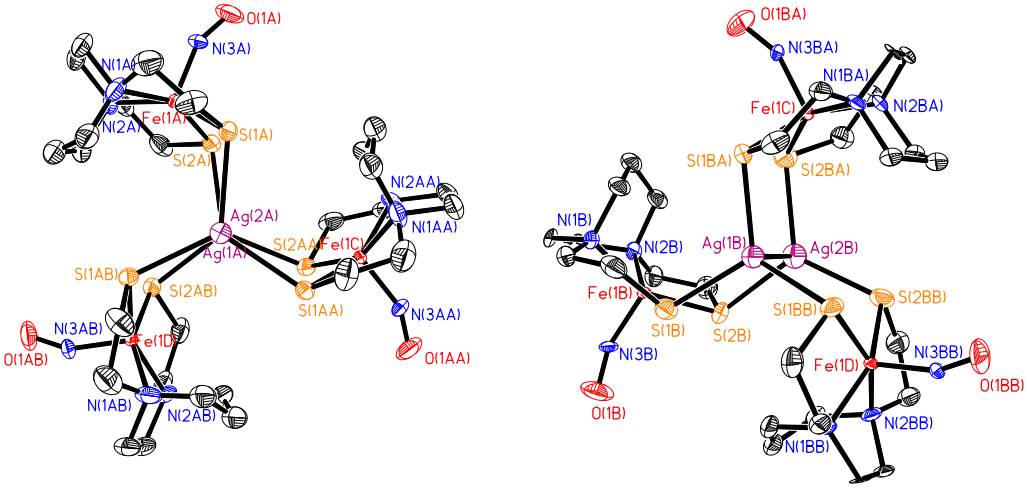

Figure V-9. Thermal ellipsoid plots of the molecular structures of the two independent molecules of {[**Fe-1'**(NO)]$_3$Ag$_2$}[BF$_4$]$_2$. Tetrafluoroborate counter anions have been removed for clarity.

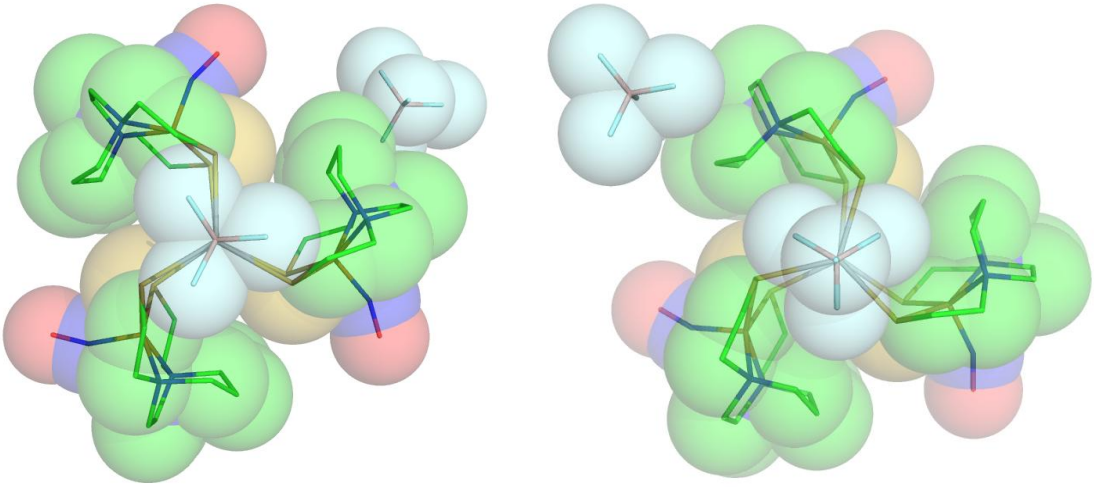

Figure V-10. Space filling diagrams corresponding with the thermal ellipsoid plots in Figure V-9 of the two independent molecules of {[**Fe-1'**(NO)]$_3$Ag$_2$}[BF$_4$]$_2$ showing close contact of one BF_4^- anion and one distant BF_4^- anion per molecule. The second diagram is rotated 180° in relation to the corresponding thermal ellipsoid plot to better see the BF_4^- anions.

A similar Ag_2^{2+} trigonal paddlewheel structure is known in which the coordinating ligands are (bme-dach)Ni, **Ni-1'**, complexes.[117] A comparison of bond distances and angles of the {[**Fe-1'**(NO)]$_3$Ag$_2$}$^{2+}$ and the {[**Ni-1'**]$_3$Ag$_2$}$^{2+}$, Table V-4, finds greatest differences in the Ag···Ag distances, the displacement of the metal of the metallodithiolate ligand from the N_2S_2 plane, and the tilt of the paddles as they are attached into the silver axle or shaft. For the **Ni-1'** derivative, the Ag···Ag distance is 3.00(1) Å, whereas for the **Fe-1'**(NO) derivative, the average is 2.866(3) Å.[117] The nickel is largely within the N_2S_2 best plane (average displacement of 0.0599 Å). In contrast, the Fe rests above the N_2S_2 best plane on average by 0.455 Å, i.e., in typical square pyramidal fashion.

The tilt of the paddles with respect to the Ag···Ag axle, i.e., the dihedral angle defined as the angle of intersection of the best N_2S_2 plane and the Ag_2S_2 best plane to which it is joined, is 82.9° for the **Ni-1'** paddlewheel as compared to 68.7° for the **Fe-1'**(NO) analogue. The smaller dihedral angle of the **Fe-1'**(NO) paddlewheel may arise from increased steric interaction of the NO ligands with the neighboring diazacycloheptane rings.

Table V-4. Selected bond distances and bond angles of **Fe-1'**(NO),[73] {[**Fe-1'**(NO)]Ag_2}(BF_4) (both molecules in the unit cell), and [(**Ni-1'**)$_3Ag_2$]$(ClO_4)_2$.[117] See Figure V-9 for atom labeling.

Complex	**Fe-1'**(NO)	{[**Fe-1'**(NO)]-Ag_2}(BF_4) [1]	{[**Fe-1'**(NO)]-Ag_2}(BF_4) [2]	[(**Ni-1'**)$_3Ag_2$] $(ClO_4)_2^+$
Ag···Ag	--	2.883(3)	2.849(3)	3.00(1)
M-N (NO)	1.705(2)	1.693(9)	1.683(9)	--
Ag(1)-M	--	3.920	3.834	3.380
Ag(2)-M	--	3.879	3.967	3.350
Ag(1)-S(1)	--	2.524(3)	2.482(3)	2.518(1)
Ag(2)-S(2)	--	2.464(3)	2.561(4)	2.511(2)
M-S_{avg}	2.2314(7)	2.234(5)	2.239(4)	2.170(2)
M-N_{avg} (N_2S_2)	2.013(2)	2.023(5)	1.997(10)	1.932(5)
M-N_2S_2 disp[a]	0.5525	0.4625	0.4472	0.0599
Torsion angle (S-Ag-Ag-S)	--	11.84(9)	4.06(10)	3.95(5)
S(1)-M-S(2)	94.91(3)	95.13(14)	96.03(15)	94.80(7)
N(1)-M-N(2)	79.03(9)	78.7(5)	79.9(4)	82.8(2)
S(1)-Ag(1)-S(1)	--	119.997(2)	116.71(6)	119.997(1)
S(2)-Ag(2)-S(2)	--	117.55(5)	119.996(2)	119.327(12)
Ag(1)-S(1)-M	--	110.63(13)	108.27(14)	91.11(6)
Ag(2)-S(2)-M	--	111.35(14)	111.50(15)	91.93(6)
M-N-O	148_{avg}	153.8(9)	156.1(9)	--
Dihedral[b]	--	68.3	69.1	82.9

[a] Displacement of M from N_2S_2 best plane

[b] Angle between the N_2S_2 best plane and the S_2Ag_2 best plane

Comparisons of the bond angles and distances of the **Fe-1'**(NO) paddlewheel and the parent **Fe-1'**(NO) ligand can also be found in Table V-4. On complexation to the silver ions the Fe-N-O angle is increased by roughly 7° (155°$_{avg}$ in the paddlewheel vs. 148°$_{avg}$ in the free ligand). There is also a significant difference in the Fe displacement from the N_2S_2 best plane (0.455 Å in the paddlewheel and 0.5525 Å in the parent metalloligand). In summary, binding of the **Fe-1'**(NO) ligands to Ag^+ results in a C_3 paddlewheel that bears structural similarity to the previously reported **Ni-1'** analogue. The differences in geometrical parameters of the {Fe(NO)} unit within the free metallodithiolate and within the paddlewheel structure arise from the combination of steric and electronic effects due to the NO ligand, which is manifested in a smaller paddle to axle dihedral angle, an increased Fe-N-O angle, and a decrease in the displacement of the Fe from the N_2S_2 plane.

Spectroscopic Characterization

The IR spectrum of the target compound, {[**Fe-1'**(NO)]$_3$Ag$_2$}[BF$_4$]$_2$ was measured in CH_3CN solution with a focus on the sentinel ν(NO) band at 1690 cm^{-1}. As the parent metalloligand, **Fe-1'**(NO), also in CH_3CN solution, displays a ν(NO) band at 1633 cm^{-1}, the positive shift of 57 cm^{-1} in the pentametallic aggregate indicates a withdrawal of electron density from the Fe(NO) unit through the thiolate sulfurs to the silvers, in keeping with typical σ-donor/ π-back-bonding arguments.[107] Interestingly, the ν(NO) band in the [**Fe-1'**(NO)]W(CO)$_4$ adduct is observed at a similar position as in the silver paddlewheel: 1697 cm^{-1} (CH_2Cl_2 solution),[106] i.e., shifted by 64 cm^{-1}.

The {[**Fe-1'**(NO)]$_3$Ag$_2$}[BF$_4$]$_2$ is paramagnetic with a μ_{obs} value of 3.4 ±0.1 at 22° C (Evans method[55-57]) resulting from three S = ½ {Fe(NO)}^{7} units. The EPR spectrum shows a single isotropic signal with a g value of 2.024. The experimental (frozen DMF solution) and simulated spectra are shown in Figure V-11. A similar isotropic signal is seen for the parent ligand, **Fe-1'**(NO) in which the g value is 2.030.[73] ^{14}N hyperfine splitting was not observed in either spectrum.

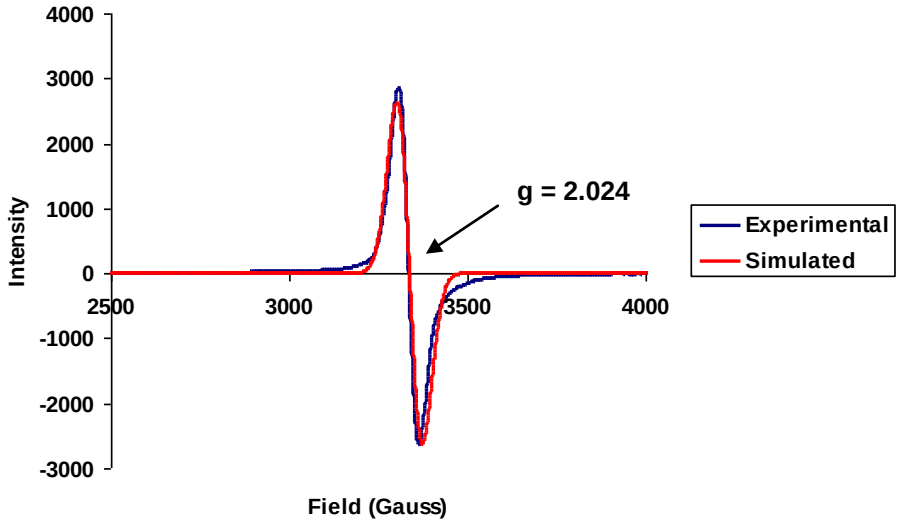

Figure V-11. Experimental and simulated EPR spectra of {[**Fe-1'**(NO)]$_3$Ag$_2$}[BF$_4$]$_2$ at 9 K in DMF solution(glass).

Variable Temperature Magnetic Susceptibility Studies

Direct current magnetic susceptibility measurements were taken by Mark Young on powdered crystalline samples of **Fe-1'**(NO) and {[**Fe-1'**(NO)]$_3$Ag$_2$}[BF$_4$]$_2$ in the 2-300 K temperature range. Temperature independent paramagnetism (TIP) was present in both samples. A 1,000 Oe field was used for **Fe-1'**(NO), yielding a spin-only moment of 0.394 emu-K/mol at 2 K. A 10,000 Oe field was used for the variable temperature sweep of {[**Fe-1'**(NO)]$_3$Ag$_2$}[BF$_4$]$_2$ to eliminate the TIP from the measurements. The data in terms of χT vs. T are plotted in Figure V-12. The χT value for the trigonal paddlewheel is nearly constant at 1.17 emu-K/mol, i.e., three times that of the single **Fe-1'**(NO) unit, until a marked increase begins at ca. 20 K. As antiferromagnetic coupling should lead to a decrease in χT, the temperature dependent behavior is attributed to ferromagnetic coupling between the {Fe(NO)}^{7} centers. The data was modeled using the equation

$$\chi T = \frac{N\beta^2 g^2}{4k}\left(\frac{1+5\exp\left(3J/2kT\right)}{1+\exp\left(3J/2kT\right)}\right)$$

where N is Avogadro's number, β is the Bohr magneton, k is the Boltzmann constant, and J is the spin-spin coupling constant. This fit yields values of g = 2.03 and J = +1 cm^{-1} with an R value of 0.982, confirming the weak ferromagnetic coupling. The g-value is also in agreement with that found experimentally via EPR spectroscopy. The basis of the ferromagnetic coupling is presumed to lie in the p-orbital pathway through the bridging sulfur atoms as mediated by the diamagnetic silver ions.[121]

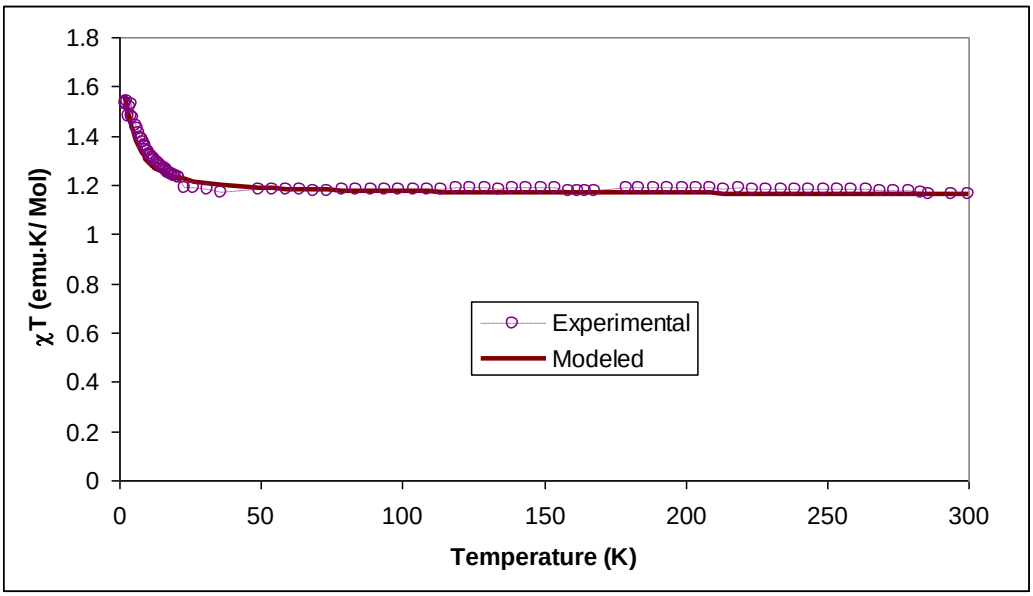

Figure V-12. χT vs. T plot of {[**Fe-1'**(NO)]$_3$Ag$_2$}[BF$_4$]$_2$ displaying weak ferromagnetic coupling at T < 20 K.

Electrochemistry: Cyclic Voltammetry

In DMF solution the cyclic voltammogram of **Fe-1'**(NO) shows a reversible one-electron reduction centered at -1.08 V. Upon complexation to W(CO)$_4$, this reduction event shifts to -0.47 V indicating the greater ease of electron uptake by the **Fe-1'**(NO) in the bimetallic which shares the thiolate S-donors.[106] Consistent with the similar ν(NO) IR shifts of **Fe-1'**(NO) on complexation to W(CO)$_4$ and to two Ag$^+$ ions in the silver paddlewheel complex, an irreversible reduction event is observed at -0.55 V. Greater reversibility is seen in a second event where the E$_{1/2}$ is -1.06 V relative to NHE. A third irreversible event is observed at -1.82 V. Assuming that the {[**Fe-1'**(NO)]$_3$Ag$_2$}$^{2+}$ cation remains intact, the first two reductions may be interpreted according to the following:

$$\{[\text{Fe-1'(NO)}]_3\text{Ag}_2\}^{2+} \overset{e^-}{\rightleftharpoons} \{[\text{Fe-1'(NO)}]^{-1}[\text{Fe-1'(NO)}]_2\text{Ag}_2\}^{+} \overset{e^-}{\rightleftharpoons} \{([\text{Fe-1'(NO)}]^{-1})_2[\text{Fe-1'(NO)}]\text{Ag}_2\}^{0}$$

Multiple redox events shifted positively from the free metallodithiolate ligand are also observed in polymetallics based on (bme-dach)Ni as binucleating ligand.[91]

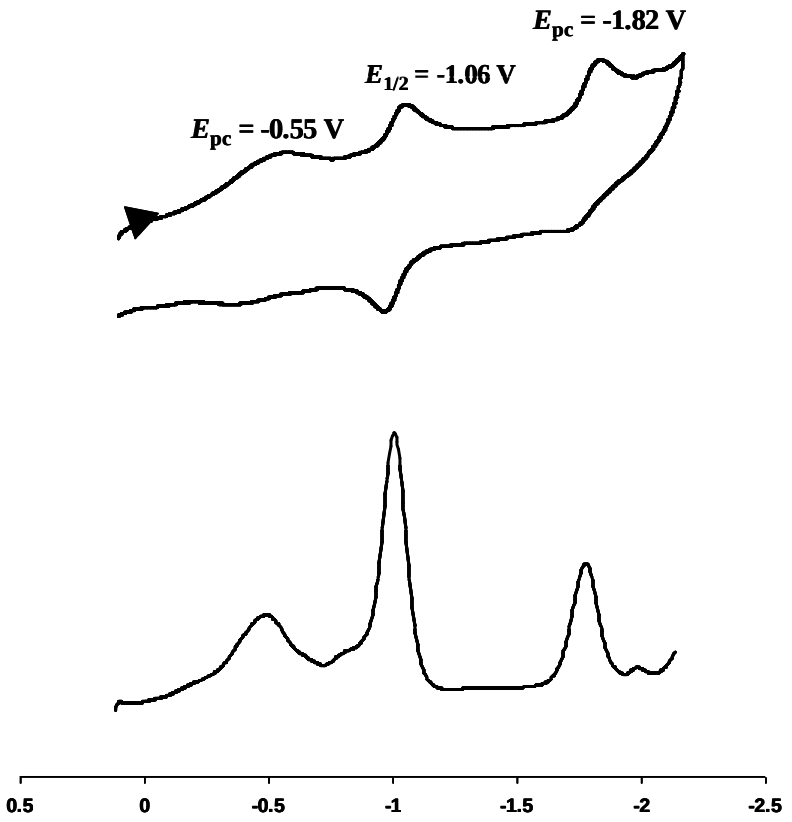

Figure V-13. Cyclic and square-wave voltammograms of DMF solution of {[**Fe-1'**$(NO)]_3Ag_2\}[BF_4]_2$ in 0.1 M n-Bu_4NBF_4 with a glassy carbon electrode at a scan rate of 200 mV/s. All potentials scaled to NHE as referenced to a Cp_2Fe/Cp_2Fe^+ standard ($E_{1/2}^{NHE}$ = 0.692 V).[122]

In summary, we have demonstrated that a metallodithiolate ligand shown to be a poorer donor than an analogous NiN_2S_2 complex can nevertheless serve as a

binucleating agent in the construction of a C_3 paddlewheel complex of silver that exists as clockwise and counterclockwise rotation isomers. The structure is unremarkable with the exception of evidence of steric interference between the paddles arising from the NO ligands between each **Fe-1'**(NO) paddle resulting in a smaller dihedral plane in the attachment of the ligand into the disilver shaft and a smaller displacement of Fe from the N_2S_2 centroid. Over a wide temperature range magnetism of the paddlewheel is a summation of the single unpaired electrons on each **Fe-1'**(NO) unit; ferromagnetic coupling becomes evident below T = 20K.

Conclusion

The effect of steric and electronic properties of ligands on acceptor metals is typically documented by various spectroscopic techniques that probe changes in the electron distribution about the acceptor metal. The opposite, that is, the changes in the donor ligand as a result of complexation, is less well established. The unique set of ligands that we have studied, containing redox-active metals amenable to solution electrochemistry and, in this case, an additional reporter unit in the guise of an NO ligand, has permitted a view of electronic shifts from the metallodithiolato ligand resulting from ligation. Such a view of both the acceptor and donor is useful to deconvolute heterobimetallics with bridging thiolate ligands into a donor and an acceptor site. Using these simple systems as models, it is expected that more complicated heteropolymetallics might be better understood. A specific example of a thiolate-bridged biological bimetallic system is within the active site of the Acetyl co-A synthase

in which a cysteine-glycine-cysteine tripeptide furnishes a Ni^{II} binding site and a (N_2S_2)Ni dithiolate donor to the second nickel, which is catalytically active toward C-C coupling processes.[123-128] Thiolate-bridged bimetallics are also prominent in the active sites of [FeFe]- and [NiFe]-hydrogenases. The extent to which each monometallic unit participates in donor versus acceptor interactions may be used in the design of small-molecule synthetic analogues for practical use.

CHAPTER VI

CONCLUSIONS AND FUTURE DIRECTIONS

Using the presence of nitric oxide and dinitrosyl iron complexes (DNICs) in biological systems as inspiration, a series of N-heterocyclic carbene (NHC)-containing inorganic DNICs have been prepared as mimics of imidazole- and histidine-containing DNICs. Characterizations of these complexes demonstrate similar steric properties as well as electron donor properties between the imidazoles and the NHCs suggesting that the NHCs are suitable mimics of imidazoles. Further synthetic studies revealed that upon deprotonation, imidazoles can lead to aggregation forming molecular squares containing four $\{Fe(NO)_2\}^9$ units. Additionally, synthetic models of a mononitrosyl Fe-containing enzyme, nitrile hydratase, have exhibited sulfur-based reactivity resulting in the formation of polymetallic complexes.

Nitric oxide (NO) can exists in three oxidation states as NO^+, NO•, and NO^-. In fact, the NO binding modes of these different oxidation states in mononitrosyl complexes are well documented and are typically determined by the M-N-O angle. For example, NO^+, a 2 e^- donor isoelectronic with CO binds to metals in a linear fashion, with ∠M-N-O of about 180°, while NO• and NO^- bind in a bent fashion with ∠M-N-O of about 150° and 120°, respectively (Figure VI-1).[34,107,129] These trends are clearly demonstrated in the Fe and $Co(N_2S_2)$ complexes reported in Chapter V. For Fe-1′(NO) and [Fe-1′(NO)]$W(CO)_4$, the ∠M-N-O are 148° and 155°, respectively, which are consistent with a NO• bound to formally Fe^{II} or $\{Fe(NO)\}^7$ in Enemark-Feltham

notation. For Co-1′(NO) and [Co-1′(NO)]$W(CO)_4$, the ∠M-N-O are 124° and 123°, respectively. These NO ligands are much more bent resulting in assignment of Co^{III} bound to NO^- or $\{Co(NO)\}^8$. While the correlation between ∠M-N-O and the NO binding mode for the mononitrosyl complexes follows a "textbook" description, this is not so for the dinitrosyl iron complexes.

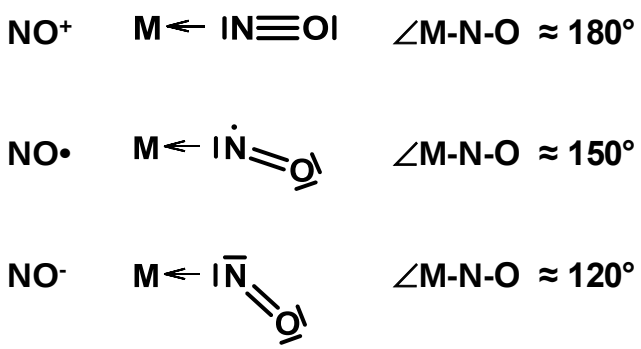

Figure VI-1. Three oxidation states of NO with the corresponding metal-binding mode as indicated by the M-N-O angle.

The Fe-N-O angle in DNICs typically ranges from 160° to 180°. While many may consider angles in the 160° range to be only a slight deviation from linear, and thus, an NO^+ binding mode, there is no appreciable correlation between ∠Fe-N-O and oxidation state of the $Fe(NO)_2$ unit as so clearly defined by the mononitrosyl cases. For example, as discussed in Chapter III, the (NHC-iPr)$Fe(NO)_2$ reduced $\{Fe(NO)_2\}^{10}$ complex has an average ∠Fe-N-O of 174°. Alternatively, the (NHC-iPr)(PhS)$Fe(NO)_2$

oxidized $\{Fe(NO)_2\}^9$ complex has an average ∠Fe-N-O of 167°. Though a distinct difference between the ∠Fe-N-O in these two complexes may initially seem as an indicator of the reduced or oxidized form, it should be noted that an analogous reduced $\{Fe(NO)_2\}^{10}$ complex, $(Imid\text{-}Me)_2Fe(NO)_2$ has average ∠Fe-N-O of 168°.[35] With linear NO, it is expected that the N-O bond would be shorter and stronger resulting in a higher stretching frequency in the infrared spectrum. Again, this is not the case. The abovementioned reduced $(NHC\text{-}iPr)Fe(NO)_2$ has ν(NO) of 1664 and 1619 cm^{-1}, whereas oxidized $(NHC\text{-}iPr)(PhS)Fe(NO)_2$ with more bent ∠Fe-N-O has ν(NO) of 1757 and 1712 cm^{-1}. Furthermore, as there are no great deviations amongst the average N-O distances for the series of oxidized and reduced DNICs discussed in Chapters III and IV, perhaps the NO infrared stretching frequency is a better indicator of NO binding mode instead of the ∠Fe-N-O for DNICs.

From the demonstrated syntheses and reactivity discussed in Chapters III and IV, and chemical precedent, it can be concluded that the $\{Fe(NO)_2\}^{10}$ unit most favorably coexists with neutral ligands such as CO, phosphines, NHCs, and imidazoles. The $\{Fe(NO)_2\}^9$ unit is stable in the presence of anionic ligands such as SR^-, deprotonated imidazoles or mixed anionic/neutral ligand sets, neutral ligands being NHCs. Additionally, the precursors to $\{Fe(NO)_2\}^{10}$ and $\{Fe(NO)_2\}^9$, $Fe(CO)_2(NO)_2$ and $(\mu\text{-}RS)_2[Fe(NO)_2]_2$, respectively, are both susceptible to reaction with imidazoles as well as NHCs. In the latter case, trinitrosyl iron complexes may be derived. N-heterocyclic carbene ligands also stabilize neutral $\{Fe(NO)_2\}^{10}$, neutral $\{Fe(NO)_2\}^9$ and cationic $\{Fe(NO)_2\}^9$ DNICs. It should be noted that very few examples of DNICs containing the

same ligand set exist as oxidized and reduced redox pairs.[38] The NO-releasing order with respect to NO capture by $Fe(N_2S_2)$ or Co(porphyrin) trapping agents in these derivatives is established as follows:

$\{Fe(NO)_3\}^{10}$ TNICs > $\{Fe(NO)_2\}^9$ DNICS >> $\{Fe(NO)_2\}^{10}$ DNICs

Within the $\{Fe(NO)_2\}^9$ DNIC series, the NO-release/transfer ability of these complexes is as follows:

$[(NHC)_2Fe(NO)_2]^+$ > $[(NHC)(RS)Fe(NO)_2]^0$ > $(\mu\text{-}SR)_2[Fe(NO)_2]_2$

Nevertheless, the mechanism of NO-release/transfer in these systems is unknown.

While the TNICs may be too reactive towards NO release for use as therapeutic NO donors, more potential exists within the oxidized bis-NHC and mixed (NHC)(RS) DNICs. Especially in the mixed (NHC)(RS) case, this complex is relatively air-stable. Unfortunately, these complexes are only soluble in organic solvents and attempts to dissolve in buffered aqueous solutions for cytotoxicity studies were unsuccessful. Enhancing the water solubility and perhaps even the biocompatibility of the supporting ligands bound to the $Fe(NO)_2$ unit may make these type of complexes more useful NO donors for biological studies. I have established, from literature precedent,[130] the synthesis of water-soluble imidazolium salts derived from carboxy-protected amino acid methyl esters (glycine, cysteine, and methionine) as NHC precursors, Figure VI-2. Utilizing the knowledge gained from the preparation and reactivity studies of the complexes in Chapter III, a series of analogous water-soluble NHC-containing

complexes may be synthesized. Exchanging the thiolate (more or less sterically bulky or weaker or stronger donor) in the mixed (NHC)(SR) complex is expected to tune the NO transfer ability of the complex.[30] These water-soluble DNICs may then be utilized as NO donors in biological media in order to establish such properties as their cytotoxicity, or in applications that require careful control of NO levels.

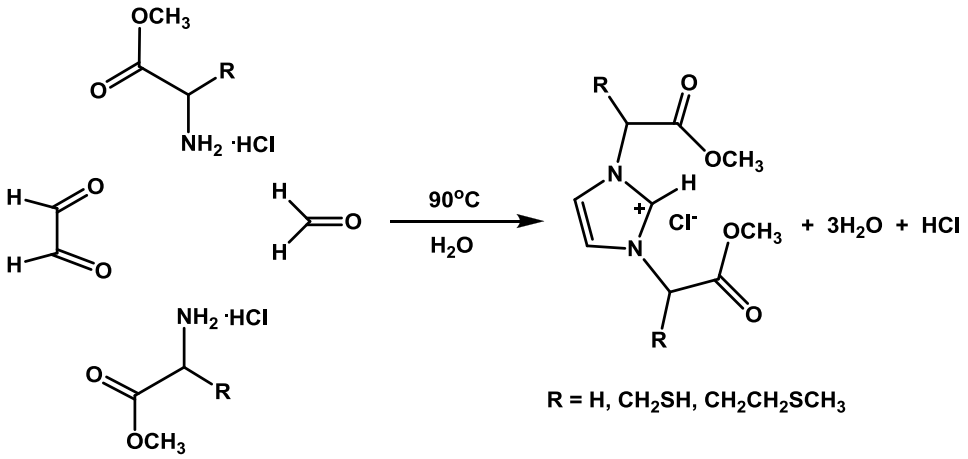

Figure VI-2. Reaction sequence depicting synthesis of water-soluble amino acid methyl ester imidazolium salts as N-heterocyclic carbene precursors.[130]

Furthermore, thiolate displacement of NHCs in the oxidized $\{Fe(NO)_2\}^9$ complexes keeps the $Fe(NO)_2$ unit intact. This holds interesting possibilities in using such complexes as "$Fe(NO)_2$ transfer" agents to such targets as proteins with an exposed thiol group to further establish the formation and possible aggregation of protein-bound DNICs. A proposed reaction scheme is given in Figure VI-3.

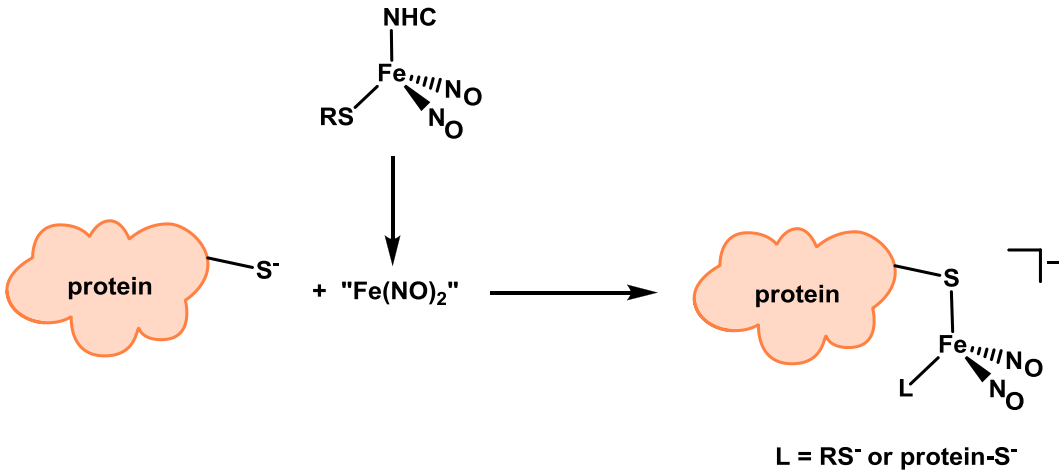

Figure VI-3. Proposed reaction scheme utilizing a (NHC)(RS)Fe(NO)$_2$ complex as a "Fe(NO)$_2$ transfer" agent to a protein with an exposed thiol group in order to synthesize a protein-bound dinitrosyl iron complex.

Histidine-containing DNICs have been observed via EPR spectroscopy upon nitrosylation of several proteins containing histidine residues, including aconitase, mammalian ferritin, and the iron-quinone complex of photosystem II.[15,16,44] From these studies, it is not clear whether the histidine residues were bound through the neutral N or the deprotonated N of the imidazole ring. Importantly, pH studies have demonstrated that deprotonation of the imidazole N-H occurs at a pKa of 14.5; however, when histidine is bound to Fe in the case of a 2Fe2S center, this pKa is lowered to 7.85.[131,132] Thus, under physiological pH conditions, it is expected that this N might be deprotonated. This opens up the possibility for aggregation of Fe/histidine-containing proteins in the presence of NO in biological systems as seen in the inorganic imidazolate-containing Fe(NO)$_2$ aggregates discussed in Chapter IV. Whether these types of clusters could form in the cellular environment or what their function might be

have yet to be discovered. Interesting conjectures regarding the stabilization and storage of NO in histidine-rich, Fe-containing proteins will doubtlessly follow such a future physiology.

Furthermore, the relative ease in which the $Fe(NO)_2$ complexes are synthesized, and their stability in the presence of a variety of ligand donors offers speculation in whether other transition metal dinitrosyl complexes may be synthesized, for example, $\{Mn(NO)_2\}^8$ or $\{Co(NO)_2\}^{10}$. In fact, several $\{Co(NO)_2\}^{10}$ complexes have been reported though little is known concerning their reactivity and redox properties.[49,133-136] I have initiated a study of a cobalt analogue of the $\{Fe(NO)_2\}^9$ imidazolate-bridged tetramers as presented in Chapter IV. As a cobalt-containing analogue would be diamagnetic, variable temperature ^1H NMR studies may provide interesting information regarding the orientation of the bound imidazolates when the complex is in solution as well as temperature dependent conformers. The well-known black-brown $[Co(NO)_2Cl]_2$ precursor[137] was used and cleaved with excess deprotonated benzimidazolate to produce a dark green solid (Figure VI-4). The ν(NO) are 1844 and 1771 cm^{-1} in THF solution. Though the $Co(NO)_2$ stretching frequencies cannot necessarily be correlated with the $Fe(NO)_2$ series, the pattern of the ν(NO) bands and the partial solubility of the dark green solid in organic solvents such as hexanes, pentane, and ether are similar to the Fe-containing tetramers, suggesting that the Co-containing tetramer has formed. Definitive assignment of the structure and reactivity of this complex awaits future study.

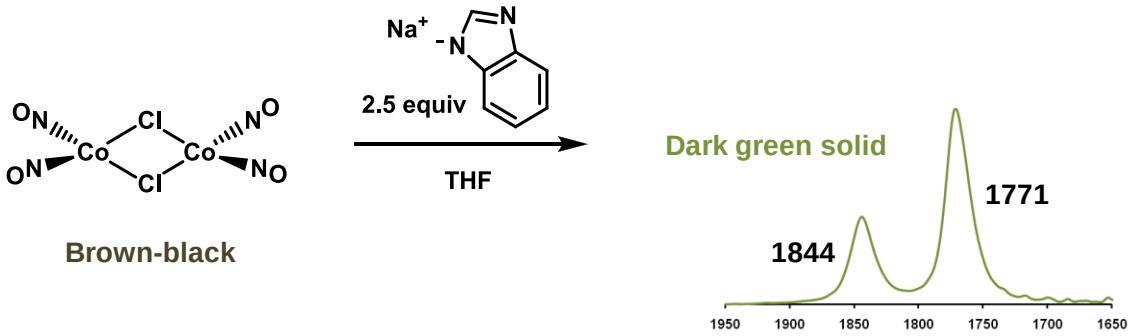

Figure VI-4. Reaction sequence and ν(NO) infrared spectrum of a cobalt-containing nitrosyl complex in an attempt to synthesize a Co-containing tetramer. Further characterization is the subject of a future study.

Through the course of this dissertation work, I have characterized and studied the reactivity of a variety of mono, di, and trinitrosyl complexes. Though the vast majority of *in vivo* DNICs presumably in the paramagnetic, oxidized form $[RS_2Fe(NO)_2]^-$ have been detected via EPR spectroscopy, it is feasible that other diamagnetic monomeric, dimeric, or polymeric $Fe(NO)_2$ complexes may form *in vivo* but go unnoticed. Difficulty in extracting and isolating these biological DNICs results in a lack of their full characterization beyond EPR spectroscopy. Thus, synthesizing these types of inorganic DNICs and fully characterizing and studying their reactivity is an excellent way to model DNICs found in biological systems as well as a way to further understand their formation and function. Possibly, the most significant contribution of Chapter IV is the Mössbauer data collected for a series of DNICs in both the reduced and oxidized states with a variety of donor ligands. Though a large number of synthetic DNICs are reported in the literature, very few have been studied with Mössbauer spectroscopy.[41,46] As

Mössbauer data is only valuable when correlated with a set of related compounds,[94] it is imperative to build a library of DNICs studied by Mössbauer spectroscopy in order to gather meaningful data regarding the structure and bonding of DNICs. As more Mössbauer information is obtained for DNICs, this spectroscopy may become a useful tool in detecting the presence of both oxidized and reduced DNICs in biological systems.

Insight into the NO transfer ability of oxidized $\{Fe(NO)_2\}^9$ complexes in comparison to reduced $\{Fe(NO)_2\}^9$ complexes may suggest a link between DNIC-related NO storage and release to redox form in biological systems. Aggregation of the $Fe(NO)_2$ units or aggregation assisted by reactive thiolate sulfurs when bound to a M-NO unit may find biological significance concerning products formed upon protein disassembly or deactivation in the presence of NO. Overall, this work serves to examine the fundamental characteristics of iron nitrosyl complexes with the consideration that small model complexes may provide information to compare to and hopefully understand more about intricate NO-containing biomolecules.

REFERENCES

1. Culotta, E.; Koshland, D. E. Jr. *Science* **1992**, *258*, 1862-1865.
2. Szacilowski, K.; Chmura, A.; Stasicka, Z. *Coordination Chemistry Reviews* **2005**, *249*, 2408-2436.
3. Vanin, A. F. *Nitric Oxide* **2009**, *21*, 1-13.
4. Santolini, J. *J. Inorg. Biochem.* **2011**, *105*, 127-141.
5. Daff, S. *Nitric Oxide* **2010**, *23*, 1-11.
6. Richardson, D. R.; Lok, H. C. *Biochim. Biophys. Acta* **2008**, *1780*, 638-651.
7. Miller, MR; Megson, IL. *Br. J. Pharmacol.* **2007**, *151*, 305-321.
8. Vanin, A. F. *Biochemistry (Moscow, Russ. Fed.)* **1998**, *63*, 782-793.
9. Woolum, J. C.; Commoner, B. *Biochim. Biophys. Acta* **1970**, *201*, 131-140.
10. Vanin, A. F.; Nalbandyan, R. M. *Biofizika* **1965**, *10*, 167-168.
11. Vanin, A. F.; Nalbandyan, R. M. *Biofizika* **1966**, *11*, 178-179.
12. Nalbandyan, R. M.; Shifman, L. A. *Biofizika* **1966**, *11*, 359-361.
13. McDonald, C. C.; Phillips, W. D.; Mower, H. F. *J. Am. Chem. Soc.* **1965**, *87*, 3319-3326.
14. Sellers, V. M.; Johnson, M. K.; Dailey, H. A. *Biochemistry* **1996**, *35*, 2699-2704.
15. Kennedy, M. C.; Antholine, W. E.; Beinert, H. *J. Biol. Chem.* **1997**, *272*, 20340-20347.
16. Lee, M.; Arosio, P.; Cozzi, A.; Chasteen, M. D. *Biochemistry* **1994**, *33*, 3679-3687.

17. D'Autréaux, B.; Horner, O.; Oddou, J.-L.; Jeandey, C.; Gambarelli, S.; Berthomieu, C.; Latour, J.-M.; Michaud-Soret, I. *J. Am. Chem. Soc.* **2004**, *126*, 6005-6016.

18. Foster, M. W.; Cowan, J. A. *J. Am. Chem. Soc.* **1999**, *121*, 4093-4100.

19. Cruz-Ramos, H.; Crack, J.; Wu, G.; Hughes, M. N.; Scott, C.; Thomson, A. J.; Green, J.; Poole, R. K.; *EMBO J.* **2002**, *12*, 3235-3244.

20. Toledo, J. C., Jr.; Bosworth, C. A.; Hennon, S. W.; Mahtani, H. A.; Bergonia, H. A.; Lancaster, J. R., Jr. *J. Biol. Chem*. **2008**, *283*, 28926-28933.

21. Mülsch, A.; Mordvintcev, P.; Vanin, A. F.; Busse, R. *FEBS Lett.* **1991**, *294*, 252-256.

22. Ding, H.; Demple, B.; *Proc. Natl. Acad. Sci. U.S.A.* **2000**, *97*, 5146-5150.

23. Cesareo, E.; Parker, L. J.; Pedersen, J. Z.; Nuccetelli, M.; Mazzetti, A. P.; Pastore, A.; Federici, G.; Caccuri, A. M.; Ricci, G.; Adams, J. J.; Parker, M. W.; Lo Bello, M. *J. Biol. Chem*. **2005**, *280*, 42172-42180.

24. Hou, Y.; Wang, J.; Andreana, P. R.; Cantauria, G.; Tarasia, S.; Sharp, L.; Braunscheweiger, P. G.; Wang, P. G. Bioorg. *Med. Chem. Lett.* **1999**, *9*, 2255-2258.

25. Maragos, C. M.; Wang, J. M.; Hrabie, J. A.; Oppenheim, J. J.; Keefer, L. K. *Cancer Res.* **1993**, *53*, 564-568.

26. Stuehr, D. J.; Nathan, C. F. *J. Exp. Med.* **1989**, *169*, 1543-1555.

27. Ignarro, L. J.; Napoli, C.; Loscalzo, *J. Circ. Res*. **2002**, *90*, 21-28.

28. Cook, S.; Scherrer, U. *Fundam. Clin. Pharmacol.* **2002**, *16*, 441-453.

29. Chiang, C.-Y.; Miller, M. L.; Reibenspies, J. H.; Darensbourg, M. Y. *J. Am. Chem. Soc*. **2004**, *126*, 10867-10874.

30. Tsai, F.-T.; Chiou, S.-J.; Tsai, M.-C.; Tsai, M.-L.; Huang, H.-W.; Chiang, M.-H. Liaw, W.-F. *Inorg. Chem*. **2005**, *44*, 5872-5881.

31. Hung, M.-C.; Tsai, M.-C.; Lee, G.-H.; Liaw, W.-F. *Inorg. Chem*. **2006**, *45*, 6041-6047.

32. Chiou, S.-J.; Wang, C.-C.; Chang, C.-M. *J. Organomet. Chem*. **2008**, *693*, 3582-3586.

33. Lu, T.-T.; Tsou, C.-C.; Huang, H.-W.; Hsu, I.-J.; Chen, J.-M.; Kuo, T.-S.; Wang, Y.; Liaw, W.-F. *Inorg. Chem*. **2008**, *47*, 6040-6050.

34. Enemark, J. H.; Feltham, R. D. *Coord. Chem. Rev.* **1974**, *13*, 339-406.

35. Reginato, N.; McCrory, C. T. C.; Pervitsky, D.; Li, L. *J. Am. Chem. Soc*. **1999**, *121*, 10217-10218.

36. Huang, H.-W.; Tsou, C.-C.; Kuo, T.-S.; Liaw, W.-F. *Inorg. Chem*. **2008**, *47*, 2196-2204.

37. Chen, C.-H.; Ho, Y.-C.; Lee, G.-H. *J. Organomet. Chem*. **2009**, *694*, 3395-3400.

38. Tonzetich, Z. J.; Do, L. H.; Lippard, S. J. *J. Am. Chem. Soc.* **2009**, *131*, 7964-7965.

39. Tsai, M.-L.; Liaw, W.-F. *Inorg. Chem.* **2006**, *45*, 6583-6585.

40. Albano, V. G.; Araneo, A.; Bellon, P. L.; Ciani, G.; Manassero, M. *J. Organomet. Chem.* **1974**, *67*, 413-422.

41. Tsai, M.-L.; Hsieh, C.-H.; Liaw, W.-F. *Inorg. Chem.* **2007**, *46*, 5110-5117.

42. Boese, M.; Mordvintcev, P. I.; Vanin, A. F.; Busse, R.; Mülsch, A. *J. Biol. Chem.* **1995**, *270*, 29244-29249.

43. Welter, R.; Yu, L.; Yu, C.-A.; *Arch. Biochem. Biophys.* **1996**, *331*, 9-14.

44. Goussias, C.; Deligiannakis, Y.; Sanakis, Y.; Ioannidis, N.; Petrouleas, V. *Biochemistry* **2002**, *41*, 15212-15223.

45. Tinberg, C. E.; Tonzetich, Z. J.; Wang, H.; Do, L. H.; Yoda, Y.; Cramer, S. P.; Lippard, S. J. *J. Am. Chem. Soc.* **2010**, *132*, 18168-18176.

46. Harrop, T. C.; Tonzetich, Z. J.; Reisner, E.; Lippard, S. J. *J. Am. Chem. Soc.* **2008**, *130*, 15602-15610.

47. Li, L. *Comments Inorg. Chem.* **2002**, *23*, 335-353.

48. Chen, Y.-J.; Ku, W.-C.; Feng, L.-T.; Tsai, M.-L.; Hsieh, C.-H.; Hsu, W.-H.; Liaw, W.-F.; Hung, C.-H.; Chen, Y.-J. *J. Am. Chem. Soc.* **2008**, *130*, 10929-10938.

49. Tonzetich, Z. J.; Héroguel, F.; Do, L. H.; Lippard, S. J. *Inorg. Chem.* **2011**, *50*, 1570-1579.

50. Chiang, C.-Y.; Darensbourg, M. Y. *J. Biol. Inorg. Chem.* **2006**, *11*, 359-370.

51. Nagashima, S.; Nakasako, M.; Dohmae, N.; Tsujimura, M.; Takio, K.; Odaka, M.; Yohda, M.; Kamiya, N.; Endo, I. *Nat. Struct. Biol.* **1998**, *5*, 347-351.

52. Endo, I.; Nojiri, M.; Tsujimura, M.; Nakasako, M.; Nagashima, S.; Yohda, M.; Odaka, M.; *J. Inorg. Biochem.* **2001**, *83*, 247-253.

53. Sari, M.-A.; Moali, C.; Boucher, J.-L.; Jaouen, M.; Mansuy, D. *Biochem. Biophys. Res. Commun.* **1998**, *250*, 364-368.

54. *WINEPR Simfonia,* Version 1.25; Bruker Analytische Messtechnik GmbH: Berlin, **1996**.

55. Evans, D. F. *J. Chem. Soc.* **1959**, 2003-2005.

56. Grant, D. H. *J. Chem. Educ.* **1995**, *72*, 39-40.

57. Girolami, G. S.; Rauchfuss, T. B.; Angelici, R. J. *Synthesis and Technique in Inorganic Chemistry; A Laboratory Manual*; University Science Books: New York, 3rd ed., 1999.

58. *SMART: Program for Data Collection on Area Detectors*, Version 5.632; Bruker AXS Inc.: Madison, WI, **2005**.

59. *APEX2*, Version 2009.7-0; Bruker AXS Inc.: Madison, WI, **2007**.

60. *SAINTPLUS: Program for Reduction of Area Detector Data*, Version 6.63; Bruker AXS Inc.: Madison, WI, **2007**.

61. Sheldrick, G. M. *SADABS: Program for Absorption Correction of Area Detector Frames*; Bruker AXS Inc.: Madison, WI, **2001**.

62. Sheldrick, G. M. *SHELXS-97: Program for Crystal Structure Solution*; Universität Göttingen: Göttingen, Germany, **1997**.

63. Sheldrick, G. M. *SHELXL-97: Program for Crystal Structure Refinement*; Universität Göttingen: Göttingen, Germany, **1997**.

64. Barbour, L. *X-Seed 2.0*; University of Stellenbosch: Stellenbosch, South Africa, **2008**.

65. Macrae, C. F.; Edgington, P. R.; McCabe, P.; Pidcock, E.; Shields, G. P.; Taylor, R.; Towler, M.; van de Streek, J. *J. Appl. Crytsallogr.* **2006**, *39*, 453-457.

66. *The PyMOL Molecular Graphics System*, Version 1.3, Schrödinger, LLC; New York, **2011**.

67. McBride, D. W.; Stafford, S. L.; Stone, F. G. A. *Inorg. Chem*. **1962**, *1*, 386-388.

68. Connelly, N. G.; Gardner, C. *J. Chem. Soc., Dalton Trans*. **1976**, 1525-1527.

69. Schaub, T.; Backes, M.; Radius, U. *Organometallics* **2006**, *25*, 4196-4206.

70. Rauchfuss, T. B.; Weatherill, T. D. *Inorg. Chem*. **1982**, *21*, 827-830.

71. Wang, X.; Sundberg, E. B.; Li, L.; Kantardjieff, K. A.; Herron, S. R.; Lim, M.; Ford, P. C. *Chem. Commun*. **2005**, 477-479.

72. Darensbourg, D. J.; Kump, R. L. *Inorg. Chem.* **1978**, *17*, 2680–2682.

73. Chiang, C.-Y.; Lee, J.; Dalrymple, C.; Sarahan, M. C.; Reibenspies, J. H.; Darensbourg, M. Y. *Inorg. Chem.* **2005**, *44*, 9007–9016.

74. Rabiniwitz, H. N.; Karlin, K. D.; Lippard, S. J. *J. Am. Chem. Soc.* **1976**, *98*, 6951–6957.

75. Cornils, B.; Herrmann, W. A. *Aqueous-Phase Organometallic Catalysis*, 2nd ed.; Wiley-VCH: Weinheim, Germany, 2004.

76. de Frémont, P.; Marion, N.; Nolan, S. P. *Coord. Chem. Rev*. **2009**, *253*, 862-892.

77. Hsieh, C.-H.; Darensbourg, M. Y. *J. Am. Chem. Soc*. **2010**, *132*, 14118-14125.

78. Jenkins, R. M.; Singleton, M. L.; Leamer, L. A.; Reibenspies, J. H.; Darensbourg, M. Y. *Inorg. Chem*. **2010**, *49*, 5503-5514.

79. Sini, G.; Eisenstein, O.; Crabtree, R. H. *Inorg. Chem*. **2002**, *41*, 602-604.

80. Hannig, F.; Kehr, G.; Fröhlich, R.; Erker, G. *J. Organomet. Chem*. **2005**, *690*, 5959-5972.

81. Dillinger, S. A. T.; Schmalle, H. W.; Fox, T.; Berke, H. *Dalton Trans.* **2007**, 3562-3571.

82. Hayton, T. W.; McNeil, W. S.; Patrick, B. O.; Legzdins, P. *J. Am. Chem. Soc.* **2003**, *125*, 12935-12944.

83. Wang, R.; Wang, X.; Sundberg, E. B.; Nguyen, P.; Grant, G. P. G.; Sheth, C. Zhao, Q.; Herron, S.; Kantardjieff, K. A.; Li, L. *Inorg. Chem*. **2009**, *48*, 9779-9785.

84. Vanin, A. F.; Poltorakov, A. P.; Mikoyan, V. D.; Kubrina, L. N.; Burbaev, D. S. *Nitric Oxide* **2010**, *23*, 136-149.

85. a) Volbeda, A.; Charon, M. H.; Piras, C.; Hatchikian, E. C.; Frey, M.; Fontecilla-Camps, J. C. *Nature*, **1995**, *373*, 580-587. b) Bagley, K. A.; Duin, E. C.; Roseboom, W.; Albracht, S. P. J.; Woodruff, W. H. *Biochemistry* **1995**, *34*, 5527-5535.

86. a) Richardson, J. S.; Thomas, K. A.; Rubin, B. H.; Richardson, D. C. *Proc. Nat. Acad. Sci. USA* **1975**, *72*, 1349-1353. b) Tainer, J. A.; Getzoff, E. D.; Beem, K. M.; Richardson, J. S.; Richardson, D. C. *J. Mol. Biol.* **1982**, *160*, 181-217.

87. Kolks, G.; Lippard, S. J.; Waszczak, J. V.; Lilienthal, H. R. *J. Am. Chem. Soc.* **1982**, *104*, 717-725.

88. Chaudhuri, P.; Karpenstein, I.; Winter, M.; Lengen, M.; Butzlaff, C.; Bill, E.; Trautwein, A. X.; Flörke, U.; Haupt, H.-J. *Inorg. Chem.* **1993**, *32*, 888-894.

89. Groysman, S.; Holm, R. H. *Inorg. Chem.* **2009**, *48*, 621-627.

90. Hess, J. L.; Hsieh, C.-H.; Reibenspies, J. H.; Darensbourg, M. Y. *Inorg. Chem.* **2011**, ASAP.

91. Musie, G.; Farmer, P. J.; Tuntulani, T.; Reibenspies, J. H.; Darensbourg, M. Y. *Inorg. Chem.* **1996**, *35*, 2176-2183.

92. Jeffery, S. P.; Lee, J.; Darensbourg, M. Y. *Chem. Commun.* **2005**, 1122-1124.

93. Richardson, H. E.; Taube, H. *Inorg. Chem.* **1981**, *20*, 1278-1285.

94. Parish, R. V. Mössbauer Spectroscopy. *The Organic Chemistry of Iron, Volume 1. Organometallic Series*; Koerner von Gustorf, E. A., Grevels, F. W., Fischler, I., Eds.; Academic Press: London, England; **1978**; pp. 175-211.

95. Ye, S.; Neese, F. *J. Am. Chem. Soc.* **2010**, *132*, 3646-3647.

96. Angaridis, P.; Kampf, J. W.; Pecoraro, V. L. *Inorg. Chem.* **2005**, *44*, 3626-3635.

97. Selmeczi, K.; Gizzi, P.; Champmartin, D.; Rubini, P.; Aubert, E.; Dahaoui, S.; Henry, B. *Inorg. Chem*. **2010**, *49*, 8222-8229.

98. Smee, J. J.; Miller, M. L.; Grapperhaus, C. G.; Reibenspies, J. H.; Darensbourg, M. Y. *Inorg. Chem.* **2001**, *41*, 3601-3605.

99. Bouwman, E.; Reedijk, J. *Coord. Chem. Rev.* **2005**, *249*, 1555-1581.

100. Smee, J. J.; Miller, M. L.; Grapperhaus, C. A.; Reibenspies, J. H.; Darensbourg, M. Y. *Inorg. Chem.* **2001**, *40*, 3601-3605.

101. Farmer, P. J.; Reibenspies, J. H.; Lindahl, P. A.; Darensbourg, M. Y. *J. Am. Chem. Soc.* **1993**, *115*, 4665-4674.

102. Grapperhaus, C. A.; Darensbourg, M. Y. *Acc. Chem. Res.* **1998**, *31*, 451-459.

103. Rampersad, M. V.; Jeffery, S. P.; Golden, M. L.; Lee, J.; Reibenspies, J. H.; Darensbourg, D. J.; Darensbourg, M. Y. *J. Am. Chem. Soc.* **2005**, *127*, 17323-17334.

104. Rampersad, M. V.; Jeffery, S. P.; Reibenspies, J. H.; Ortiz, C. G.; Darensbourg, D. J.; Darensbourg, M. Y. *Angew. Chem., Int. Ed.* **2005**, *44*, 1217-1220.

105. Wayland, B. B.; Olson, L. W. *J. Am. Chem. Soc.* **1974**, *96*, 6037-6041.

106. Hess, J. L.; Conder, H. L.; Green, K. N.; Darensbourg, M. Y. *Inorg. Chem.* **2008**, *47*, 2056-2063.

107. Crabtree, R. H. *The Organometallic Chemistry of the Transition Metals*, 4th ed.; John Wiley & Sons, Inc.: New York, **2005**, pp 88-90.

108. Hall, M. B. *Inorg. Chem.* **1978**, *17*, 2261-2269.

109. Scheidt, W. R.; Ellison, M. K. *Acc. Chem. Res.* **1999**, *32*, 350-359.

110. Jeffery, S. P.; Green, K. N.; Rampersad, M. V.; Reibenspies, J. H.; Darensbourg, M. Y. *Dalton Trans.* **2006**, 4244-4252.

111. Golden, M. L.; Jeffery, S. P.; Miller, M. L.; Reibenspies, J. H.; Darensbourg, M. Y. *Eur. J. Inorg. Chem.* **2004**, 231-236.

112. Hatlevik, O.; Blanksma, M. C.; Mathrubootham, V.; Arif, A. M.; Hegg, E. L.; *J. Biol. Inorg. Chem.* **2004**, *9*, 238-246.

113. Amoroso, A. J.; Chung, S. S. M.; Spencer, D. J. E.; Danks, J. P.; Glenny, M. W.; Blake, A. J.; Cooke, P. A.; Wilson, C.; Schröder, M. *Chem. Commun*. **2003**, 2020-2021.

114. Huang, Y.; Drake, R. J.; Stephan, D. W. *Inorg. Chem.* **1993**, *32*, 3022-3028.

115. Miller, M. L.; Ibrahaim, S. A.; Golden, M. L.; Darensbourg, M. Y. *Inorg. Chem.* **2003**, *42*, 2999-3007.

116. Golden, M. L.; Rampersad, M. V.; Reibenspies, J. H.; Darensbourg, M. Y. *Chem. Commun.* **2003**, 1824-1825.

117. Golden, M. L.; Whaley, C. M.; Rampersad, M. V.; Reibenspies, J. H.; Hancock, R. D.; Darensbourg, M. Y. *Inorg. Chem.* **2005**, *44*, 875-883.

118. Jeffery, S. P.; Singleton, M. L.; Darensbourg, M. Y. *Inorg. Chem*. **2007**, *46*, 179-185.

119. Cotton, F. A.; Walton, R. A. *Multiple Bonds between Metal Atoms*, 2nd ed.; Oxford University Press: Oxford, 1993.

120. Green, K. N.; Brothers, M. B.; Jenkins, R. M.; Carson, C. E.; Grapperhaus, C. A.; Darensbourg, M. Y. *Inorg. Chem.* **2007**, *46*, 7536-7544.

121. Shatruk, M.; Dragulescu-Andrasi, A.; Chambers, K. E.; Stoian, S. A.; Bominaar, E. L.; Achim, C.; Dunbar, K. R. *J. Am. Chem. Soc.* **2007**, *129*, 6104-6116.

122. Connelly, N. G.; Geiger, W. E. *Chem. Rev.* **1996**, *96*, 877-910.

123. Darnault, C.; Volbeda, A.; Kim, E. J.; Legrand, P.; Vernède, X.; Lindahl, P. A.; Fontecilla-Camps, J. C. *Nat. Struct. Biol.* **2003**, *10*, 271-279.

124. Doukov, T. I.; Iverson, T. M.; Seravilli, J.; Ragsdale, S. W.; Drennan, C. L. *Science* **2002**, *298*, 567-572.

125. Svetlitchnyi, V.; Dobbek, H.; Meyer-Klaucke, W.; Meins, T.; Thiele, B.; Romer, P.; Huber, R.; Meyer, O. *Proc. Natl. Acad. Sci. USA* **2004**, *101*, 446-451.

126. Seravalli, J.; Xiao, Y.; Gu, W.; Cramer, S. P.; Antholine, W. E.; Krymov, V.; Gerfen, G. J.; Ragsdale, S. W. *Biochemistry* **2004**, *43*, 3944-3955.

127. Webster, C. E.; Darensbourg, M. Y.; Lindahl, P. A.; Hall, M. B. *J. Am. Chem. Soc.* **2004**, *126*, 3410-3411.

128. Amara, P.; Volbeda, A.; Fontecilla-Camps, J. C.; Field, M. J. *J. Am. Chem. Soc.* **2005**, *127*, 2776-2784.

129. Eisenberg, R.; Meyer, C. D. *Acc. Chem. Res.* **1975**, *8*, 26-34.

130. Kühl, O.; Palm, G. *Tetrahedron: Asymmetry* **2010**, *21*, 393-397.

131. Konkle, M. E.; Elsenheimer, K. N.; Hakala, K.; Robicheaux, J. C.; Weintraub, S. T.; Hunsicker-Wang, L. M. *Biochemistry* **2010**, *49*, 7272-7281.

132. Hsueh, K.; Westler, W. M.; Markley, J. L. *J. Am. Chem. Soc.* **2010**, *132*, 7908-7918.

133. Tennyson, A. G.; Dhar, S.; Lippard, S. J. *J. Am. Chem. Soc.* **2008**, *130*, 15087-15098.

134. Martin, R. L.; Taylor, D. *Inorg. Chem.* **1976**, *15*, 2970-2976.

135. Haymore, B. L.; Huffman, J. C.; Butler, N. E. *Inorg. Chem.* **1983**, *22*, 168-170.

136. Kaduk, J. A.; Ibers, J. A. *Inorg. Chem.* **1977**, *16*, 3283–3287.

137. Sacco, A.; Rossi, M.; Nobile, C. F. *Ann. Chim. (Rome)* **1967**, *57*, 499-507.

VITA

Jennifer Lynn Hess received her Bachelor of Science degree in chemistry from Grove City College in 2006, graduating *Magna cum Laude*. She began her graduate studies at Texas A&M University in the summer of 2006 under the direction of Marcetta Y. Darensbourg. Correspondence may be made through Marcetta Y. Darensbourg at: Department of Chemistry, Texas A&M University, Mail Stop 3255, College Station, TX 77843-3255 or at marcetta@chem.tamu.edu.